

# Quantum Optical Multiple Scattering

**Ott, Johan Raunkjær**

*Publication date:*
2012

*Document Version*
Publisher's PDF, also known as Version of record

DTU Fotonik
Department of Photonics Engineering

Technical University
of Denmark

# Quantum Optical Multiple Scattering

**Johan Raunkjær Ott**
**Ph.D. Thesis**

Supervisors:

Professor N. Asger Mortensen,
Technical University of Denmark

Professor Peter Lodahl,
Copenhagen University

Associate Professor Martijn Wubs,
Technical University of Denmark

**DTU Fotonik**
Kgs. Lyngby,
November 22, 2012

Johan Raunkjær Ott

# Abstract

This thesis concerns the theoretical investigation of interference phenomena related to elastic and inelastic scattering of quantized light. The presented work is naturally divided into two parts, the first is concerning elastic scattering while the second explores inelastic scattering.

In the first part we use a scattering-matrix formalism combined with results from random-matrix theory to investigate the interference of quantum optical states on a multiple scattering medium. We investigate a single realization of a scattering medium thereby showing that it is possible to create entangled states by interference of squeezed beams. Mixing photon states on the single realization also shows that quantum interference naturally arises by interfering quantum states. We further investigate the ensemble averaged transmission properties of the quantized light and see that the induced quantum interference survives even after disorder averaging. The quantum interference manifests itself through increased photon correlations. Furthermore, the theoretical description of a measurement procedure is presented. In this work we relate the noise power spectrum of the total transmitted or reflected light to the photon correlations after ensemble averaging. This analysis enables us to describe an experimental observation of the quantum nature of light that survives the averaging over disorder.

In the second part we investigate inelastic scattering. This we do by first treating the scattering of light on dipoles embedded in an arbitrary dielectric environment. By considering the two different models for dipole interaction known as the minimal-coupling and electric-dipole interaction Hamiltonians, we find exact relations between the electric field and the dipole operators in the Heisenberg picture, while keeping the model of the dipoles arbitrary. Due to the exact treatment of the electric-field operators, we obtain kernels known from classical scattering theory to describe the propagation of the field from the dipoles. Using the found electric field operators we derive the Heisenberg equations of motion for the dipoles while treating them as quantum two-level systems and using the Born–Markov and rotating-wave approximations. Postponing the rotating-wave approximation to the very end of the formal calculations allows us to identify the different physical parameters of the dipole evolution in terms of physical quantities known from optics. Finally, we use our Heisenberg picture formalism to treat a dilute cloud of two-level atoms, by simplifying the equations of motion using a single-scattering approximation for the interaction between the atoms. This

enables us to derive expressions for the steady-state population and fluorescence spectrum, where we find cooperative effects in both the elastic and the inelastic spectra.

# Resumé

Denne afhandling omhandler den teoretiske undersøgelse af interferens fænomener relaterede til elastisk og inelastisk spredning af kvantiseret lys. Det præsenterede arbejde er naturligt opdelt i to dele, den første vedrører elastisk spredning mens den anden udforsker inelastisk spredning.

I den første del benytter vi sprednings matrice formalismen kombineret med resultater fra teorien om tilfældige matricer til at undersøge interferensen af kvanteoptiske tilstande på et multipelt spredende medie. Vi undersøger en enkelt realisation af et spredende medie hvorved det vises at det er muligt at frembringe sammenfiltrede tilstande ved at interferere squeezed lysstråler. Ved at blande foton tilstande på denne enkelte realisation viser også at kvanteinterferens naturligt opstår ved at interferere kvantetilstande. Derefter undersøger vi de ensembel midlede transmissions egenskaber af kvantiseret lys og ser at den inducerede kvanteinterferens overlever selv efter midling af uordenen. Kvanteinterferensen manifesterer sig gennem øgede foton korrelationer. Derudover præsenteres en teoretisk beskrivelse af en målemetode. I dette arbejde relaterer vi støj spektret af det totale transmitterede og reflekterede lys til foton korrelationerne efter ensemble midling. Denne analyse gør det muligt for os at beskrive en eksperimentel observation af at den kvantemekaniske natur for lys overlever midling over uorden.

I den anden del undersøger vi inelastisk spredning. Dette gør vi ved først at behandle spredning af lys på dipoler indlejret i et arbitrært dielektrisk materiale. Ved at undersøge to forskellige modeller for dipol interaktionen, kendt som minimal-kobling og elektrisk-dipol interaktions Hamiltonerne, finder vi eksakte relationer mellem det elektriske felt og dipol operatorerne i Heisenberg billedet, mens vi lader modellen for dipolerne være valgfri. På grund af den eksakte behandling af operatorerne for det elektriske felt opnår vi elementer kendt fra klassisk sprednings teori til at beskrive udbredelsen af feltet fra dipolerne. Ved at bruge de fundne operatorer fra det elektriske felt udleder vi Heisenbergs bevægelses ligninger for dipolerne som vi beskriver som kvantemekaniske to-niveau systemer og benytter Born-Markov og roterende-bølge approksimationerne. Ved at udsætte brugen af roterende-bølge approksimationen til slutningen af vores udledning gør det muligt for os at identificere forskellige fysiske parametre for dipol evolutionen i forhold til fysiske kvantiteter kendt fra optikken. Til slut benytter vi vores Heisenberg formalisme til at beskrive en tynd sky af to-niveau atomer ved at simplificere bevægelsesligningerne med en enkelt spredning approksimation for interaktionen atomerne imellem. Dette gør det muligt for os at udlede udtryk for slut tilstanden

for populationen of fluorescence spektret hvor vi finder kooperative effekter i både de elastiske og inelastiske spektre.

# Preface

This thesis is submitted in partial fulfillment of the requirements for obtaining the Philosophiea Doctor (Ph.D.) degree at the Department of Photonics Engeneering, Technical University of Denmark. The work presented in the thesis was carried out between April 2009 and March 2012.

First of all, I would like to thank my main supervisor Professor N. Asger Mortensen for always having a positive attitude towards new ideas. Furthermore, it has been a great pleasure being part of Asgers group, the Structured Electromagnetic Materials group. As the name suggest this group could practically cover all areas of physics where light is considered and at times it even felt this way as well. It was thus always interesting to come to the group meetings, where subjects such as Dirac dispersion in graphene, non-local effects of plasmons, cloaking of macroscopic objects, and Casimir effects in gain media have all been brought up.

My Ph.D. work was further co-supervised by Professor Peter Lodahl and during the last half also Associate Professor Martijn Wubs. I am grateful of having had the chance of stimulating interaction with the experimentalists in the Quantum Photonics group of Peter. Even though both Peter and his group changed affiliation to the Niels Bohr Institute, University of Copenhagen, Peters door has always been open if needed. Next, I would like to sincerely thank Martijn, also in Asgers group, who, even before he became my co-supervisor when Peter left, always have had time to answer my questions and even spend evenings at home going through my calculations to help me.

Apart from the supervisors who were formally attached to my studies I would also like to thank Professor Antti-Pekka Jauho with whom I had many interesting discussions about diagrams and alike.

Part of the research was carried out at the Group of Professor Robin Kaiser at Institut Non Lineaire de Nice, Centre National de la Recherche Scientifique in Sophia-Antipolis in France. I would like to thank Robin and his team in the Cold Atom Group for their great hospitality during my stay in the spring of 2011. It has been a great pleasure being part of this enthusiastic research environment and even being invited into their homes. Furthermore, I did not complain of having to live in southern France for half a year.

While carrying out my explorations I have had the pleasure to share the ups and downs of the life of a Ph.D. with my office mates through the years: Jesper Goor Pedersen (from whom I got the LaTeX style of this thesis), Giovanni Gilardi (the most Italian of Italians), Søren Raza (the real OG),

Jeppe Clausen (the experimental input in the otherwise theoretical office), and especially Jure Grgic who started just before me and thus followed me all the way. Furthermore, I would also thank the rest of the members of the Structured Electromagnetic Materials and Quantum Photonics groups who all made my Ph.D. a journey I will never forget.

I would also like to thank Associate Professor Mads Brandbyge, Professor Klaus Mølmer, and Professor Allard P. Mosk for serving on the evaluation committee of my thesis.

Finally, I thank Anne from the bottom of my heart. I don't know how I would have gotten through this without you. Let us explore the world together, not only that of physics.

Johan Raunkjær Ott
March 2012

# List of Publications

## Journal Papers Included in the Thesis

[J1] S. Smolka, **J. R. Ott**, A. Huck, U. L. Andersen, and P. Lodahl,
"Continuous-wave spatial quantum correlations of light induced by multiple scattering",
Physical Review A **86**, 033814 (2012).

[J2] **J. R. Ott**, N. A. Mortensen, and P. Lodahl,
"Quantum interference and entanglement induced by multiple scattering of light",
Physical Review Letters **105**, 090501, (2010).

## Other Journal Papers

[J3] J. Grgic, **J. R. Ott**, F. Wang, O. Sigmund, A.-P. Jauho, J. Mørk, and N. A. Mortensen,
"Fundamental limits to gain enhancement in periodic media and waveguides",
Physical Review Letters **108**, 183903 (2012) (featured in Nature Photonics **6**, 413 (2012)).

[J4] H. Steffensen, **J. R. Ott**, K. Rottwitt, and C. J. McKinstrie,
"Full and semi-analytic analysis of two-pump parametric amplification with pump depletion",
Optics Express **19**, pp. 6648-6656 (2011).

[J5] **J. R. Ott**, M. E. V. Pedersen, and K. Rottwitt,
"Self-oscillation threshold of Raman amplified Brillouin fiber cavities",
Optics Express **17**, pp. 16166-16176 (2009).

[J6] **J. R. Ott**, M. Heuck, C. Agger, P. D. Rasmussen, and O. Bang,
"Label-free and selective nonlinear fiber-optical biosensing",
Optics Express **16**, pp. 20834-20847 (2008).

## Peer-Reviewed Conference Contributions

[C1] J. Grgic, **J. R. Ott**, F. Wang, O. Sigmund, A.-P. Jauho, J. Mørk, and N. A. Mortensen,
"Fundamental limitations to gain enhancement in slow-light photonic structures",
CLEO:QELS 2012, San Jose, California, USA (2011).

[C2] **J. R. Ott**, M. Wubs, N. A. Mortensen, and P. Lodahl,
"Scattering induced quantum interference of multiple quantum optical states",
TaCoNa Photonics, Bad Honnef, Germany, AIP Conf. Proc. **1398**, 82 (2011).

[C3] **J. R. Ott**, N. A. Mortensen, and P. Lodahl,
"Multiple scattering of quantum optical states",
CLEO:ECOC, Munich, Germany (2011).

[C4] **J. R. Ott**, N. A. Mortensen, and P. Lodahl,
"Quantum interference of multiple beams induced by multiple scattering",
CLEO:QELS 2011, Baltimore, Maryland, USA (2011).

[C5] **J. R. Ott**, N. A. Mortensen, and P. Lodahl,
"Quantum interference and entanglement induced by multiple scattering of light",
PECS IX, Granada, Spain (2010).

[C6] O. Bang, **J. R. Ott**, M. Heuck , C. Agger, P. D. Rasmussen, R. B. Simonsen, and M. Frosz,
"Label-free and selective four-wave mixing based nonlinear biosensing in photonic crystal fibers",
LPHYS, Barcelona, Spain (2009).

[C7] K. Rottwitt, **J. R. Ott**, H. Steffensen, S. Ramachandran,
"Spontaneous emission from saturated parametric amplifiers",
ICTON, Island of São Miguel, Azores, Portugal (2009).

[C8] M. E. V. Pedersen, **J. R. Ott**, and K. Rottwitt,
"Self-pulsation in Raman fiber amplifiers",
ICTON, Island of Sao Miguel, Azores, Portugal (2009).

# Contents

# 1 Introduction

## 1.1

We have been taught throughout our life that light propagates as waves, giving rise to constructive and destructive interference. It is thus often not considered strange when the light quanta, known as photons, are found to make similar interference patterns. Opposite to electrons or other quantum particles, the quantum nature of light is often thought of being the particle properties and not the wave properties.

Let us try to illustrate the weirdness of the quantum optics by the simple scattering setup known as the double-slit or Young's experiment. It consist of a detector hidden at some distance behind a plate with two slits, which is then illuminated by a light source. This give rise to the detection of a regular pattern which is caused by the interference between the light passing through the different slits. This makes perfect sense because we learned this in one of the first physics classes in school. Let us now imagine that we send in a single photon onto the double slit. Of course, the detector will only be able to detect a single hit since there is only one photon, but if we redo the experiment a large number of times the same pattern will appear. The photon, even though it is a single quantum, is thus able to interfere with itself. This surprisingly simple, yet mind-boggling experiment was first conducted by Taylor in 1909 [1].

By increasing the complexity of scattering of classical waves, studies of elastic scattering of waves have revealed a range of fascinating wave phenomena, including Anderson localization [2], enhanced coherent backscattering [3, 4], and universal conductance fluctuations [5]. These phenomena originate from wave interference and appear even after averaging over all configurations of disorder [6, 7]. Recently it was shown experimentally that light-matter interaction is strongly enhanced in disordered photonic crystal waveguides, enabling cavity quantum electrodynamics with Anderson-localized modes [8]. This, along with the advancement of controlling the

light-matter interaction between in cold atom experiments lead to the need of a formalism which can deal with multiple elastic and inelastic scattering of light in a quantum mechanical setting. This is the topic of this thesis.

## 1.2 Thesis Outline

The thesis is naturally divided into two parts, one concerning elastic scattering while the other concern inelastic scattering. The first part concerning elastic scattering consist of Chaps. 2 to 4 while the second part is contained in Chaps. 5 and 6. The chapters are structured as follows.

In Chap. 2 we introduce some background theory of classical light propagation and multiple scattering and review the quantization of the electromagnetic field. After this we introduce the concepts of quantum interference and entanglement which are illustrated by the simple scattering device known as a beam splitter.

Then, in Chap. 3, we explore the possibility to induce quantum interference and entanglement by interfering several quantum states of light on a multiple scattering medium. We first explore the interference effects of propagation through a single configuration of scatterers and then investigate the properties of interference of quantum optical states on a multiple scattering medium averaged over all configurations of the scatterers.

After this, in Chap. 4, we relate the experimentally measurable noise power spectrum to the photon correlations between two output ports. This we do in order to describe an experimental observation of the preserved quantum nature of light after averaging the scattering configurations.

In the second part of the thesis we include inelastic effects through the scattering on dipoles. This is done in Chap. 5, where the scattering of light on point dipoles embedded in an arbitrary dielectric structure is treated quantum mechanically. Using two models for the interaction, known as the electric-dipole and minimal-coupling interaction Hamiltonians, we describe the general evolution of the electric-field operators through an arbitrary dielectric medium with dipoles in the Heisenberg picture, first without introducing a specific model for the dipoles. This is then used to derive the Heisenberg equations of motion for $N$ dipoles each described as a quantum two-level model system.

Finally, in Chap. 6 we consider a dilute cloud of two-level atoms driven by a laser field. Using the equations of motion derived in the previous chapter along with a single-scattering assumption, we derive analytic expressions for the steady-state population and fluorescence spectrum.

The results of the thesis are summarized in Chap. 7.

# Part I

# Quantum Optical Correlations from Random Elastic Scattering

# 2

# Background Theory

Since this thesis deals with multiple scattering of quantized light it is advantageous to know some quantum optics and multiple scattering formalisms. The purpose of this chapter is to briefly review the two fields in order to make readers more familiar with some of the concepts used throughout the thesis. We will start out in Sec. 2.1 by going through a bit of classical optics ending up with the expression for the energy of the electromagnetic radiation in terms of the vector potential. Next in Sec. 2.2 the basics of classical elastic multiple scattering is explained through some Green function analysis and scattering matrix theory. After this in Sec. 2.3, using the results of the previous sections, we quantize the electric field and introduce two quantum phenomena, quantum interference and entanglement. Then, in Sec. 2.4 we illustrate the scattering formalism for quantum optics and discuss the introduced quantum phenomena by analyzing the scattering of quantum optical states on one of the simplest scatterers imaginable, the beam splitter. At last we summarize the findings of the chapter in Sec. 2.5. Let us start out with some classical optics.

## 2.1 Classical Light Propagation

In this section we will briefly review classical light propagation using usual potential theory to derive the total energy of the electromagnetic field and relate it to the energy of a sum of harmonic oscillators. As always we start out with Maxwell's equations [9, 10] (see also any textbook on light propagation)

$$\nabla \times \mathbf{E}(\mathbf{r},t) = -\frac{\partial \mathbf{B}(\mathbf{r},t)}{\partial t}, \tag{2.1.1a}$$

$$\nabla \times \mathbf{H}(\mathbf{r},t) = \frac{\partial \mathbf{D}(\mathbf{r},t)}{\partial t} + \mathbf{J}(\mathbf{r},t), \tag{2.1.1b}$$

$$\nabla \cdot \mathbf{D}(\mathbf{r},t) = \sigma(\mathbf{r},t), \tag{2.1.1c}$$

$$\nabla \cdot \mathbf{B}(\mathbf{r},t) = 0, \tag{2.1.1d}$$

where $\sigma(\mathbf{r},t)$ and $\mathbf{J}(\mathbf{r},t)$ are respectively the charge and current densities. Furthermore, $\mathbf{E}(\mathbf{r},t)$ and $\mathbf{B}(\mathbf{r},t)$ are the electric and magnetic fields which in a local, linear, non-magnetic, dielectric medium are related to the electric displacement field, $\mathbf{D}(\mathbf{r},t)$, and the auxiliary magnetic field, $\mathbf{H}(\mathbf{r},t)$, through

$$\mathbf{D}(\mathbf{r},t) = \varepsilon_0\varepsilon(\mathbf{r})\mathbf{E}(\mathbf{r},t), \tag{2.1.2a}$$

$$\mathbf{B}(\mathbf{r},t) = \mu_0\mathbf{H}(\mathbf{r},t), \tag{2.1.2b}$$

where $\varepsilon_0$ and $\mu_0$ are the vacuum permittivity and permeability respectively. Furthermore the dielectric function, $\varepsilon(\mathbf{r})$, describing the geometric distribution of dielectric material, is considered real-valued, i.e. we assume a medium without loss or gain. In this chapter we will not consider charges and currents in the structures, but these will be included in Chap. 5.

We will now show that the energy of electromagnetic radiation is related to the energy of a sum of harmonic oscillators. This we do in order to, in a hand-waving way, introduce the first quantization in a general dielectric medium in Sec. 2.3 in a similar way as the treatment of quantization of light in vacuum, see eg. Refs. [11, 12]. A more rigorous treatment can be found in Ref. [13]. Let us thus introduce the vector potential $\mathbf{A}(\mathbf{r},t)$ by

$$\mathbf{B}(\mathbf{r},t) = \nabla \times \mathbf{A}(\mathbf{r},t) \tag{2.1.3a}$$

and furthermore the scalar potential $\phi(\mathbf{r},t)$ such that the electric field

$$\mathbf{E}(\mathbf{r},t) = -\nabla\phi(\mathbf{r},t) - \frac{\partial\mathbf{A}(\mathbf{r},t)}{\partial t} \tag{2.1.3b}$$

automatically obeys Eq. (2.1.1a). The potentials can be chosen with a certain degree of freedom since any gauge transformation $\mathbf{A}(\mathbf{r},t) = \mathbf{A}'(\mathbf{r},t) - \nabla\Xi(\mathbf{r},t)$ and $\phi(\mathbf{r},t) = \phi'(\mathbf{r},t) + \frac{\partial\Xi(\mathbf{r},t)}{\partial t}$ will leave $\mathbf{E}(\mathbf{r},t)$ and $\mathbf{B}(\mathbf{r},t)$ unaltered. Due to the absence of charges it is easy to show that we can choose the scalar potential to be zero, $\phi(\mathbf{r},t) = 0$, and thus we fix the vector potential by the so called generalized Coulomb gauge

$$\nabla \cdot [\varepsilon(\mathbf{r})\mathbf{A}(\mathbf{r},t)] = 0. \tag{2.1.4}$$

Insertion of Eq. (2.1.3a) into the Maxwell Eq. (2.1.1b) then gives the wave equation

$$\left[\hat{L} + \frac{\varepsilon(\mathbf{r})}{c^2}\frac{\partial^2}{\partial t^2}\right]\mathbf{A}(\mathbf{r},t) = 0, \tag{2.1.5}$$

with the double curl operator defined as $\hat{L} = \nabla \times \nabla\times$.

We now define the complex mode function $\mathbf{f}_\lambda(\mathbf{r})$ as the solution of the eigenvalue problem

$$\left[\hat{L} - \frac{\varepsilon(\mathbf{r})\omega_\lambda^2}{c^2}\right]\mathbf{f}_\lambda(\mathbf{r}) = 0, \tag{2.1.6}$$

which with appropriate boundary conditions is seen to be Hermitian with the normal inner product for $\mathbf{f}_\lambda(\mathbf{r}) = \mathbf{g}_\lambda(\mathbf{r})/\sqrt{\varepsilon(\mathbf{r})}$ such that the eigenfunctions $\mathbf{f}_\lambda(\mathbf{r})$ form a full set of solutions having the orthonormality condition

$$\int \mathrm{d}\mathbf{r}\, \varepsilon(\mathbf{r})\mathbf{f}_\lambda(\mathbf{r}) \cdot \mathbf{f}^*_{\lambda'}(\mathbf{r}) = \delta_{\lambda,\lambda'}, \tag{2.1.7}$$

where $\delta_{\lambda,\lambda'}$ is the Kroenecker delta function. The indices $\lambda$ label the specific independent modes of the field and we can choose $\lambda = \{\mathbf{k}, s\}$ corresponds to the specific state with momentum $\mathbf{k}$ and polarization $s$ such that the sum over $\lambda$ is a generalized sum over $\{\mathbf{k},\, s\}$. We can now make an eigenfunction expansion of the vector potential in the new eigenfunctions

$$\mathbf{A}(\mathbf{r}, t) = \sum_\lambda \left[A_\lambda(t)\mathbf{f}_\lambda(\mathbf{r}) + A^*_\lambda(t)\mathbf{f}^*_\lambda(\mathbf{r})\right], \tag{2.1.8}$$

where $A_\lambda(t)$ are some complex-valued, time-dependent expansion coefficients which by insertion into Eq. (2.1.5), using the definition of the eigenfunctions, Eq. (2.1.6), and the orthonormality condition, Eq. (2.1.7), are found to evolve harmonically as $A_\lambda(t) = A_\lambda(0)e^{-i\omega_\lambda t}$. For vacuum ($\varepsilon(\mathbf{r}) = 1$) the expansion reduces to the usual plane-wave mode expansion known from textbooks, see eg. Refs. [12, 11]. The energy of the electromagnetic radiation is given by the volume integral of the sum of the energy densities of the electric field and the magnetic field,

$$\mathcal{E}_\mathrm{R} = \frac{1}{2}\int \mathrm{d}\mathbf{r}\left[\varepsilon_0\varepsilon(\mathbf{r})\mathbf{E}(\mathbf{r}, t) \cdot \mathbf{E}(\mathbf{r}, t) + \frac{1}{\mu_0}\mathbf{B}(\mathbf{r}, t) \cdot \mathbf{B}(\mathbf{r}, t)\right] \tag{2.1.9}$$

and thus by insertion of the vector potential we get a sum of time-independent contributions of the modes

$$\mathcal{E}_\mathrm{R} = \varepsilon_0 \sum_\lambda \omega_\lambda^2 \left[A_\lambda(t)A^*_\lambda(t) + A^*_\lambda(t)A_\lambda(t)\right], \tag{2.1.10}$$

where we have left the order of the mode coefficients even though they of course commute in the classical case. If we now introduce the real-valued coefficients $Q_\lambda(t) = A_\lambda(t) + A^*_\lambda(t)$ and $P_\lambda(t) = -i\omega\left[A_\lambda - A^*_\lambda(t)\right]$ we get

$$\mathcal{E}_\mathrm{R} = \frac{\varepsilon_0}{2}\sum_\lambda \left[P^2_\lambda(t) + \omega^2_\lambda Q^2_\lambda(t)\right], \tag{2.1.11}$$

which strongly resembles a sum of individual harmonic oscillators. This resemblance is not a coincidence, but rather is caused by the explicit use of "matter in motion" in the original derivation of Maxwell [10]. It is thus more curious that Maxwell's equations also describe light propagation in vacuum. In Sec. 2.3 we put hats on the mode coefficients and call them operators and relate the energy to the energy of the quantum mechanical harmonic oscillator. This is of course a too simplified way to carry out the first quantization, but it is sufficient for the present purpose. In the following section we will go through the basics of classical light propagation through multiple scattering systems.

## 2.2 Classical Multiple Scattering

In the previous section we introduced some rather general results from classical optics. Here we investigate the effect of multiple scattering of classical light. This will give the reader a strong feeling of classical wave scattering and the related formalism. This we do by first in Sec. 2.2.1 revisiting the method of Green functions to give a simple and intuitive microscopic way of treating weak multiple scattering. This is used to introduce the so-called scattering matrix which makes it possible to investigate scattering in a macroscopic description by the use of random matrix theory which is discussed in Sec. 2.2.2. This will give an intuitive understanding of intensity correlations in classical multiple scattering.

### 2.2.1 The Green Function and Scattering Matrix

Now we will use the Green function method to find the time evolution of the electric field. We then use the intuitive physical interpretation of the Green function as a way to investigate propagation in a scattering medium. After this we relate the Green function to the scattering matrix.

By taking the curl of Eq. (2.1.1a) and performing the Fourier transform we get the wave equation for the electric field

$$\left[\hat{L} - \frac{\omega^2 \varepsilon(\mathbf{r})}{c^2}\right] \mathbf{E}(\mathbf{r}, \omega) = 0. \tag{2.2.1}$$

If we now assume the medium to be homogeneous $\varepsilon(\mathbf{r}) = \varepsilon_b$, where the subscript $b$ is for background, and phenomenologically add a source term $\mathbf{S}(\mathbf{r}, \omega)$ we get

$$\left[\hat{L} - \frac{\omega^2 \varepsilon_b}{c^2}\right] \mathbf{E}_b(\mathbf{r}, \omega) = \mathbf{S}(\mathbf{r}, \omega). \tag{2.2.2}$$

We will now find the resulting field due to the source using the Green function method. The source could be interpreted as the field at some initial stage and we thus investigate the time evolution of such an initial field.

The dyadic Green function is defined as the solution of

$$\left[\hat{L} - \frac{\omega^2 \varepsilon_b}{c^2}\right] \mathbf{G}_b(\mathbf{r}, \mathbf{r}', \omega) = \delta(\mathbf{r} - \mathbf{r}')\mathbf{I} \tag{2.2.3}$$

where $\mathbf{I}$ is the unit matrix, such that, using that the operator in Eq. (2.2.2) is Hermitian, we have that

$$\mathbf{E}_b(\mathbf{r}, \omega) = \int \mathrm{d}\mathbf{r}' \mathbf{G}_b(\mathbf{r}, \mathbf{r}', \omega) \cdot \mathbf{S}(\mathbf{r}', \omega). \tag{2.2.4}$$

The Green function gives the probability amplitude for the light to go from $\mathbf{r}'$ to $\mathbf{r}$. Now let us introduce the scattering elements into the structure by including the geometric distribution of dielectric material, $\varepsilon(\mathbf{r})$. This we do by defining the difference $\delta\varepsilon(\mathbf{r}) = \varepsilon_b - \varepsilon(\mathbf{r})$ such that

$$\left[\hat{L} - \frac{\varepsilon(\mathbf{r})\omega^2}{c^2}\right] \mathbf{E}(\mathbf{r}, \omega) = \mathbf{S}(\mathbf{r}, \omega). \tag{2.2.5}$$

We see that this can be written as

$$\left[\hat{L} - \frac{\varepsilon_b \omega^2}{c^2}\right] \mathbf{E}(\mathbf{r}, \omega) = \mathbf{S}(\mathbf{r}, \omega) + \frac{\delta\varepsilon(\mathbf{r})\omega^2}{c^2} \mathbf{E}(\mathbf{r}, \omega) \tag{2.2.6}$$

which has the formal solution

$$\mathbf{E}(\mathbf{r}, \omega) = \mathbf{E}_b(\mathbf{r}, \omega) + \frac{\omega^2}{c^2} \int \mathrm{d}\mathbf{r}' \mathbf{G}_b(\mathbf{r}, \mathbf{r}', \omega) \cdot \delta\varepsilon(\mathbf{r}') \mathbf{E}(\mathbf{r}', \omega). \tag{2.2.7}$$

This has the clear physical interpretation that by introducing some change in the scattering environment, $\delta\varepsilon(\mathbf{r}')$, the field at $\mathbf{r}$, $\mathbf{E}(\mathbf{r}, \omega)$ is given by the field without the change $\mathbf{E}_b$ plus a scattering term being an implicit integral of the field over all the positions where the environment is changed, $\mathbf{r}'$, and weighted with the amount it is changed at that position, $\delta\varepsilon(\mathbf{r}')$. If we assume that the scattering is weak, such that $\mathbf{G}_b(\mathbf{r}, \mathbf{r}', \omega)\delta\varepsilon(\mathbf{r}')$ is small, then we can iterate once on this implicit equation, Eq. (2.2.7), and assume all second- and higher-order terms to be negligible

$$\begin{aligned}
\mathbf{E}(\mathbf{r}, \omega) &= \mathbf{E}_b(\mathbf{r}, \omega) + \frac{\omega^2}{c^2} \int \mathrm{d}\mathbf{r}' \mathbf{G}_b(\mathbf{r}, \mathbf{r}', \omega) \cdot \delta\varepsilon(\mathbf{r}') \mathbf{E}_b(\mathbf{r}', \omega) \\
&\quad + \frac{\omega^4}{c^4} \int \mathrm{d}\mathbf{r}' \mathbf{G}_b(\mathbf{r}, \mathbf{r}', \omega) \cdot \delta\varepsilon(\mathbf{r}') \int \mathrm{d}\mathbf{r}'' \mathbf{G}_b(\mathbf{r}', \mathbf{r}'', \omega) \cdot \delta\varepsilon(\mathbf{r}'') \mathbf{E}(\mathbf{r}'', \omega) \\
&\approx \mathbf{E}_b(\mathbf{r}, \omega) + \frac{\omega^2}{c^2} \int \mathrm{d}\mathbf{r}' \mathbf{G}_b(\mathbf{r}, \mathbf{r}', \omega) \cdot \delta\varepsilon(\mathbf{r}') \mathbf{E}_b(\mathbf{r}', \omega).
\end{aligned} \tag{2.2.8}$$

This is known as the first-order Born approximation and describes how the electric field at position $\mathbf{r}$ is approximated by the light that would have arrived there without the change in the scattering environment plus the light scattered once and arriving at $\mathbf{r}$. If the change in the scattering environment was due to a collection of isotropic point scatterers $\delta\varepsilon(\mathbf{r}) = \sum_m \delta\varepsilon_m \delta(\mathbf{r} - \mathbf{r}_m)$ then

$$\begin{aligned}\mathbf{E}(\mathbf{r},\omega) &= \mathbf{E}_b(\mathbf{r},\omega) + \frac{\omega^2}{c^2}\sum_m \mathbf{G}_b(\mathbf{r},\mathbf{r}_m,\omega)\cdot\delta\varepsilon_m\mathbf{E}_b(\mathbf{r}_m,\omega) \\ &\quad + \frac{\omega^4}{c^4}\sum_m\sum_n \delta\varepsilon_m\delta\varepsilon_n\mathbf{G}_b(\mathbf{r},\mathbf{r}_m,\omega)\cdot\mathbf{G}_b(\mathbf{r}_m,\mathbf{r}_n,\omega)\cdot\mathbf{E}(\mathbf{r}_n,\omega) \\ &\approx \mathbf{E}_b(\mathbf{r},\omega) + \frac{\omega^2}{c^2}\sum_m \mathbf{G}_b(\mathbf{r},\mathbf{r}_m,\omega)\cdot\delta\varepsilon_m\mathbf{E}_b(\mathbf{r}_m,\omega), \qquad (2.2.9)\end{aligned}$$

which is seen to be valid if either the scattering strengths $\delta\varepsilon_m$ are small or the probability of going from $\mathbf{r}_m$ to $\mathbf{r}_n$, $\mathbf{G}_b(\mathbf{r}_n,\mathbf{r}_m,\omega)$ is small, i.e. if the probability of scattering between different scatterers is small. This approximation will be used in Chap. 6 to calculate the fluorescence spectrum of a driven cloud of cold atoms.

When scattering is not weak it is not always preferable to use the microscopic approach of Green functions since the explicit propagation path is not usually important for the end result. Therefore one often uses the scattering-matrix approach, a macroscopic approach which only consider the probability of a mode $i$ to propagate to another mode $\alpha$[1]. The scattering matrix, $\mathbf{S}$, is related to the Green function through the Fisher–Lee relation [14]. The relation is not stated here since it not explicitly used, but one could in principle use the relation to calculate the scattering matrix elements given the knowledge of the Green function of the full scattering medium. The scattering matrix method is however only applicable when the transport is linear [15] and will thus not be used in the second part of the thesis concerning strong light-matter interaction.

### 2.2.2 Classical Correlations by Multiple Scattering

Let us now use the scattering matrix method to describe multiple scattering. Since the present work consider scattering processes with random distributions of scatterers the usual way to describe such type of propagation is to

[1]Here and in the following we use the notation that Roman letters correspond to incoming modes while Greek letters indicate outgoing modes. Furthermore we use the notion "modes" while the term "states" is also often used in the literature. We will reserve the use of "states" to quantum states.

investigate its ensemble-averaged properties. Due to the randomness one might expect that performing an average would wash out all correlations in the system, but as we will see this is not the case.

Here we perform the ensemble average by using the scattering matrix theory and then use random-matrix theory on the products of scattering matrix elements, see eg. Ref. [7]. Random matrix theory builds on using the general properties of the scattering matrices concerning the specific physical situation under investigation. For example energy conservation and time-reversal symmetry of light propagation in multiple scattering media lead to unitarity and hermiticity of the scattering matrix. Furthermore random matrix theory assumes that the eigenvalues of the scattering matrix has some statistical distribution. Specifically we look at the transport through a disordered waveguide and use the expressions for the averaged products of two or four scattering matrix elements obtained in Ref. [16] using the Dorokhov–Mello–Pereyra–Kumar (DMPK) scaling equation [17, 18]. The DMPK equation is built on only a few general properties, namely of flux conservation, time-reversal symmetry and the maximum entropy hypothesis [19].

Let us look at the intensity of a given output mode $\alpha$ after transmission which is generally given by

$$I_\alpha = \sum_i \sum_j t_{i\alpha} t_{j\alpha}^* E_i E_j^* \tag{2.2.10}$$

where $t_{\alpha i}$ is the scattering matrix element giving the probability amplitude of the field amplitude incident in mode $i$, $E_i$, to be *transmitted* to the output mode $\alpha$, and the sum is over all $N$ possible modes of the structure. If we now perform an ensemble average we obtain

$$I_\alpha = \sum_i \sum_j \overline{t_{i\alpha} t_{j\alpha}^*} E_i E_j^* = \tau \sum_i I_i \tag{2.2.11}$$

where the overline denotes the averaging, $\overline{t_{i\alpha} t_{j\alpha}^*} = \overline{T_{i\alpha}}\delta_{ij} = \tau\delta_{ij}$ is the average single channel intensity transmission coefficient, with $T_{i\alpha}$ being the intensity transmission coefficient, and $I_i = |E_i|^2$ is the intensity of the light incident in the $i$'th mode. We thus see that the intensity transmission is given by the average conductance $g = N^2\tau$ through the medium. Furthermore, only the intensity transmission coefficients rather than the individual amplitude transmission coefficients contribute to the transmitted intensity. From this, one might expect that all correlations between the intensities of different modes would wash out since the averaging procedure would seem to remove all phase information. This is however only partially true. Due to constructive and destructive interference amongst different paths, some

intensity correlations will in fact survive ensemble-averaging. The correlation function for scalar wave propagation through disordered media was first found using a diagrammatic technique to have the form [20]

$$C_{\alpha i\beta j} = \frac{\overline{T_{i\alpha}T_{j\beta}}}{\overline{T_{i\alpha}}\,\overline{T_{j\beta}}} - 1 = C^{(1)}_{i\alpha j\beta} + C^{(2)}_{i\alpha j\beta} + C^{(3)}_{i\alpha j\beta}, \tag{2.2.12}$$

independent of the details of the scattering mechanisms. The same form was later found using random matrix theory giving [21, 22]

$$C_{i\alpha j\beta} = C_1\delta_{\alpha\beta}\delta_{ij} + C_2(\delta_{\alpha\beta} + \delta_{ij}) + C_3. \tag{2.2.13}$$

The different coefficients has a transparent physical interpretation which will be explained in the following. The three coefficients $C_1$, $C_2$, and $C_3$ correspond respectively to the so-called short-range, long-range, and infinite-range correlations. We will spend the rest of this section describing in detail the dependence of $g$, $C_1$, $C_2$, and $C_3$ on the degree of scattering to be explained in a moment. Furthermore, it is explained how these coefficients are related to the fluctuations and correlations of the speckle pattern produced in a classical multiple scattering experiment. The discussion will also lead us to define the ballistic, weak scattering, and localized regimes.

In general, $g$, $C_1$, $C_2$, and $C_3$ only depend on two quantities, $i$) the number of possible modes of the structure, $N$, and $ii$) the ratio, $s = \frac{L}{\ell}$, between the length of the scattering region of the medium, $L$, and the scattering mean free path, $\ell$ [7]. Since systems with different $N$ have qualitatively the same dependence on $s$, we will illustrate $C_1$, $C_2$, $C_3$, and $g$ using a waveguide having $N = 20$ with data generously supplied by L. S. Froufe-Pérez, Ref. [16]. In the following we describe the four different quantities seperately.

**Conductance** $g$ : The conductance, $g$, has its name from electronic transport where disorder was first investigated. It describes the average number of modes that are conducting, i.e. where light can pass through the sample. Intuitively it is expected that the conductance decreases as the amount of scattering, $s$, increases, this can be seen in the upper plot in Fig. 2.1. Furthermore we see that as we increase $s$, we reach a point where $g < 1$ which signifies that, on average, less than one mode will be conducting. The $g = 1$, see dashed lines in Fig. 2.1, thus marks the conducting to insulating transition and the region $g < 1$ is defined as the localized regime. The precise value of $s$ at the transition depends on the number of modes $N$ and increases with $N$.

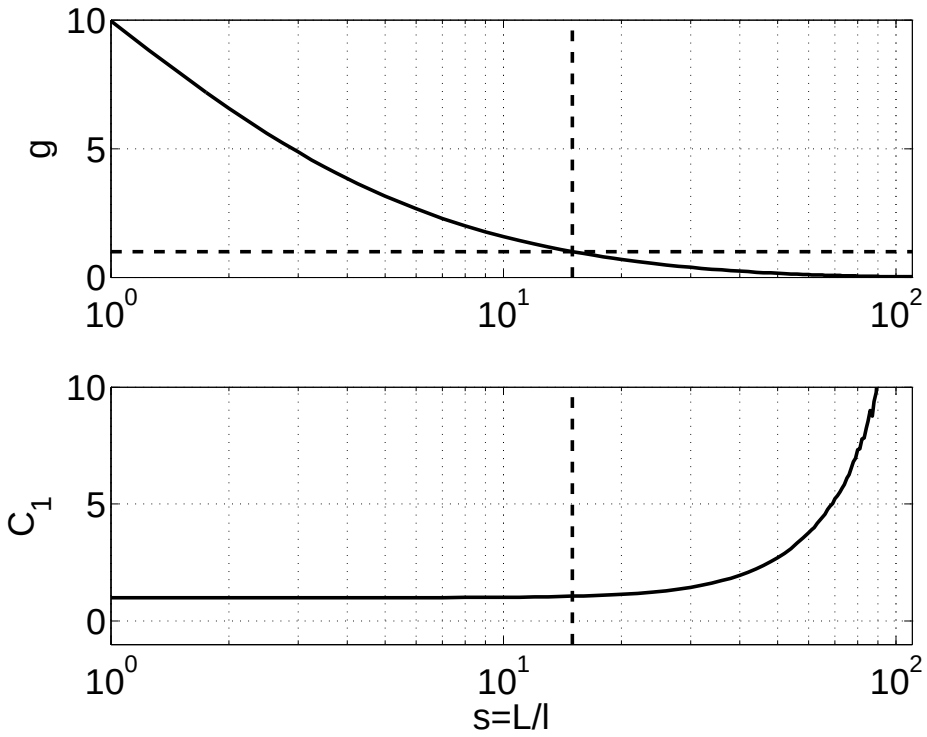


**Figure 2.1** The dependence of $g$ and $C_1$ versus $s = L/\ell$. The upper plot shows the conductance $g$ as a function of the amount of scattering $s = L/\ell$. At $g = 1$ there is a transition from conducting to becoming insulating defining the localized regime. The lower plot shows the short-range correlation $C_1$, also as function of $s$. The quantity $C_1$ is also identified as the single speckle intensity fluctuations and in the localized regime $C_1$ increases dramatically. The plot is for a disordered waveguide with $N = 20$ modes with the data gratefully supplied by L. S. Froufe-Pérez published in Ref. [16]. Systems with different $N$ have qualitatively the same dependence of $s$.

**Short-range correlation** $C_1$ : The short range correlation, $C_1$, is often identified as the so-called speckle contrast or single-speckle intensity fluctuations since it is the leading term in $C_{\alpha i \beta j}$ with $\alpha = \beta$ and $i = j$ [19]. That is, it is the leading term when considering a single input channel, i.e. $i = j$, and a single output channel, i.e. $\alpha = \beta$. In the lower plot in Fig. 2.1 the dependence of $C_1$ as a function of $s$ is shown. First of all we see that up until the localized regime, we have $C_1 \approx 1$ indicating small sample-to-sample speckle intensity fluctuations. Furthermore we notice a dramatic increase of $C_1$ in the localized regime. The reason is that most often light will not pass through when the system becomes insulating, but for a few realizations it will, thus giving rise to large fluctuations in the sample- to- sample speckle intensity.

**Long-range correlation** $C_2$ : The long-range correlations $C_2$ can be identified as the intensity correlations between different speckles in the speckle pattern since it is the leading term in $C_{\alpha i \beta j}$ with $\alpha \neq \beta$ and $i = j$ [19]. That is, it is the leading term when considering a single input channel, i.e. $i = j$, and two different output channel, i.e. $\alpha \neq \beta$. The dependence of $C_2$ versus $s$ is shown in the upper plot of Fig. 2.2 showing a similar behavior as $C_1$ except for two striking features. Firstly, we see that $C_2 \approx 0$ below the localized regime which signifies that the different speckles are almost uncorrelated. This would be expected from weak scattering or diffusion theory which build on the ansatz that all phase information is averaged out and thus no correlations caused by interference can occur. Secondly, we notice that for small amounts of scattering $C_2$ actually becomes negative which signifies that the intensity of two speckles becomes anti-correlated. This can be explained follows. As the amount of scatterers decreases the propagation becomes ballistic. Since we are considering transmission from only one input channel, ballistic propagation would signify that observation of high intensity in one speckle will decrease the possibility of high intensity in another speckle. The extreme case is free space propagation which of cause would only give a single speckle spot from the laser itself. This transition from negative to positive $C_2$ thus marks the transition from the ballistic regime to the weak scattering regime. It occurs at $s \approx 2$, independent of $N$ [23]. Let us now take a look at the behavior of $C_2$ in the localized regime. As mentioned, the dependence is very similar to that of $C_1$ and in fact as we can see by the solid line in the lower plot of Fig. 2.2 the difference $C_1 - C_2$ actually goes to zero in the localized regime. This is because in the localized regime the system turns insulating and thus, since less than one mode is propagating through the structure, two speckles in the same speckle pattern will result from the same mode such that $C_1$ and $C_2$ actually probe the same transmitted mode.

**Infinite-range correlation** $C_3$ : Finally, the infinite-range correlations, $C_3$, are actually equal to $C_1 - 1$ [16] which can be seen from the dash dotted line in the lower plot of Fig. 2.2. We have thus seen that, in classical wave propagation through disordered media, correlations between intensities of different output modes persist ensemble averaging and that correlations are actually increased as the amount of scattering increases. This along with the knowledge about the dependence of $g$, $C_1$, $C_2$, and $C_3$ is used in the next chapter where quantum optical phenomena in connection to multiple scattering are investigated. However, to that end we first need to introduce quantum optics which is the subject of the next section.

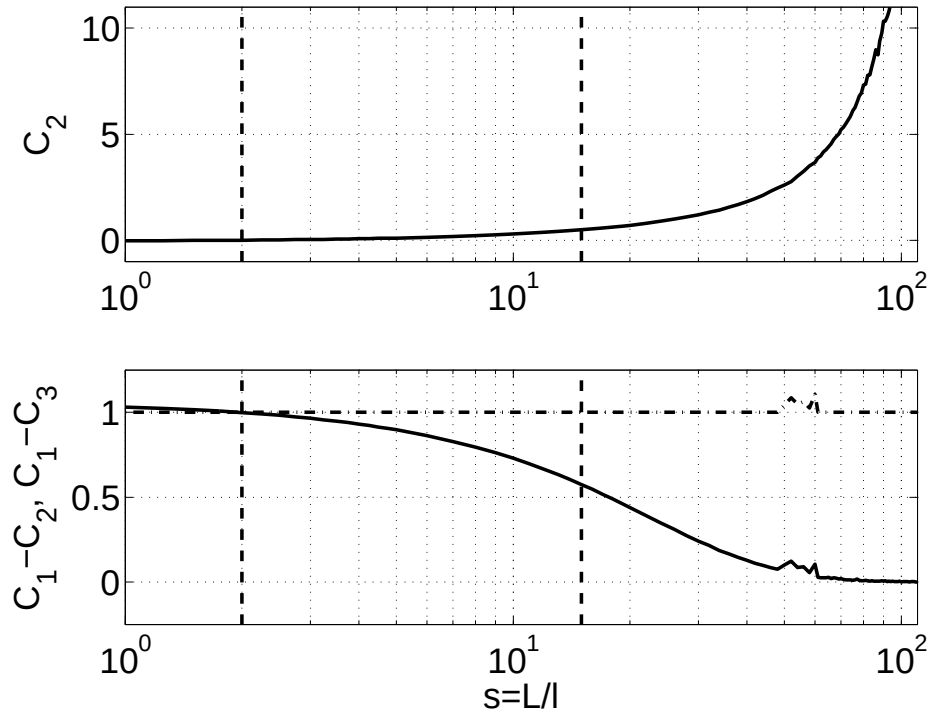


**Figure 2.2** The evolution of $C_2$ and $C_1 - C_2$ and $C_1 - C_3$ versus $s = L/\ell$. The upper plot shows the long-range correlations, $C_2$, as a function of the amount of scattering, $s$. The quantity $C_2$ is also identified as the speckle intensity correlation function and is observed to be approximately zero in the weak scattering regime having a transition from negative to positive around $s \approx 2$ corresponding to the transition from ballistic to weak scattering. In the localized regime $C_2$ approach $C_1$ as is seen from the solid line in the lower plot. The dash-dotted horizontal line correspond to $C_1 - C_3$ showing that $C_3 = C_1 - 1$. The vertical lines correspond to the transitions from ballistic to weak scattering and from weak scattering to localized respectively. The small ripples in the curve around $s \approx 60$ are due to an incomplete convergence in the numerical ensemble averaging. The plot is for a disordered waveguide with $N = 20$ modes with the data gratefully supplied by L. S. Froufe-Pérez published in Ref. [16]. Systems with different $N$ have qualitatively the same dependence of $s$.

## 2.3 Quantization of Light

In the previous sections we have reviewed classical light propagation and multiple scattering. In the present section we will turn our attention to the procedure of quantization of light and the connection between multiple scattering and quantum optics. We will start out in Sec. 2.3.1 by briefly going through the quantum treatment of the harmonic oscillator and relate it to the energy of the radiation found in the beginning of this chapter. Then in Sec. 2.3.2 we will use this approach to find the quantized electric field

and relate this to the scattering matrix approach discussed in the previous section. This will enable us to describe multiple scattering in a quantum optical setting.

### 2.3.1 The Quantum-Mechanical Harmonic Oscillator

Let us take a look at the quantum mechanical description of the harmonic oscillator which we will write in a form that looks like the energy of the classical electric field found in Sec. 2.1. We will start with the Hamiltonian of a one-dimensional quantum-mechanical harmonic oscillator (QHO)

$$\mathcal{H}_{\mathrm{QHO}} = \frac{\hat{p}^2(t)}{2m} + \frac{1}{2}m\omega^2\hat{q}^2(t), \tag{2.3.1}$$

which is found by taking the total energy of the classical system and promoting the canonical variables to operators by adding hats on them and assume the usual commutation relation $[\hat{q}(t), \hat{p}(t)] = i\hbar$, see eg. Refs. [11, 12, 24]. By defining the operators

$$\hat{a}(t) = \frac{1}{\sqrt{2\hbar\omega}}\left[m\omega\hat{q}(t) + i\hat{p}(t)\right], \tag{2.3.2a}$$

$$\hat{a}^\dagger(t) = \frac{1}{\sqrt{n\hbar\omega}}\left[m\omega\hat{q}(t) - i\hat{p}(t)\right], \tag{2.3.2b}$$

where $[\hat{a}(t), \hat{a}^\dagger(t)] = 1$, such that we can write the Hamiltonian as

$$\mathcal{H}_{\mathrm{QHO}} = \frac{1}{2}\hbar\omega\left[\hat{a}(t)\hat{a}^\dagger(t) + \hat{a}^\dagger(t)\hat{a}(t)\right] = \hbar\omega\left[\hat{a}^\dagger(t)\hat{a}(t) + \frac{1}{2}\right]. \tag{2.3.3}$$

The observant reader will already have noticed the similarities to the total energy of the radiation field Eqs. (2.1.10) and (2.1.11) and we will make use of this shortly.

In order to understand the physical meaning of the operators $\hat{a}(t)$ and $\hat{a}^\dagger(t)$ we define the eigenstates $|n\rangle$ and eigenenergies $E_n$ such that $\mathcal{H}|n\rangle = E_n|n\rangle$. Using the commutation relations of $\hat{a}(t)$ and $\hat{a}^\dagger(t)$ we then get that $\mathcal{H}\hat{a}^\dagger(t)|n\rangle = (E_n + \hbar\omega)\hat{a}^\dagger(t)|n\rangle$ and $\mathcal{H}\hat{a}(t)|n\rangle = (E_n - \hbar\omega)\hat{a}(t)|n\rangle$. We thus see that $\hat{a}^\dagger(t)|n\rangle$ and $\hat{a}(t)|n\rangle$ are eigenstates of the harmonic oscillator with respective eigenenergies $\hbar\omega$ higher or lower than $E_n$. This signifies that the QHO has equally spaced discrete eigenenergies, but since the potential and kinetic energies of the oscillator are positive quantities there must be a lowest energy level $E_0$ which we define as $\hat{a}(t)|0\rangle = 0$. If we now use the Hamiltonian, Eq. (2.3.3), we get that $\mathcal{H}|0\rangle = \frac{1}{2}\hbar\omega|0\rangle$. That is, very different from classical mechanics, the oscillator has a ground state energy

$E_0 = \frac{1}{2}\hbar\omega$, known as the vacuum energy, different from zero. From repeated use of $\mathcal{H}\hat{a}^\dagger(t)\,|n\rangle = (E_n + \hbar\omega)\hat{a}^\dagger(t)\,|n\rangle$ we get that the discrete eigenenergies of the the quantum harmonic oscillator are $E_n = \hbar\omega(n + \frac{1}{2})$. Finally, we define the operator $\hat{n}(t) = \hat{a}^\dagger(t)\hat{a}(t)$ which commutes with the Hamiltonian and thus has the same eigenstates as $\mathcal{H}$. From Eq. (2.3.3) along with $E_n$ we have that $\hat{n}(t)\,|n\rangle = n\,|n\rangle$, i.e. the operator $\hat{n}(t)$ probes the specific energy level of the state of a QHO.

In the theory of the QHO the eigenstates are eigenoscillations of the system having separate eigenenergies. In quantum optics, on the other hand, the eigenstates correspond to the number of photons in the specific mode and $\hat{n}(t)$ is thus known as the photon number operator. Furthermore, $\hat{a}^\dagger(t)$ and $\hat{a}(t)$ are known as the creation and annihilation operators since applying them on an eigenstate respectively increase and decrease the number of photons in that state, i.e.

$$\hat{a}^\dagger(t)\,|n\rangle = \sqrt{n+1}\,|n+1\rangle\,, \tag{2.3.4a}$$

$$\hat{a}(t)\,|n\rangle = \sqrt{n}\,|n-1\rangle\,. \tag{2.3.4b}$$

Furthermore, it is useful to defined the quadrature operators

$$\hat{X}(t) = \frac{1}{\sqrt{2}}\left[\hat{a}^\dagger(t) + \hat{a}(t)\right], \tag{2.3.5a}$$

$$\hat{Y}(t) = \frac{i}{\sqrt{2}}\left[\hat{a}^\dagger(t) - \hat{a}(t)\right], \tag{2.3.5b}$$

describing the real and imaginary parts of the field amplitude. The operators $\hat{a}(t)$ and $\hat{a}^\dagger(t)$ are very important in quantum optics and will reappear throughout the remaining of this thesis while $\hat{X}(t)$, $\hat{Y}(t)$, and $\hat{n}(t)$ are used extensively in this and the next two chapters.

### 2.3.2 Quantization of the Electromagnetic Field

Let us now turn to the quantization of the electromagnetic field. Similar to the QHO discussion we write the quantum-mechanical Hamiltonian of the electric field by taking the expression for the total energy of the classical field and stating that the modes are now operators. This is of course a somewhat backwards way to do quantization. The more strict mathematical way is to first derive the classical Lagrangian and identifying the canonical variables, see eg. Ref. [25], then turn the canonical variables into operators in the Lagrangian and use this to find the Hamiltonian from the Euler–Lagrange equations. See eg. Ref. [24] for a general treatment of quantization and Ref. [13] for a treatment of field quantization in dielectric structures. In the

current case the two methods though give the same results [13] and thus without further ado we simply write

$$\mathcal{H}_{\mathrm{R}} = \varepsilon_0 \sum_{\lambda} \omega_{\lambda}^2 \left[ \hat{A}_{\lambda}(t)\hat{A}_{\lambda}^{\dagger}(t) + \hat{A}_{\lambda}^{\dagger}(t)\hat{A}_{\lambda}(t) \right]. \tag{2.3.6}$$

The resemblance between the terms of the sum in $\mathcal{H}_{\mathrm{R}}$ and the QHO Hamiltonian, Eq. (2.3.3), is striking and we thus associate a quantum mechanical harmonic oscillator to each mode $\lambda$ by writing

$$\hat{A}_{\lambda}(t) = \sqrt{\frac{\hbar}{2\varepsilon_0 \omega_{\lambda}}} \hat{a}_{\lambda}(t) \tag{2.3.7}$$

such that

$$\mathcal{H}_{\mathrm{R}} = \sum_{\lambda} \hbar\omega_{\lambda} \left[ \hat{a}_{\lambda}^{\dagger}(t)\hat{a}_{\lambda}(t) + \frac{1}{2} \right]. \tag{2.3.8}$$

Since the terms in the sum are equal to the Hamiltonian for the QHO we can attribute the same relations to $\hat{a}_{\lambda}$ and $\hat{a}_{\lambda}^{\dagger}$ as of $\hat{a}$ and $\hat{a}^{\dagger}$ in Sec. 2.3.1, while all operators with different $\lambda$ commute.

Using Eq. (2.3.7) we get the vector potential operator

$$\hat{\mathbf{A}}(\mathbf{r}, t) = \sum_{\lambda} \sqrt{\frac{\hbar}{2\varepsilon_0 \omega_{\lambda}}} \left[ \hat{a}_{\lambda}(0) e^{-i\omega_{\lambda} t} \mathbf{f}_{\lambda}(\mathbf{r}) + \hat{a}_{\lambda}^{\dagger}(0) e^{i\omega_{\lambda} t} \mathbf{f}_{\lambda}^{*}(\mathbf{r}) \right], \tag{2.3.9}$$

such that the electric field operator is

$$\hat{\mathbf{E}}(\mathbf{r}, t) = -\frac{\partial \hat{\mathbf{A}}(\mathbf{r}, t)}{\partial t} = i \sum_{\lambda} \sqrt{\frac{\hbar\omega_{\lambda}}{2\varepsilon_0}} \left[ \hat{a}_{\lambda}(0) e^{-i\omega_{\lambda} t} \mathbf{f}_{\lambda}(\mathbf{r}) - \hat{a}_{\lambda}^{\dagger}(0) e^{i\omega_{\lambda} t} \mathbf{f}_{\lambda}^{*}(\mathbf{r}) \right]. \tag{2.3.10}$$

There is a tradition of writing the electric field as a sum of two contributions $\hat{\mathbf{E}}^{(\pm)}(\mathbf{r}, t)$ known as the positive- and negative-frequency components, i.e.

$$\hat{\mathbf{E}}^{(+)}(\mathbf{r}, t) = i \sum_{\lambda} \sqrt{\frac{\hbar\omega_{\lambda}}{2\varepsilon_0}} \hat{a}_{\lambda}(0) e^{-i\omega_{\lambda} t} \mathbf{f}_{\lambda}(\mathbf{r}), \tag{2.3.11a}$$

$$\hat{\mathbf{E}}^{(-)}(\mathbf{r}, t) = -i \sum_{\lambda} \sqrt{\frac{\hbar\omega_{\lambda}}{2\varepsilon_0}} \hat{a}_{\lambda}^{\dagger}(0) e^{i\omega_{\lambda} t} \mathbf{f}_{\lambda}^{*}(\mathbf{r}), \tag{2.3.11b}$$

owing to the fact that Eq. (2.3.10) resemble the positive and negative parts of a Fourier integral [26] and we will use this notation throughout the thesis.

Let us for a moment dwell on the significance of Eqs. (2.3.11). First of all we notice that the spatial mode profile and dynamics of the electric-field operators is the same as for the classical field, i.e. $e^{-i\omega_\lambda}\mathbf{f}_\lambda(\mathbf{r})$. The quantum electrodynamics description thus seems to give rise to the same interference patterns as in the classical case. This is indeed often true when considering amplitude or intensity propagation, such as for example the double-slit experiment described in Chap. 1. The difference between the classical and the quantum treatment do arise because not all operators commute. This gives rise to differences when we look at higher-order moments of the field, such as photon fluctuations, coincidences, and noise.

For simplicity we will in the rest of this chapter and the next consider stationary single-mode excitations which is often sufficient to describe quantum optical experiments in non-interacting systems [11] and we thus only need to look at the evolution of the optical operators of the individual modes using the scattering matrix approach. That is, we can write the operator of an output mode $\alpha$ as a sum of the contributions from the input modes $i$ through the scattering-matrix elements $s_{\alpha i}$, i.e. [27, 28]

$$\hat{a}_\alpha = \sum_i s_{\alpha i}\hat{a}_i. \tag{2.3.12}$$

This will be used in the next section to illustrate quantum optical phenomena on the simple scattering on a beam splitter and, more importantly, in the next chapter to describe the propagation of quantum optical states through a multiple scattering medium.

## 2.4 A Simple Example - The Beam Splitter

The key elements in most linear quantum information protocols are the phase shifter, the beam splitter (BS) and the quarter- and half-plates [29]. These elements can be described by unitary transforms having two input ports and two output ports, i.e. having two by two scattering or transmission matrices. In the following the model of the lossless BS is briefly reviewed. Then, in Sec. 2.4.1, the photon number correlation function is defined and used to illustrate quantum interference. Finally, in Sec. 2.4.2 we introduce the degree of quadrature entanglement, an entanglement measure, and use the BS as a simple illustrative example of how to obtain entangled states.

The input-output relation for a BS, illustrated in Fig. 2.3, can in general be written as

$$\hat{\mathbf{a}}_\alpha = \mathbf{S}\hat{\mathbf{a}}_i, \tag{2.4.1}$$

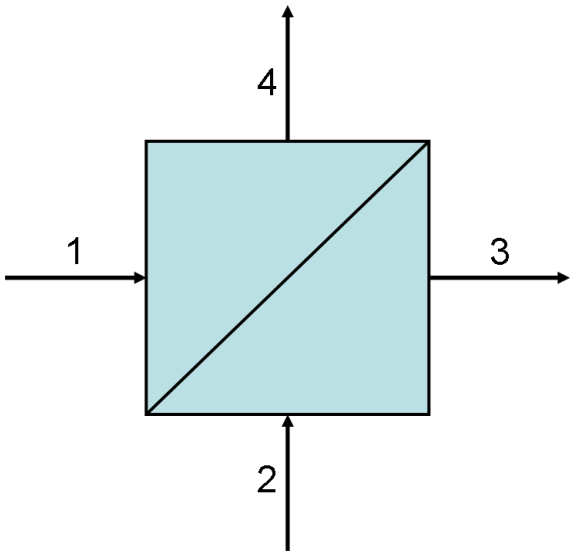


**Figure 2.3** A sketch of a beam splitter. Light is incident from mode 1 or 2 and is scattered into modes 3 and 4.

where $\hat{\mathbf{a}}_\alpha$ and $\hat{\mathbf{a}}_i$ are vectors containing the annihilation operators of the outgoing and incident fields, respectively, and $\mathbf{S}$ is the scattering matrix. In reality the BS has 4 modes, but the mode pairs 1 and 2 do not couple and likewise the modes 3 and 4. Therefore we can limit ourself to consider the 2 by 2 system consisting of one of the off-diagonal block elements in the scattering matrix. We thus take $\hat{\mathbf{a}}_i = (\hat{a}_1, \hat{a}_2)$ and $\hat{\mathbf{a}}_\alpha = (\hat{a}_3, \hat{a}_4)$ as respectively the input and output annihilation operators and the unitary scattering matrix, $\mathbf{S}$, is given by

$$\mathbf{S} = \begin{pmatrix} t_{31} & r_{32} \\ r_{41} & t_{42} \end{pmatrix}. \tag{2.4.2}$$

Due to the unitarity, the coefficients are related as $r_{32} = \sqrt{\mathcal{R}} e^{i(\phi_R + \phi_0)}$, $r_{41} = \sqrt{\mathcal{R}} e^{-i(\phi_R - \phi_0)}$, $t_{31} = i\sqrt{\mathcal{T}} e^{-i(\phi_T - \phi_0)}$ and $t_{42} = -i\sqrt{\mathcal{T}} e^{i(\phi_T + \phi_0)}$, i.e.

$$\mathbf{S} = e^{i\phi_0} \begin{pmatrix} \sqrt{\mathcal{T}} e^{i\phi_T} & \sqrt{\mathcal{R}} e^{i\phi_R} \\ \sqrt{\mathcal{R}} e^{-i\phi_R} & -\sqrt{\mathcal{T}} e^{-i\phi_T} \end{pmatrix}, \tag{2.4.3}$$

with $\mathcal{R}$ and $\mathcal{T}$ being the real-valued intensity reflection and transmission coefficients with $\mathcal{R} + \mathcal{T} = 1$ and $\phi_T - \phi_R = \pm\pi$ [30]. Since $\phi_T - \phi_R = \pm\pi$ one can eliminate $\phi_R$. This yields that the general system can be described by the scattering matrix

$$\mathbf{S} = \begin{pmatrix} -\sqrt{\mathcal{T}} e^{i\phi_I} & \sqrt{\mathcal{R}} e^{i\phi_I} \\ \sqrt{\mathcal{R}} e^{-i\phi_I} & \sqrt{\mathcal{T}} e^{-i\phi_I} \end{pmatrix}, \tag{2.4.4}$$

where $\phi_I$ is the inherent BS phase. This looks very similar to the classical treatment of a BS and indeed the scattering matrix is the same as the classical since the mode wave-function is the same as the classical as described in Sec. 2.3. The quantum character however allready appears if we consider the simplest case possible: transmission of light incident only in a single mode of the beam splitter, say mode 1. In the classical case we would then simply put the field in mode 2 to zero and not worry about this for further calculations. If one naively does the same in the quantum optical case, i.e. taking $\hat{a}_2 = 0$, then the operator commutation relations become violated, e.g. giving $[\hat{a}_3; \hat{a}_4^\dagger] = \mathcal{RT}e^{2i\phi_I} \neq 0$. This would signify that the output modes were suddenly not independent which is of course not the case since they are separate eigenmodes of the electric field. The error is easily corrected by simply including the operator of the mode where no field is incident thereby fixing the commutation relations. It is thus evident that the discrepancy is caused by the lack of inclusion of the vacuum field which, in stark contrast to classical optics, is important for describing even the simplest of scattering systems.

A valid question is now; does this have any physical implications or is it simply a mathematical artifact which demands the inclusion vacuum modes? We will answer the question in the following section by investigating the photon correlations after transmission through the beam splitter. This will further lead us to the introduction of a concept called quantum interference for which the photon correlation function is seen to be a good measure.

### 2.4.1 Spatial Correlations

Let us introduce a measure of the quantum correlations between the intensity of two distinct modes defined as the covariance of the intensity in the modes $\alpha$ and $\beta$ and normalized with respect to the respective intensities. Since the intensity of a mode is proportional to the number of photons we have, see eg. Ref. [11],

$$C_{\alpha\beta} = \frac{\langle \hat{n}_\alpha \hat{n}_\beta \rangle - \langle \hat{n}_\alpha \rangle \langle \hat{n}_\beta \rangle}{\langle \hat{n}_\alpha \rangle \langle \hat{n}_\beta \rangle} = \frac{\left\langle \hat{a}_\alpha^\dagger \hat{a}_\alpha \hat{a}_\beta^\dagger \hat{a}_\beta \right\rangle - \left\langle \hat{a}_\alpha^\dagger \hat{a}_\alpha \right\rangle \left\langle \hat{a}_\beta^\dagger \hat{a}_\beta \right\rangle}{\left\langle \hat{a}_\alpha^\dagger \hat{a}_\alpha \right\rangle \left\langle \hat{a}_\beta^\dagger \hat{a}_\beta \right\rangle}. \tag{2.4.5}$$

This corresponds to the conditional probability that, given the measurement of a photon in one mode what is the probability to measure a photon in the other. A negative value of $C_{\alpha\beta}$ thus corresponds to anti-correlated modes, i.e. that detection in one mode reduces the probability of detection in the other, and similarly $C_{\alpha\beta} > 0$ correspond to correlated modes. The limiting case of $C_{\alpha\beta} = 0$ corresponds to the two output modes being uncorrelated

and is often known as the classical limit since $C_{\alpha\beta} < 0$ is impossible for classical light [11]. In the case of a multiple-scattering medium as in the next chapter the modes correspond to two different output directions. In the present section the situation corresponds to the two output modes of the BS and the setup is known as Hanbury Brown–Twiss interferometry [31].

If we first look at the case of an arbitrary input state in mode 1 and vacuum input in mode 2, $|\psi_{\text{in}}\rangle = |\phi_1, 0_2\rangle$, such that $\hat{a}_2 |\phi_1, 0_2\rangle = 0$, then we obtain

$$\begin{aligned}\langle \hat{n}_3 \hat{n}_4 \rangle &= \mathcal{R}\mathcal{T} \left[ \langle \hat{n}_1^2 \rangle - \left\langle \hat{a}_1 \hat{a}_2 \hat{a}_2^\dagger \hat{a}_1 \right\rangle \right] \\ &= \mathcal{R}\mathcal{T} \left[ \langle \hat{n}_1^2 \rangle - \left\langle \hat{a}_1 (\hat{a}_2^\dagger \hat{a}_2 + 1) \hat{a}_1 \right\rangle \right] \\ &= \mathcal{R}\mathcal{T} \left[ \langle \hat{n}_1^2 \rangle - \langle \hat{n}_1 \rangle \right]. \end{aligned} \tag{2.4.6}$$

Notice that the included calculations, even though they are trivial, constitute prime examples of the difference between classical and quantum theory. In classical theory everything commutes and we would obtain $\langle \hat{n}_3 \hat{n}_4 \rangle = \mathcal{R}\mathcal{T} \langle \hat{n}_1^2 \rangle = \langle \hat{n}_3 \rangle \langle \hat{n}_4 \rangle$ such that, no matter the type of input state in mode 1 we would have uncorrelated photon output. In quantum optics on the other hand we need to take the effect of the vacuum field and its commutation relation into account. As we see from the first to the second line the commutation relation of the vacuum field adds a contribution to the correlation similar to the introduction of an extra photon and is thus identified as a contribution of vacuum fluctuations to spatial correlations.

We will now take two examples of specific input states. If we first consider a so-called coherent state (or Glauber state) of amplitude $a_1$ as the input state, $|\psi_{\text{in}}\rangle = |a_1, 0_2\rangle$, such that $\hat{a}_1 |a_1, 0_2\rangle = a_1 |a_1, 0_2\rangle$, then we readily obtain $\langle \hat{n}_3 \hat{n}_4 \rangle = \mathcal{R}\mathcal{T} |a_1|^4 = \langle \hat{n}_3 \rangle \langle \hat{n}_4 \rangle$ giving exactly the classical result of uncorrelated photon statistics of the output modes. This is because the coherent state is the quantum mechanical counterpart of classical light. If, on the other hand, we consider an incident $n_1$ photon Fock state, $|\psi_{\text{in}}\rangle = |n_1, 0_2\rangle$, such that $\hat{n}_1 |n_1, 0_2\rangle = n_1 |n_1, 0_2\rangle$, then we get $\langle \hat{n}_3 \hat{n}_4 \rangle = \mathcal{R}\mathcal{T} n_1 (n_1 - 1)$, which for $n_1 = 1$ shows the striking result $\langle \hat{n}_3 \hat{n}_4 \rangle = 0$. This has the clear physical interpretation that when only a single photon is incident, then measuring a photon in one mode will leave it impossible to measure a photon in the other mode.

In order to identify what is often meant by quantum interference (QI) we will consider the case when single-photon Fock states are incident in each input mode, i.e. $|\psi_{\text{in}}\rangle = |1_1, 1_2\rangle$, giving $\langle \hat{n}_3 \hat{n}_4 \rangle = (\mathcal{T} - \mathcal{R})^2$. For a symmetric BS, $\mathcal{T} = \mathcal{R} = \frac{1}{2}$, we see that the two photons will interfere and leave the BS through the same mode. Thus it is impossible to make a

coinciding measurement of photons in the two output modes, that is, either both photons exit in mode 3 or in mode 4. This effect is called QI and stems from the fact that the two photons are indistinguishable quantum particles. Therefore the photon probability amplitudes of the two photon paths corresponding to the photons exiting separately must be added before forming the absolute value in order to get the probability outcome. Due to the phase shift of reflection and transmission the two paths are exactly $\pi$ out of phase and thus cancel [12]. It might not seem surprising that photons interfere since we are perfectly used to the interference of light as waves, but one should remember that when considering photons we are considering the "particle" properties of light for which interference might seem impossible.

For reference, we note that for general Fock states incident in the two BS modes, the correlation function is always less than or equal to zero since detection of a photon in one of the output modes will decrease the number of photons in the system and thus the two output modes will be anti-correlated or at most uncorrelated. Peculiarly this is not the case for transmission through multiple scattering media as we will find in Chap. 3, but first we will introduce an entanglement measure and illustrate its properties on the simple BS.

### 2.4.2 Degree of Quadrature Entanglement

Finally, we introduce a measure for continuous-variable quantum entanglement between the quadratures of two different modes and illustrate its properties with the example of a BS. The measure we will use is the Duan–Simon criterion determining the degree of separability of two different continuous-variable operators [32, 33]. We will use the quadrature operators as our continuous-variable operators for which the degree of entanglement is quantified in terms of the quadrature variance product (QVP) [34]

$$\varepsilon_{\alpha\beta} = \Delta(\hat{X}_\alpha - \hat{X}_\beta)^2 \Delta(\hat{Y}_\alpha + \hat{Y}_\beta)^2. \tag{2.4.7}$$

This product determines the degree of separability of the quadratures of two distinct modes $\alpha$ and $\beta$. Physically, the QVP determines the ability to predict a noise measurement in mode $\beta$ given the result of a noise measurement on mode $\alpha$, and for $\varepsilon_{\alpha\beta} < 1$ ($> 1$) the outcome is predictable below (above) the quantum noise limit, $\varepsilon_{\alpha\beta} = 1$. Thus $\varepsilon_{\alpha\beta} < 1$ implies that the quantum state of the two output modes $\alpha$ and $\beta$ is unseparable, i.e. entangled [34]. Furthermore, if $\varepsilon_{\alpha\beta} < \frac{1}{4}$ the states are called EPR entangled [35] and obey the very strict entanglement criteria introduced by Bell [36] making them especially useful for quantum information processing [29, 35].

The QVP will be used in the next chapter to investigate the possibility of creating entangled states between two separate modes by interference of squeezed states on a multiple scattering medium. In this section we will illustrate the phenomena using the example of a BS. First of all, it is easy to show (see App. A.1) that mixing any coherent states, i.e. classical laser light, on the BS simply gives a QVP equal to unity corresponding to the quantum noise limit. This is because the BS is a linear device and thus cannot create quantum effects out of classical states. Let us instead take a look at the effect of mixing two quadrature squeezed states on a BS. For illustrative purposes we will look at the simple case of a symmetric phase-less BS and squeezed states with equal squeezing amplitude, $s$, while a more general treatment is found in App. A.1. The phase-less symmetric BS and equal amplitude squeezed states give us

$$\Delta(\hat{X}_3 - \hat{X}_4)^2 = \sin^2\left(\frac{\theta_1}{2}\right) e^{2s} + \cos^2\left(\frac{\theta_1}{2}\right) e^{-2s}, \tag{2.4.8a}$$

$$\Delta(\hat{Y}_3 + \hat{Y}_4)^2 = \cos^2\left(\frac{\theta_2}{2}\right) e^{2s} + \sin^2\left(\frac{\theta_2}{2}\right) e^{-2s}, \tag{2.4.8b}$$

with $\theta_i$ being the squeezing phase of the state incident in mode $i$. We note that $s = 0$, corresponding to a coherent state, again gives the quantum noise limit as it should. Let us instead play around with the squeezing phases by noticing that for $\theta_1 = 0$, we have $\Delta(\hat{X}_3 - \hat{X}_4)^2 = e^{-2s}$, while if $\theta_1 = \pi$, then $\Delta(\hat{X}_3 - \hat{X}_4)^2 = e^{2s}$, and opposite for $\theta_2$ and $\Delta(\hat{Y}_3 + \hat{Y}_4)^2$. We thus get that if $\theta_1 = \theta_2 = 0$ then $\varepsilon_{3,4} = 1$ again corresponding to the quantum noise limit. If, instead, the two states have $\theta_1 = 0$ and $\theta_2 = \pi$ then $\varepsilon_{3,4} = e^{-4s}$ which is always below unity and thus the two output modes are mutually entangled whereas for $\theta_1 = \pi$ and $\theta_2 = 0$ we have $\varepsilon_{3,4} = e^{4s}$ and the two outputs are not entangled. Furthermore, for $\theta_1 = 0$ and $\theta_2 = \pi$ it is possible to achieve EPR entanglement by cranking the squeezing strength up to above $s > \frac{1}{2}\ln(2)$. It is thus possible to create entangled states by mixing two squeezed states on the simplest imaginable scatterer. We will see in the next chapter that this also holds for for a more complicated system of scatterers.

## 2.5 Chapter Summary

In this chapter we introduced and reviewed some of the theoretical concepts of multiple scattering and quantum optics which serve as the background of the new results of the following chapters.

We began the chapter by revisiting classical optics where we found the energy of the classical electrodynamics in terms of the vector potential. We

further introduced the Green function as a means to investigate multiple scattering at a microscopic level, which we will find useful in Chaps. 5 and 6. Then we introduced the scattering matrix which in connection with random-matrix theory is able to describe multiple scattering at a macroscopic level which we will use in Chaps. 3 and 4.

We then turned our attention to quantum optics. We first carried out the quantization of the electromagnetic field in an arbitrary dielectric environment which will be used throughout the thesis, but will become especially useful in Chap. 5. Then we introduced the photon-number correlation function and the degree of continuous-variable entanglement as measures for quantum interference and entanglement, respectively. Finally, we illustrated the formalism and phenomena by analyzing the scattering of quantum optical states off one of the simplest scatterers imaginable, the beam splitter.

# 3

# Quantum Optics in Elastic Scattering Waveguides

In this chapter, we use the scattering matrix theory described in the previous chapter combined with results from random matrix theory. This let us investigate quantum interference (QI) induced by combining an arbitrary number of independent quantum states in a random multiple scattering medium in the mesoscopic regime. We identify the role of QI on the degree of photon number correlations between two transmission paths through the medium and the degree of continuous variable entanglement. Surprisingly QI of photons is found to survive after averaging over all configurations of disorder, i.e. the induced quantum correlations have deterministic character despite the underlying random multiple scattering processes. We furthermore discuss the feasibility of experimentally verifying our theoretical predictions. The chapter is primarily built on Paper J2; J. R. Ott, *et al.*, Phys. Rev. Letters **105**, 090501 [37], which is a generalization of the work in Ref. [38].

We begin in Sec. 3.1 by describing the calculation of light propagation through a multiple scattering medium using the scattering matrix formalism. Then in Sec. 3.2 we illustrate the existence of quantum interference and creation of continuous variable entanglement induced by multiple scattering in a single realization of disorder. Finally, in Sec. 3.3 we show that interestingly, some of the found quantum optical phenomena survive even after ensemble averaging.

## 3.1 Discrete-Mode Theory of Multiple Scattering

Let us introduce the model for propagation of quantized light through a linear, elastic, multiple scattering medium of length $L$ and transport mean free path $\ell$, see Fig. 3.1. We apply the scattering matrix for the propagation of light and use random matrix theory on the scattering elements as described

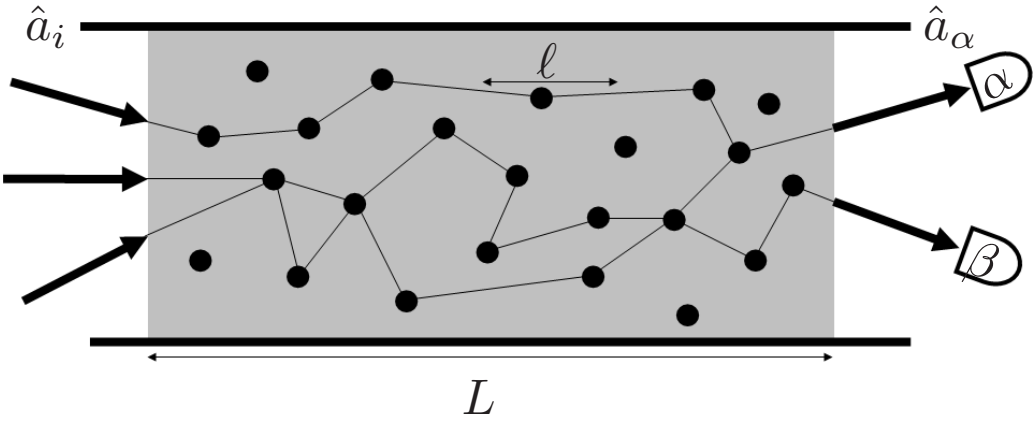


**Figure 3.1** (color online). Sketch of propagation through a disordered waveguide of length $L$ and transport mean free path $\ell$. Quantized light is incident to the left and the correlations between two output modes on the right are analyzed. The operators $\hat{a}_i$ and $\hat{a}_\alpha$ correspond to the annihilation operators of modes $i$ and $\alpha$, where Roman and Greek subscripts denote input and output modes respectively. The correlations between the two different output modes $\alpha$ and $\beta$ are analyzed. Figure from Paper J2.

in Chap. 2. The approach describes effectively a quasi-1D model of an $N$-mode waveguide, but is known also to accurately predict propagation in 3D slab geometries [7]. We relate the photon annihilation operators $\hat{a}_\alpha$ ($\hat{a}_i$) of output (input) modes $\alpha$ ($i$) by $\hat{a}_\alpha = \sum_i s_{\alpha i}\hat{a}_i$, where the summation is over all $N$ possible input modes at each end of the waveguide and $s_{\alpha i}$ denotes the complex scattering matrix element. Experimentally, such a system could, e.g., be realized in titania powder samples, see next Chap. 4, or disordered photonic crystal waveguides [8, 39]. It is important to note that, as with the beamsplitter in Sec. 2.4, in the quantum optical description it is necessary to include all modes, even those with vacuum input, in order to obtain correct physical results.

As described in Chap. 2 a measure of QI is the two-channel photon correlation function

$$C_{\alpha\beta} = \frac{\langle \hat{n}_\alpha \hat{n}_\beta \rangle - \langle \hat{n}_\alpha \rangle \langle \hat{n}_\beta \rangle}{\langle \hat{n}_\alpha \rangle \langle \hat{n}_\beta \rangle}. \tag{3.1.1}$$

The brackets denote quantum mechanical expectation values and $\hat{n}_\alpha = \hat{a}_\alpha^\dagger \hat{a}_\alpha$ is the output photon number operator. The degree of entanglement is quantified in terms of the quadrature variance product (QVP) [34]

$$\varepsilon_{\alpha\beta} = \Delta(\hat{X}_\alpha - \hat{X}_\beta)^2 \Delta(\hat{Y}_\alpha + \hat{Y}_\beta)^2, \tag{3.1.2}$$

where $\hat{X}_\alpha = \frac{1}{\sqrt{2}}(\hat{a}_\alpha^\dagger + \hat{a}_\alpha)$ and $\hat{Y}_\alpha = \frac{i}{\sqrt{2}}(\hat{a}_\alpha^\dagger - \hat{a}_\alpha)$ are the quadrature operators. The QVP determines the ability to predict a measurement in mode $\beta$ given

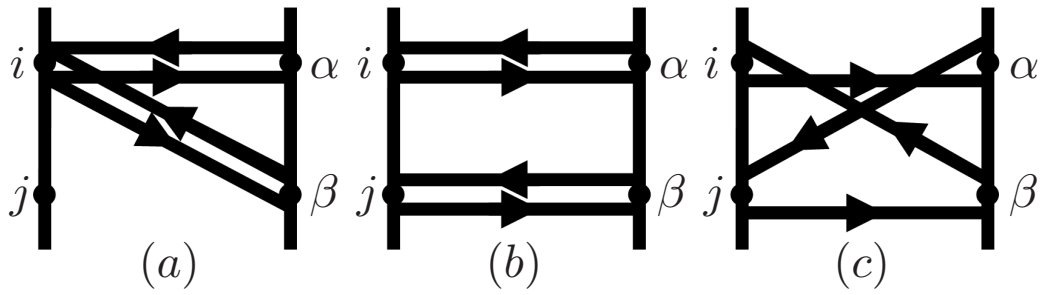


**Figure 3.2** A diagrammatic representation of three terms of the form $t^*_{\alpha i}t^*_{\beta j}t_{\beta k}t_{\alpha l}\left\langle \hat{a}^\dagger_i\hat{a}^\dagger_j\hat{a}_k\hat{a}_l\right\rangle$. Diagrams ($a$) and ($b$) involve only intensity transmission of the input modes while ($c$) shows quantum interference between two input states. The three diagrams are the only ones that survive ensemble averaging. Figure from Paper J2.

the result of a measurement on mode $\alpha$, and for $\varepsilon_{\alpha\beta} < 1$ ($> 1$) the outcome is predictable below (above) the quantum noise limit. Thus, $\varepsilon_{\alpha\beta} < 1$ implies that the quantum state of the two output modes $\alpha$ and $\beta$ is unseparable, i.e. entangled [34].

Since we consider transmission we only obtain transmission scattering matrix elements, $t_{\alpha i}$, in our calculations. Eqs. (3.1.1) and (3.1.2) can conveniently be evaluated diagrammatically, by representing the propagator $t_{\alpha i}\hat{a}_i$ by an arrow connecting input mode $i$ to output mode $\alpha$. Since the scattering matrix is unitary, $t^*_{\alpha i}\hat{a}^\dagger_i$ represents the time-reversed path. E.g. considering two input modes, evaluating Eq. (3.1.1) yields $2^4$ different terms of the form $t^*_{\alpha i}t^*_{\beta j}t_{\beta k}t_{\alpha l}\left\langle \hat{a}^\dagger_i\hat{a}^\dagger_j\hat{a}_k\hat{a}_l\right\rangle$. Three typical diagrams are shown in Fig. 3.2. As an example, the contribution from diagram ($a$) is $|t_{\alpha i}|^2|t_{\beta i}|^2\left\langle :\hat{n}^2_i:\right\rangle$, where $\langle :\cdot:\rangle$ denotes normal ordering. The diagrams can be classified into intensity and interference diagrams. The former corresponds to incoherent addition of the intensities associated with the different propagation paths through the medium, as it is the case for the diagrams ($a$) and ($b$). The latter gives rise to QI between the input states and diagram ($c$) is such an example. We note that all additional diagrams not shown in Fig. 3.2 are interference diagrams and only the three shown diagrams survive ensemble averaging.

## 3.2 Single Realization of Disorder

For diffusive transport the intensity transmission coefficients are exponentially distributed while the phase is uniformly distributed [40], i.e. the system can be simulated exactly. To be specific, we choose a waveguide of $N = 10^2$

so that the average single channel transmission is $\tau = g/N^2 = 1/300$ [1], where $g$ is the normalized average conductance. We keep output mode $\alpha$ fixed while varying output mode $\beta$ in a 10 by 10 grid to represent spatial wavevectors in the transverse plane ($k_x$, $k_y$).

Similar to the discussion of the BS in Sec. 2.4, we start out by evaluating the two-channel photon correlation function between the two output modes, $\alpha$ and $\beta$, using Fock states $|n_i\rangle$ as input. By illuminating only a single input channel with a two-photon Fock state $|2\rangle$ we get that $C_{\alpha\beta} = -1/2$ for all modes $\alpha$ and $\beta$, independent of the realization of disorder. For single photons incident in two different input modes $|1,1\rangle$ the spatial photon correlations fluctuate between -1 and 0, see Fig. 3.3 ($a$). This is a manifestation of QI in a speckle pattern as observed in Ref. [41].

Next, we evaluate $\varepsilon_{\alpha\beta}$ for two quadrature-squeezed input states $|\zeta_i\rangle = \exp[\frac{1}{2}\zeta_i^*\hat{a}^2 - \frac{1}{2}\zeta_i(\hat{a}^\dagger)^2]\,|0\rangle$, where $\zeta_i = s_i e^{i\theta_i}$ contains the squeezing amplitude, $s_i$, and phase, $\theta_i$, [11]. We investigate two orthogonally oriented squeezed

[1] For diffusive transport the average single channel transmission is $g \approx N/(1 + L/\ell)$ [7] and $s = L/\ell \approx 2$ [23] giving an average amplitude transmission of $\tau = 1/300$ for $N = 10^2$.

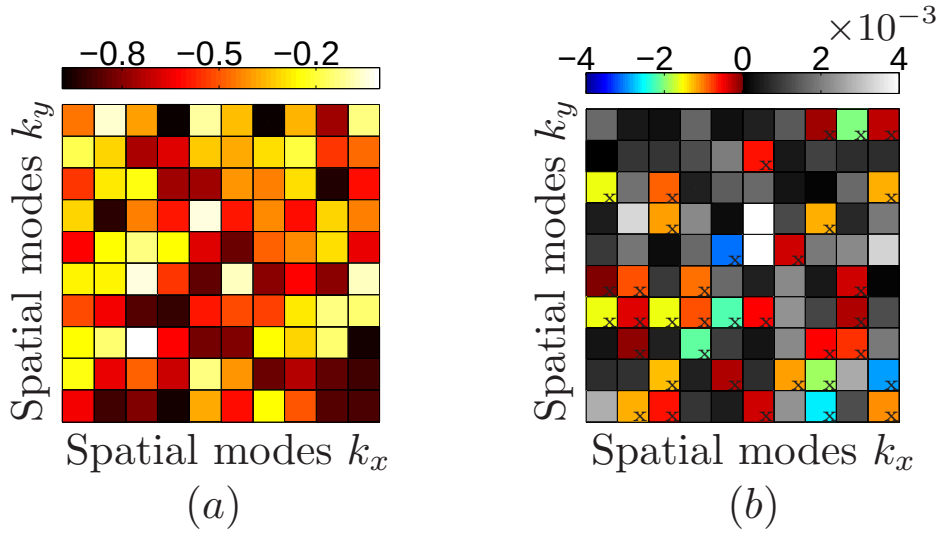


**Figure 3.3** (color online). ($a$) The 2-photon correlation $C_{\alpha\beta}$ for two single-photon Fock input states, $|1,1\rangle$, showing large fluctuations due to quantum interference. ($b$) The degree of entanglement $\log_{10}(\varepsilon_{\alpha\beta})$ for the two quadrature squeezed input states described in the text, where the gray-scale corresponds to non-entangled states $(\log_{10}(\varepsilon_{\alpha\beta}) \geq 0)$ while the colored areas with crosses display the entangled states $(\log_{10}(\varepsilon_{\alpha\beta}) < 0)$. ($a$) and ($b$) are obtained with the same realization of disorder for diffusive transport, where the phase is uniformly distributed and the intensity transmission coefficients obey the distribution $P(|t_{\alpha i}|^2) = \exp(-|t_{\alpha i}|^2/\overline{|t_{\alpha i}|^2})$ with $\overline{|t_{\alpha i}|^2} = \tau$ the average single-channel transmission [40]. Figure from Paper J2.

beams, i.e. $\theta_1 = 0$ and $\theta_2 = \pi$ and choose both incident squeezed beams to have $s_i = 0.15$ corresponding to experimentally obtainable parameters [42]. For the squeezed states incident in two different arbitrary modes we evaluate $\varepsilon_{\alpha\beta}$ between the two different output modes $\alpha$ and $\beta$. This is shown in Fig. 3.3 $(b)$, which visualizes that pairwise entanglement ($\varepsilon_{\alpha\beta} < 1$) can be induced by multiple scattering. By changing the squeezing phases of the input states the modes that display entanglement change. From knowledge of the transmission matrix one could thus specify the modes between which the entanglement should occur by changing the phases of the squeezed beams. This could potentially be achieved with the recent scheme to measure the complex transmission matrix for light propagation through a disordered medium [43]. The inherent ability of a multiple scattering medium to mix many modes shows the scalability of the approach of potential use in quantum information processing.

## 3.3 Ensemble Averaged Phenomena

Let us next consider the effects of QI after ensemble averaging. The averaged amplitude transmission coefficients are given by [16]

$$\overline{t^*_{\alpha i} t_{\alpha j}} = \tau \delta_{ij}, \tag{3.3.1a}$$

$$\overline{t^*_{\alpha i} t^*_{\beta j} t_{\beta k} t_{\alpha l}} = \tau^2 \left( C_1 \delta_{il} \delta_{jk} + C_2 \delta_{ik} \delta_{jl} \right), \tag{3.3.1b}$$

with $C_1$ and $C_2$ the short and long-range correlation functions respectively, and the bar denotes ensemble averaging. After the ensemble averaging only loop-type diagrams survive, i.e. only those shown in Fig. 3.2. The values of diagrams $(a)$ and $(b)$ are proportional to $C_1 + C_2$ and $C_1$ respectively, while diagram $(c)$ is proportional to $C_2$. This can be intuitively understood since $C_1$ expresses the intensity fluctuations in a single speckle spot, while $C_2$ is related to the intensity correlations between two speckles as explained in section 2.2. Therefore, since diagram $(a)$ corresponds to light incident in the same mode, $i$, passing through the medium exiting in two different modes, $\alpha$ and $\beta$. The term thus contributes to both the single speckle fluctuation, $C_1$, and the two speckle correlation, $C_2$. Diagram $(b)$ on the other hand only involves intensity propagation from one incident mode to another and thus only the single speckle fluctuations is of importance. At last, diagram $(c)$ displays the only QI term that survives ensemble averaging. From the values of $C_2$ and the normalized average conductance $g$, we define the transitions from the quasi-ballistic to the weakly disordered regime ($C_2 = 0$) and from the weakly disordered to the localized regime ($g = 1$). The mesoscopic regime is defined as the regime in which two speckle spots are correlated

after ensemble averaging ($C_2 > 0$). The values of $C_1$ and $C_2$ depend on the number of modes $N$ and the degree of disorder, which is contained in $s = L/\ell$ and $g^{-1}$. [2]

We define the ensemble-averaged two-channel correlation function as the ensemble average of the nominator and denominator separately, i.e.

$$\overline{C}_{\alpha\beta} = \frac{\overline{\langle \hat{n}_\alpha \hat{n}_\beta \rangle} - \overline{\langle \hat{n}_\alpha \rangle \langle \hat{n}_\beta \rangle}}{\overline{\langle \hat{n}_\alpha \rangle \langle \hat{n}_\beta \rangle}}. \tag{3.3.2}$$

Notice how this differs from the definition of the classical multiple scattering correlation function Eq. (2.2.13). With the current definition the classical states trivially give $\overline{C}_{\alpha\beta} = 0$, making a clear distinction between classical and quantum effects. By this definition the ensemble average gives

$$\overline{C}_{\alpha\beta} = \frac{(C_1 + C_2)\left[\left(\sum_i \langle \hat{n}_i \rangle\right)^2 + \sum_i (\Delta \hat{n}_i^2 - \langle \hat{n}_i \rangle)\right]}{C_1\left(\sum_i \langle \hat{n}_i \rangle\right)^2 + C_2\left(\sum_i \langle \hat{n}_i \rangle^2 + 2\sum_{i,j>i} |\left\langle \hat{a}_i^\dagger \hat{a}_j \right\rangle|^2\right)} - 1, \tag{3.3.3}$$

while the ensemble averaged QVP is

$$\overline{\varepsilon}_{\alpha\beta} = 1 + 4\tau \sum_i \Delta \hat{a}_i^\dagger \hat{a}_i + 4\tau^2 \left[C_1\left(\sum_i \Delta \hat{a}_i^\dagger \hat{a}_i\right)^2 + C_2 \sum_{i,j} \Delta \hat{a}_i^\dagger \hat{a}_j \Delta \hat{a}_j^\dagger \hat{a}_i\right]. \tag{3.3.4}$$

In Fig. 3.4, $\overline{C}_{\alpha\beta}$ and $\log_{10}(\overline{\varepsilon}_{\alpha\beta})$ are plotted versus $s$. For Fock input states the $s$ dependence of $\overline{C}_{\alpha\beta}$ is a direct measure of QI since disregarding the QI terms implies that $\overline{C}_{\alpha\beta}$ only depends on the total number of input photons. First, consider having two photons incident in only one mode, $|2\rangle$, then $\overline{C}_{\alpha\beta} = -\frac{1}{2}$ independent of $s$. With the photons in two different input modes, $|1,1\rangle$, the correlations on the contrary depend on $s$. Only at the transition to the mesoscopic regime ($C_2 = 0$) we have $\overline{C}_{\alpha\beta} = -\frac{1}{2}$ independent of wether the light is incident in one or two modes. This value corresponds to the correlation between two equally probable output modes for two classical

[2] The values of $C_1$ and $C_2$ are independent of $N$ on the transition between the quasi-ballistic and the mesoscopic regimes, $s \approx 2$, and tend toward the same value far into the localized regime, $g^{-1} \ll 1$ [23]. The values of $C_1$ and $C_2$ has qualitatively the same behaviors versus disorder in the various regimes for different $N$. The calculation of $g$, $C_1$, and $C_2$ is discussed in Refs. [16] and [23] and references therein.

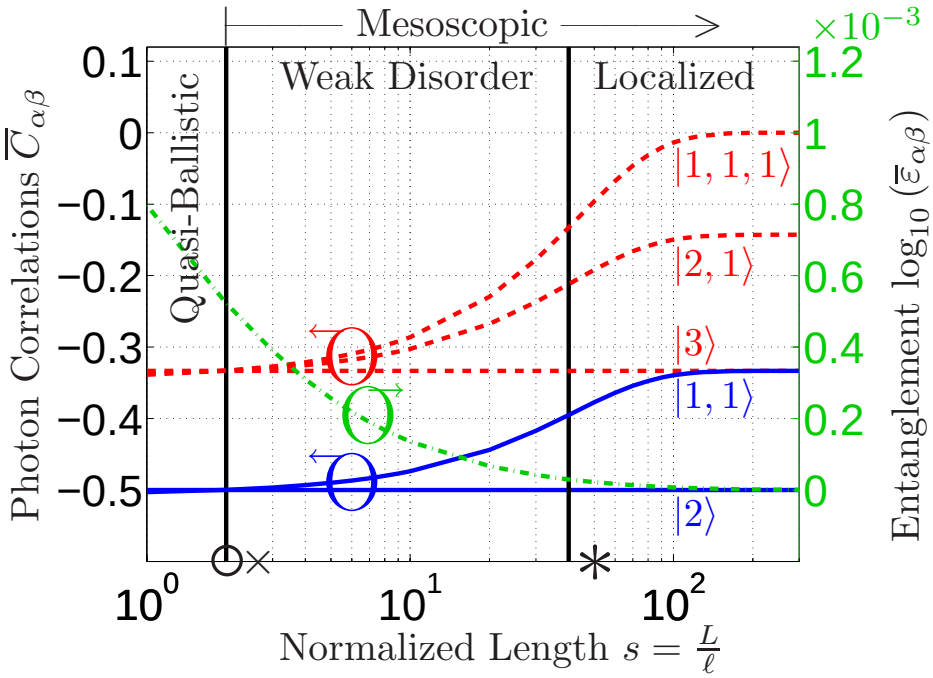


**Figure 3.4** (color online). The ensemble averaged 2-channel photon correlations, $\overline{C}_{\alpha\beta}$ and the degree of entanglement $\log_{10}(\overline{\varepsilon}_{\alpha\beta})$ versus $s = L/\ell$ for $N = 50$. Solid blue curves show $\overline{C}_{\alpha\beta}$ for Fock input states with a total of two photons and dashed red curves are for three photons. The difference in $\overline{C}_{\alpha\beta}$ between having one and more input states is due to quantum interference. The green dash-dotted line shows $\log_{10}(\overline{\varepsilon}_{\alpha\beta})$ for the two quadrature squeezed input states described in the text. The vertical line at $s = 2$ indicates the crossover from the quasi-ballistic to the mesoscopic regime $(C_2 = 0)$ and the one at $s \approx 40$ shows the transition to the localized regime $(g = 1)$. The symbols $\circ$, $\times$, and $*$ on the abscissa correspond to the experimental structures studied in Refs. [41], [42], and [39], as discussed further in the main text. Figure from Paper J2.

non-interacting particles. This is due to two simple reasons: (i) the ensemble averaging makes all output modes equally possible and (ii) transport is diffusive and thus all interference effects are washed out. As disorder is increased, $\overline{C}_{\alpha\beta}$ increases signifying that the probability that the two photons arrive at two different positions increases although remaining anti-correlated $(\overline{C}_{\alpha\beta} < 0)$. The increased correlations saturate in the localized regime since $C_2$ tends towards $C_1$ [23]. The variations in $\overline{C}_{\alpha\beta}$ can be attributed to QI amongst the input channels, which causes the photons to anti-bunch. The anti-bunching of photons originates from the correlations between different modes induced in the mesoscopic, and especially the localized, regime. Investigating three photon Fock states shows that having more incident modes increases the effects of QI. For $|1,1,1\rangle$, $\overline{C}_{\alpha\beta}$ tends towards zero in the localized regime signifying that the output modes become uncorrelated. If the

number of input modes is increased further the output modes will become correlated ($\overline{C}_{\alpha\beta} > 0$) in the localized regime. This means that detection of a photon in one mode on average increases the probability of the detection of a photon in another mode, which is in striking contrast to the behavior of diffusive transport of Fock states. Having single-photon states in $n$ input modes and letting $n$ go to infinity makes $\overline{C}_{\alpha\beta}$ approach unity far into the localized regime, which is the value obtained for thermal light. The variation of $\overline{\varepsilon}_{\alpha\beta}$ with $s$ is plotted as the green curve in Fig. 3.4 for the same quadrature-squeezed inputs as for the single realization of Fig. 3.3. In the mesoscopic regime both $C_1$ and $C_2$ are positive and thus $\overline{\varepsilon}_{\alpha\beta} \geq 1$. The value of $\overline{\varepsilon}_{\alpha\beta}$ approaches unity in the localized regime since the transmission decreases so that contributions from vacuum fluctuations dominate. Continuous variable entanglement in the transmission is therefore on average predicted to vanish after ensemble averaging.

Finally, we address the experimental feasibility of the proposal. In Fig. 3.4 we indicate the position of three existing multiple scattering structures from the literature, where the number of modes $N$ has been scaled to match the value used in the calculations. Ref. [41] concerns transmission through two scattering surfaces, which mimics a multiple scattering medium with $s = 2$. This corresponds to the diffusive limit where QI will be present in the speckle pattern but not survive ensemble averaging. In Ref. [42] a titania powder is used with sample length $L = 20\,\mu$m and transport mean free path $\ell \approx 0.9\,\mu$m, which corresponds to the mesoscopic regime of $s > 2$. Such sample support a large number of modes ($N > 10^3$) and thus $g \gg 1$, which means that this type of sample is in the weakly disordered regime where QI effects are modest, cf. Fig. 3.4. This illustrates the importance of using multiple scattering samples supporting only few modes in order to observe QI. A disordered multimode photonic crystal waveguide is exactly such a system and for $N \approx 5$ together with the typical experimental parameters of $\ell \approx 20\,\mu$m and $L = 100\,\mu$m [39] gives rise to sizeable QI effects that will be observable in an experiment, cf. Fig. 3.4.

## 3.4 Chapter Summary

In this chapter we investigated the impact of interfering multiple quantum optical states transmitted through a random multiple scattering medium in the mesoscopic regime.

First we analyzed quantized light propagation through a single realization of a multiple scattering medium. We predicted that it was possible to induce continuous variable entanglement between different directions by interfering squeezed light beams on a multiple scattering medium. Like in the case of the

simple beam splitter of Chap. 2 the degree of entanglement could be varied by changing the squeezing phase of the squeezed beams. Interestingly, this shows a possible way to create directed entanglement simply by interfering beams of squeezed light on a scattering medium. We further found that mixing of photon states from different directions on the multiple-scattering medium showed large fluctuations in the photon correlations between different output directions. These fluctuations are not present when only a single direction is illuminated, since they are caused by quantum interference.

Next, we analyzed the average effects of quantum optical multiple scattering. We theoretically predicted that surprisingly parts of the quantum interference of light survives multiple scattering. By calculating the 2-channel photon correlation function in the case of Fock input states, we showed that the difference between one and several input modes for a fixed number of total photons is a direct measure of quantum interference. We predicted 2-channel photon anti-bunching in the mesoscopic regime that increases with the degree of disorder. Then, we found that continuous-variable entanglement induced by multiple scattering of squeezed light that was predicted to show up in single realizations of disorder, vanishes after ensemble averaging.

Finally, the experimental feasibility of the proposal was investigated based on existing multiple-scattering samples from the literature, and we found that multimode disordered photonic crystal waveguides are promising candidates for an experimental demonstration of quantum interference. In the following chapter we will analyze a multiple scattering experiment of a quantum state of light.

# 4

# Experimental Realization of Elastic Quantum Optical Multiple Scattering

In this chapter the theoretical analysis of the experimental study of the quantum properties of multiple scattered quantized light in Ref. [42] is presented. We start out with Sec. 4.1 where the specific experiment is introduced. Then in Sec. 4.2 the theoretical description as presented in the last chapters is modified slightly in order to describe a way to experimentally measure the quantum optical properties of light after multiple scattering. The chapter is mainly based on Paper J1 which is a longer presentation of the experimental results of Ref. [42]. The theoretical description in this chapter has furthermore led to the erratum Ref. [44].

## 4.1 Experiment

In the following the experiment performed by Smolka *et al.* [42] is briefly presented. First, the purpose of the original experiment is stated and then the experimental setup is sketched. The experimental details can be found in Ref. [42] and Paper J1.

The purpose of Ref. [42] was to experimentally verify the theoretical prediction that the quantum nature of light persists even after the light has propagated through a multiple scattering medium. This prediction was first presented by Lodahl *et al.* in Ref. [38] which deals with quantum states incident from only one direction and is thus a special case of the work described in the previous chapter and Paper J2. As described, after propagation through the multiple scattering medium the quantum nature of the light is predicted to be observable in the photon number correlations between two distinct output directions. In the special case of only one incident light beam, the ensemble averaged spatial correlations between two output directions was furthermore found in Ref. [38] to be related to the photon statistics of the

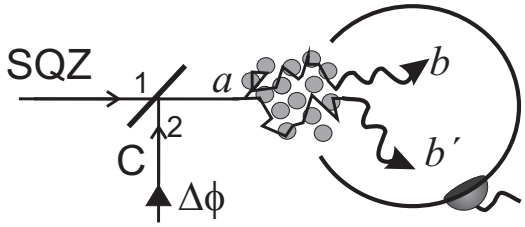


**Figure 4.1** Illustration of multiple scattering leading to spatial quantum correlations. The nonclassical light source that is used in the experiment is created by overlapping a squeezed vacuum light beam (SQZ) and a coherent light beam (C) on a beam splitter with two input ports, 1 and 2, respectively. The relative phase, $\Delta\phi$, between C and SQZ can be tuned continuously. The resultant light beam in direction $a$ is incident onto a medium with randomly distributed scatterers. Light is split into a multitude of different trajectories and the number of photons exiting the medium in a specific direction, $b$, can be correlated with the number of photons in another direction, $b'$, to a degree dependent on the quantum state of the illuminating light source. In the diffusive regime the spatial quantum correlation function can be determined from total transmission quantum noise measurements. A similar experimental scheme is applied for reflection measurements. (Figure from Paper J1.)

ensemble averaged total transmitted or reflected light. The experiment thus aims to indirectly measure the spatial photon correlation function through measurement of the photon fluctuations of the total transmitted or reflected light.

A schematic illustration of the experimental setup is displayed in Fig. 4.1. A bright squeezed state of light is created by overlapping a coherent state and a squeezed vacuum state on a beam splitter. By adjusting the relative phase between the squeezed vacuum and the coherent state the photon statistics of the bright squeezed state can be tuned continuously between sub-Poissonian and super-Poissonian corresponding to the purely quantum or classical regime [11]. The resultant bright squeezed state is then directed upon a multiple scattering medium, and the total transmitted or reflected light is collected. Notice that according to the previous chapter this setup actually also creates a multitude of mutually entangled output directions. The photon fluctuations associated with the total transmitted or reflected light are then recorded by measuring the time-dependent photo-current of the detectors. The original theoretical analysis, like in the previous chapter, was carried out using a discrete mode description and thus does not describe time dependent measurements. We thus need to introduce a continuous mode description to fully describe the experiment. This will lead to slightly different results than the discrete mode theory.

## 4.2 Continuous-Mode Theory of Multiple Scattering

In this section, we introduce a continuous-mode quantum theory that is directly applicable to the quantum noise measurements of Ref. [42].

In the experiment, the measurement is not time-independent as was implicitly assumed in the previous chapter. Instead it is necessary to consider the excitation of an infinite range of modes even when the light beam is made up from contributions of modes whose wavevectors all point in the same direction [11]. We thus define a time-dependent unidirectional annihilation operator as

$$\hat{a}_a(t) = \int \mathrm{d}\lambda \; p(\lambda)\hat{a}_{a,\lambda}(0)e^{-i\omega_{a,\lambda}t} \tag{4.2.1}$$

where $p(\lambda)$ is the continuous distribution of modes detected in the direction $a$ and $\lambda$ labels the polarizations and wavevectors pointing in the direction $a$. That is, we integrate over a subset of modes all pointing in the same direction, which we denote $a$. While the equal-time commutation relation for the usual annihilation operators are $[\hat{a}_{a,\lambda}(t); \hat{a}^\dagger_{a',\lambda'}(t)] = \delta_{\{a,\lambda\},\{a',\lambda'\}}$ the new operators will have the unequal time commutation relation

$$[\hat{a}_a(t); \hat{a}^\dagger_{a'}(t')] = \delta_{a,a'} \int \mathrm{d}\lambda |p(\lambda)|^2 e^{-i\omega_{a,\lambda}(t-t')}. \tag{4.2.2}$$

By assuming a uniform distribution $p(\lambda)$ corresponding to equal probability of detecting any of the modes in the specific direction, we get that the time dependent annihilation and creation operators obey the following commutation relation

$$[\hat{a}_a(t), \hat{a}^\dagger_{a'}(t')] = \delta_{a,a'}\, \delta(t-t'). \tag{4.2.3}$$

We will use this notation for the operators $\hat{a}_a(t)$ and $\hat{a}^\dagger_a(t)$ only in the current chapter. Furthermore, we use a different notation than in the previous chapters in that $b$'s refer to output directions while $a$'s to the input directions.

In Chaps. 2 and 3 we described that a randomly scattering medium provides $N$ spatially distinct optical input directions that are connected to $N$ output directions via multiple scattering of light. The spatial output direction $b$ is related to all input directions $a'$ through

$$\hat{a}_b(t) = \sum_{a'} s_{a'b}\hat{a}_{a'}(t), \tag{4.2.4}$$

where $s_{a'b}$ is the complex electric-field scattering coefficient corresponding to either a reflection ($r_{a'b}$) or transmission ($t_{a'b}$) channel. Eq. (4.2.4) allows us to

relate the quantum properties of the multiple scattered light to the quantum state of the incident light source. The corresponding intensity transmission coefficient is given by $T_{a'b} \equiv |t_{a'b}|^2$ and likewise the intensity reflection coefficient is $R_{a'b} = |r_{a'b}|^2$. The mean photon flux of direction $a$ is given by $\langle \hat{n}_a(t) \rangle = \left\langle \hat{a}_a^\dagger(t) \hat{a}_a(t) \right\rangle$ while the variance in the photon fluctuations is given as $\Delta n_a^2(t) = \langle \hat{n}_a^2(t) \rangle - \langle \hat{n}_a(t) \rangle^2$. In the following we focus on multiple scattering processes where the light beam is incident onto the medium through a single direction, $a$. Thus, the average incident photon flux for all other input directions equals zero. Using Eq. (4.2.4) together with the continuous-mode commutator relation, Eq. (4.2.3), the mean photon flux of the total transmitted light can be obtained by summing over all transmitted output directions, i.e. $\langle \hat{n}_T(t) \rangle = \sum_b T_{ab} \left\langle \hat{a}_a^\dagger(t) \hat{a}_a(t) \right\rangle$. In our theory the intensity transmission coefficients are random variables corresponding to a single realization of disorder. Therefore, we can only predict ensemble-averaged properties of the transport of light. For example, the total transmitted photon flux is given as

$$\overline{\langle \hat{n}_T(t) \rangle} = \overline{T_{ba}} \, \langle \hat{n}_a(t) \rangle \,, \tag{4.2.5}$$

where the bar denotes the ensemble average over all configurations of disorder [6]. A similar result can be found for the total reflection, i.e. $\overline{\langle \hat{n}_R(t) \rangle} = \overline{R_{ba}} \, \langle \hat{n}_a(t) \rangle$. In order to determine another important property of light, namely the fluctuations of the total transmitted multiply scattered light, we need to evaluate the second moment of the photon number operator. Using Eqs. (4.2.4) and (4.2.3) and the fact that only direction $a$ is illuminated, this is given by

$$\begin{aligned} \overline{\langle \hat{n}_T(t) \hat{n}_T(t+\tau) \rangle} &= \sum_{b,b'} \overline{\langle \hat{n}_b(t) \hat{n}_{b'}(t+\tau) \rangle} \\ &= \overline{T_{ba} T_{b'a}} \, \langle \hat{n}_a(t) \hat{n}_a(t+\tau) \rangle + \overline{T_{ba}(1 - T_{b'a})} \, \langle \hat{n}_a(t) \rangle \, \delta(\tau). \end{aligned} \tag{4.2.6}$$

The non-vanishing contributions to the sum in Eq. (4.2.6) for different output directions $b$ and $b'$ stem from the fact that different spatial parts of the volume speckle patterns are quantum correlated.

We define the continuous-mode spatial quantum correlation function

$$\overline{C_{bb'}^{Q}}(\tau) = \frac{\overline{\langle \hat{n}_b(t) \hat{n}_{b'}(t+\tau) \rangle}}{\overline{\langle \hat{n}_b(t) \rangle} \times \overline{\langle \hat{n}_{b'}(t+\tau) \rangle}} \tag{4.2.7}$$

describing the normalized ensemble-averaged strength of the temporal photon correlations between two output directions, $b$ and $b'$, of the multiple scattering medium. The normalization is with respect to the product of the

ensemble-averaged mean photon flux in both directions. Notice that this ensemble averaged correlation function is defined differently from the previous chapters and is more alike the classical multiple scattering correlation function of Eq. (2.2.13), Sec. 2.2.2. In the experiment of concern here, we study a statistically stationary light source whose statistical fluctuations and mean photon flux do not change in time. The spatial quantum correlation function, therefore, only depends on the time difference $\tau$ [12] and can be expressed by the photon statistics of the incident light beam using Eqs. (4.2.5) and (4.2.6), i.e.

$$\begin{aligned}\overline{C^{Q}_{bb'}}(\tau) &= \frac{\langle \hat{n}(t)\hat{n}(t+\tau)\rangle - \langle \hat{n}(t)\rangle\,\delta(\tau)}{\langle \hat{n}(t)\rangle\,\langle \hat{n}(t)\rangle}\overline{C^{C}_{bb'}}, \\ &= \frac{\Gamma_a(\tau) - \langle \hat{n}_a(t)\rangle\,\delta(\tau) + \langle \hat{n}_a(t)\rangle^2}{\langle \hat{n}_a(t)\rangle^2}\overline{C^{C}_{bb'}}. \end{aligned} \tag{4.2.8}$$

Here, $\overline{C^{C}_{bb'}} = \overline{T_{ab}T_{ab'}}/(\overline{T_{ab}} \times \overline{T_{ab'}})$ is similar to the well known classical speckle correlation function introduced in Sec. 2.2, induced by classical multiple scattering [6, 18, 20] and $\Gamma_a(\tau) = \langle \hat{n}_a(t)\hat{n}_a(t+\tau)\rangle - \langle \hat{n}_a(t)\rangle\,\langle \hat{n}_a(t+\tau)\rangle$ represents the autocorrelation function of the incoming light. Notice that the ensemble averaged correlation function, Eq. (4.2.7), factorizes into a quantum mechanical part and a classical part, as in Eq. (4.2.8), *only* if light is incident from only one direction. If light were incident from more than one direction as described in the previous chapter the correlation function would not separate except for the case of coherent input states, i.e. incident classical light.

Let us carry on by defining an ensemble-averaged autocorrelation function for the total transmitted (and similarly for reflected) light as

$$\begin{aligned}\overline{\Gamma_T(\tau)} =& \overline{\langle \hat{n}_T(t)\hat{n}_T(t+\tau)\rangle} - \overline{\langle \hat{n}_T(t)\rangle\,\langle \hat{n}_T(t+\tau)\rangle}, \\ =& \overline{T}^2\,[\Gamma_a(\tau) - \langle \hat{n}_a(t)\rangle\,\delta(\tau)] + \overline{T}\,\langle \hat{n}_a(t)\rangle\,\delta(\tau), \end{aligned} \tag{4.2.9}$$

where we utilized $\overline{T_{ab}T_{ab'}} = \overline{T_{ab}}^2$ which holds for a multimode sample in the diffusive regime [6]. The Eq. (4.2.9) shows that after averaging over all configurations of disorder the total transmitted photon fluctuations can be directly related to the quantum optical properties of the light source even in the diffusive regime despite the fact that in that regime any classical correlation would vanish.

In the experiment the photon fluctuations are studied by recording the total transmitted and reflected light with a photo diode whose photo current is linearly converted into a voltage. The photo voltage is split into a DC component that is proportional to the mean photon flux and an AC component that contains information about the photon fluctuations. Computing the

Fourier spectrum of the measured AC photo voltage allows us to study the temporal photon fluctuations in quantum noise measurements. The spectral density function at frequency $\omega$ is defined as the Fourier transformation of the auto-correlation function [12]

$$S(\omega) = \frac{1}{2\pi}\int_{-\infty}^{\infty} \mathrm{d}\tau\ \Gamma(\tau)e^{i\omega\tau}. \tag{4.2.10}$$

The variance of the temporal photon fluctuations is thus related to the noise spectrum through the inverse transform of Eq. (4.2.10), i.e. $\Delta\hat{n}^2(t) = \int_{-\infty}^{\infty}\mathrm{d}\omega S(\omega)$. The spectral density function is studied within a frequency region $\omega_{\pm} = \omega_s \pm \delta\omega/2$ so that we obtain the frequency-dependent photon variance

$$\left\langle \Delta n^2(\omega_s, \delta\omega)\right\rangle = \int_{\omega_-}^{\omega_+} \mathrm{d}\omega\, S(\omega) \tag{4.2.11}$$

that is proportional to the experimentally measured noise power. We note that the total collection and detection efficiency of a photo-diode is non-unity in any experiments and the measured transmission is $\overline{T} \to \eta_T\overline{T}$, with $0 \le \eta_T \le 1$. The total transmitted photon fluctuations, $\langle\Delta n_T^2(\omega_s, \delta\omega)\rangle$, can be related to the spectral density function of the incident light source integrated over the measured frequency range by substituting Eq. (4.2.9) into Eqs. (4.2.10) and (4.2.11), i.e.

$$\begin{aligned}\overline{\langle\Delta n_T^2(\omega_s, \delta\omega)\rangle} =& \int_{\omega_-}^{\omega_+} \mathrm{d}\omega\ \left[\eta^2\overline{T}^2\left(S_a(\omega) - \frac{\langle\hat{n}_a(t)\rangle}{2\pi}\right) + \eta\overline{T}\frac{\langle\hat{n}_a(t)\rangle}{2\pi}\right], \\ =& \eta^2\overline{T}^2\left(\left\langle\Delta n_a^2(\omega_s, \delta\omega)\right\rangle - \langle\hat{n}_a(t)\rangle\ \frac{\delta\omega}{2\pi}\right) + \eta\overline{T}\,\langle\hat{n}_a(t)\rangle\ \frac{\delta\omega}{2\pi}.\end{aligned} \tag{4.2.12}$$

Evaluating the right hand side for a coherent state yields $\overline{\langle\Delta n_T^2(\omega_s, \delta\omega)\rangle_C} = \eta\overline{T}\,\langle\hat{n}_a(t)\rangle_C\ \frac{\delta\omega}{2\pi}$, where the subscript $C$ denotes that the expectation value is with only coherent light as input state. At this point we introduce the Fano factor

$$F(\omega, \delta\omega) \equiv \frac{\langle\Delta n^2(\omega, \delta\omega)\rangle}{\langle\Delta n^2(\omega, \delta\omega)\rangle_C}, \tag{4.2.13}$$

that gauges the ratio between the photon number variance of an unknown quantum state, $\langle\Delta n^2(\omega_s, \delta\omega)\rangle$, and of a coherent state, $\langle\Delta n^2(\omega_s, \delta\omega)\rangle_C$ having the same mean photon number. Importantly, the Fano factor can be directly measured without determining the proportionality factor between the noise

power recorded with the electrical spectrum analyzer and the photon number variance. In the experiment the optical state is created by overlapping a squeezed-vacuum state with a bright-coherent state, cf. Fig. 4.1. Since the resultant bright-squeezed state has a large coherent amplitude, the average number of photons is almost equal to the average number of photons in the coherent state and Eq. (4.2.12) can be rewritten as

$$\begin{aligned}\overline{F_T}(\omega_s,\delta\omega) =& \frac{\eta_T^2\overline{T}^2\left(\langle\Delta n_a^2(\omega_s,\delta\omega)\rangle - \langle\hat{n}_a(t)\rangle\ \frac{\delta\omega}{2\pi}\right) + \eta_T\overline{T}\,\langle\hat{n}_a(t)\rangle\ \frac{\delta\omega}{2\pi}}{\eta_T\overline{T}\,\langle\hat{n}_a(t)\rangle\ \delta\omega}\\ =& 2\pi\left\{1-\eta_T\overline{T}\left[1-F_a(\omega_s,\delta\omega)\right]\right\}. \end{aligned} \tag{4.2.14}$$

A similar expression holds for the total reflected multiple scattered light which results in $\overline{F_R}(\omega_s,\delta\omega) = 2\pi\left\{1-\eta_R\overline{R}\left[1-F_a(\omega_s,\delta\omega)\right]\right\}$ with $\eta_R$ being the corresponding reflection collection efficiency. We emphasize the importance of the last expressions, Eq.(4.2.14). In Ref. [45] it was predicted that any nonclassical features in the electric field quadrature amplitudes vanish in the multiple scattering process after ensemble averaging. In contrast, Eq. (4.2.14) shows that for a quantum state with nonclassical photon fluctuations also the ensemble-averaged transmitted and reflected photon fluctuations exhibit nonclassical photon fluctuations after multiple scattering.

Analogue to the frequency-dependent photon fluctuations, Eq. (4.2.11), we can introduce the frequency-dependent spatial quantum correlation function which is the quantity extracted in the experiment. It is defined as the Fourier transformation of Eq. (4.2.8) integrated over the frequency interval $\omega_\pm = \omega_s \pm \delta\omega/2$,

$$\begin{aligned}\overline{C^Q_{bb'}}(\omega_s,\delta\omega) &= \int_{\omega_-}^{\omega^+} \mathrm{d}\omega \frac{S(\omega) - \frac{\langle\hat{n}_a(t)\rangle}{2\pi} + \langle\hat{n}_a(t)\rangle^2\,\delta(\omega)}{\langle\hat{n}_a(t)\rangle^2}\overline{C^C_{bb'}},\\ &= \frac{\left[F_a(\omega_s,\delta\omega)-1\right]\delta\omega}{\langle\hat{n}_a(t)\rangle}\overline{C^C_{bb'}}, \end{aligned} \tag{4.2.15}$$

utilizing $\langle\hat{n}_a(t)\rangle \approx \langle\hat{n}_a(t)\rangle_C = 2\pi\delta\omega^{-1}\langle\Delta\hat{n}_a^2(\omega_s,\delta\omega)\rangle_C$. This result should be compared with the discrete mode analysis of Ref. [38]. In a discrete mode analysis one obtain $\overline{C^Q_{bb'}} - 1 = (F_a - 1)/\langle\hat{n}_a\rangle\,\overline{C^C_{bb'}}$, i.e. having an extra minus one on the left hand side. This minus one term actually do appear in the first line of Eq. (4.2.15) as the $\langle\hat{n}_a(t)\rangle^2\,\delta(\omega)$ in the nominator.

From the last expression it can be seen that different output directions $b$ and $b'$ are positively correlated, i.e. the photons show spatial bunching ($\overline{C^Q_{bb'}}(\omega_s,\delta\omega) \geq 1$) when the light source exhibits classical photon fluctuations, ($F_a(\omega_s,\delta\omega) > 1$). Using a light source that exhibits non-classical photon

fluctuations ($F_a(\omega_s, \delta\omega) < 1$), we enter the purely quantum optical regime of multiple scattering where the photons between two different directions are spatially anti-correlated ($\overline{C^Q_{bb'}}(\omega_s, \delta\omega) < 1$). Alternatively, the spatial quantum correlation function can be expressed in terms of the ensemble-averaged total transmitted (reflected) Fano factor by substituting Eq. (4.2.14) into Eq. (4.2.15), leading to the expression

$$\overline{C^Q_{bb'}}(\omega_s, \delta\omega) = \frac{\left[\,\overline{F_{T/R}}(\omega_s, \delta\omega) - 1\right]\delta\omega}{\overline{\langle \hat{n}_{T/R}(t)\rangle}}\overline{C^C_{bb'}}. \tag{4.2.16}$$

Thus, in the diffusive regime ($\overline{C^C_{bb'}} = 1$) the spatial quantum correlation function can be extracted by recording two quantities *i*) the Fano factor and *ii*) the photon flux. The Fano factor is found by recording the noise power as described in Eq. (4.2.13). The photon flux is found through $\langle \hat{n}_a(t)\rangle = P/(\hbar\,\omega_0)$ by measuring the power of the light and knowing the frequency of the light. Further details on the measurement techniques and the experimental setup can be found in Paper J1 or Ref. [42].

These were exactly the quantities measured by the experiment presented in Ref. [42] and with these the correlations are calculated in Paper J1 also shown in Fig. 4.2. This figure shows the correlation function calculated using the measured photon fluctuations of the transmitted light, versus the measured photon fluctuations of the incident light and neatly illustrate the linear behavior as predicted. If one were to compare the measured correlation function in Fig. 4.2 to that of Fig. 3 in Ref. [42] one should notice three things. First, in Ref. [42] the ordinate axis shows that the measured quantity is $\overline{C_{bb'}} - 1$, as explained this is only true for the discrete mode analysis. Second, there is a five order of magnitude difference between the two! The difference is caused by the use of photon numbers in a certain measurement time as opposed to photon flux in Ref. [42]. Third, in Ref. [42] the normalized correlation function has the unit $\mathrm{Hz}^{-1}$, this is due to the previous use of a unit less number of photons as compared to the photon flux.

The experimental results shown in Fig. 4.2 illustrate that, unlike classical multiple scattering, it is possible to deterministically alter the intensity correlations by changing the photon statistics of the incident beam. Specifically, in the diffusive regime where classically the intensity of two different output directions are uncorrelated, we are able to continuously change the correlations from positive to negative by changing the photon statistics of the incident beam.

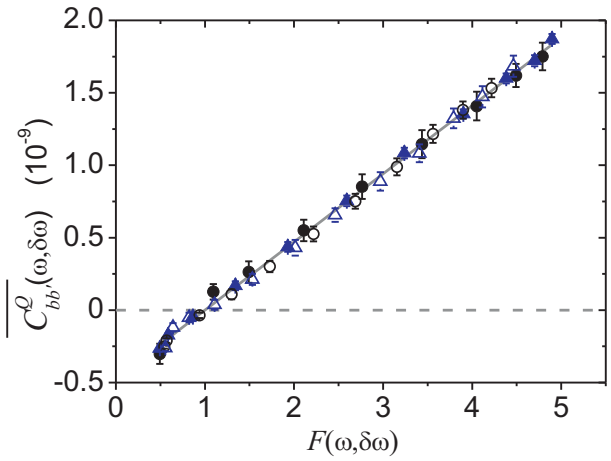


**Figure 4.2** Measured spatial quantum correlation function depending on the incident Fano factor for different sample thicknesses (triangles: $6\,\mu$m, circles: $20\,\mu$m). The spatial quantum correlation function has been measured in transmission (filled symbols) and reflection (empty symbols), respectively. The solid gray line displays the theoretical prediction while the dashed gray line represents the quantum limit of $\overline{C^{Q}_{bb'}}(\omega_s, \delta\omega) = 0$. (Figure from Paper J1).

## 4.3 Chapter Summary

In this chapter we derived the theoretical framework for the analysis of a quantum optical multiple scattering experiment. The experiment considered the propagation of squeezed light incident in a single direction upon a multiple scattering medium. The purpose of the experiment was to verify the prediction that spatial quantum correlations survive multiple scattering even after ensemble averaging.

In order to describe the measurement procedure, it was necessary to introduce the time-dependence of the operators. By doing this, it was possible to relate the noise power spectrum of the total transmitted or reflected light to the photon statistics of the incident quantum state. This was further related to the average spatial photon correlations. The derivation showed a discrepancy with the discrete-mode theory which was not taken into account in Ref. [42]. The experiment showed that, indeed as predicted by theory, the quantum nature of light persisted after multiple scattering and even survived after ensemble averaging and showed excellent agreement between the theory derived here and the experiment. This made it possible to deterministically alter the average intensity correlations by changing the photon statistics of the incident beam. Thereby it was possible to achieve both positively and

negatively correlated output intensities even in the diffusive regime, where classically output directions are uncorrelated.

An interesting next step will be to study experimentally the quantum interference of two or more independent quantum states in a multiple scattering medium as was described in Chapter 3. Another step would be to include light-matter interaction in the multiple scattering formalism in order to be able to describe phenomena such as quantum optical scattering on quantum dots in dielectrics or the fluorescence spectrum of a driven cloud of cold atoms. This is the topic of the next part of the thesis.

# Part II

# Quantum Optical Inelastic Scattering

# 5

# Quantum Scattering of Light on Dipoles

While the previous part of the thesis dealt with elastic scattering the present part will include interaction with dipoles upon which the light is scattered. This will be done using some of the concepts introduced in Chap. 2 such as quantization and Green functions. The results in this and the following chapter are unpublished and thus more calculations and details are included for transparency. The work was partially carried out at the group of Prof. Robin Kaiser at Institut Non Lineaire de Nice, Centre National de la Recherche Scientifique in France. The group of Robin Kaiser is conducting experimental cold atom physics and the collaboration has the aim to predict cooperative effects in cold atom systems.

In this chapter we will derive an exciting new formalism to investigate light-matter interaction. The formalism, carried out in the Heisenberg picture, focus on the propagation of the quantum optical operators enabling a scattering perspective. This is in contrast to the often used master equation approach which work in the Schrödinger picture and often focus on the atomic operators. The formalism is derived such that it is capable to deal with dipole scattering in any dielectric environment. The results presented in the present chapter can thus describe scattering of light on clouds of atoms, artificial atoms, i.e. quantum dots in engineered dielectric environments, and nitrogen vacancies in diamonds. In the next chapter one of the many applications of the formalism is presented by deriving analytic expressions of the fluorescence spectrum of a driven cloud of $N$ atoms.

The chapter is ordered as follows. In Sec. 5.1 the Hamiltonian due to the quantum mechanical description of interaction between light and dipoles is discussed and certain simplified versions are introduced. Then, in Sec. 5.2, the evolution of the field operators as functions of the dipole operators is found for the different interaction Hamiltonians and the significance of the introduced simplifications is investigated. At last, in Sec. 5.3, the Heisenberg equations of motion of the dipoles are derived for a two-level model. These

will be used in the following chapter for describing a driven cloud of cold atoms.

## 5.1 Light-Matter Interaction in Arbitrary Dielectric Structures

First let us look at the origin of the interaction Hamiltonian. We will now write up the Hamiltonian including the interaction between light and matter, specifically dipoles in an inhomogeneous dielectric environment. Similar to the quantization in Chap. 2 we will take the classical expression for the energy and add hats to the canonical variables. From classical electrodynamics of charged particles in fields we know that the canonical momentum of the $m$'th particle, $\mathbf{p}_m$, differs from its kinetic momentum, $\mathbf{k}_m$, and that they are related through $\mathbf{p}_m(t) = \mathbf{k}_m(t) + e\mathbf{A}(\mathbf{q}_m, t)$, where $\mathbf{q}_m$ is the canonical position of the $m$'th charge, see e.g. Ref. [46]. In the canonical dynamical variables the potential energy of the charged particle, $\mathcal{E}_{\text{pot}} = eU(\mathbf{q}_m, t)$, is thus unaltered by the field while the kinetic energy is $\mathcal{E}_{\text{kin}} = \frac{1}{2m_e}\left[\mathbf{p}_m(t) - e\mathbf{A}(\mathbf{q}_m, t)\right]^2$, where $m_e$ is the mass of the charge.

We now write the total Hamiltonian of the field and atoms by introducing hats on the canonical operators and assuming their usual commutation relations, giving

$$\begin{aligned}\mathcal{H} =& \frac{1}{2}\int \mathrm{d}\mathbf{r}\left[\varepsilon_0\varepsilon(\mathbf{r})\hat{\mathbf{E}}^2(\mathbf{r},t) + \frac{1}{\mu_0}\hat{\mathbf{B}}^2(\mathbf{r},t)\right] \\ &+ \sum_m\left[eU(\hat{\mathbf{q}}_m,t) + \frac{\hat{\mathbf{p}}_m^2(t)}{2m_e}\right] \\ &- \frac{e}{2m_e}\sum_m\left[\hat{\mathbf{p}}_m(t)\cdot\hat{\mathbf{A}}(\hat{\mathbf{q}}_m,t) + \hat{\mathbf{A}}(\hat{\mathbf{q}}_m,t)\cdot\hat{\mathbf{p}}_m(t) - e\hat{\mathbf{A}}^2(\hat{\mathbf{q}}_m,t)\right],\end{aligned} \tag{5.1.1}$$

where the three lines respectively represent the free field, $\mathcal{H}_{\text{R}}$, free charges, $\mathcal{H}_{\text{A}}$, and interaction, $\mathcal{H}_{\text{I}}$, Hamiltonians. The Hamiltonian of the free radiation field is the same as we discussed in Chap. 2, i.e. with the mode expansion in the generalized Coulomb gauge it is given by Eq. (2.3.8). The Hamiltonian for the free charges depends on the specific model of the charges and we will leave that model arbitrary for the moment. Similar to the field it can be written as an expansion in terms of its eigenstates and eigenenergies. The last term in Eq. (5.1.1) deals with the interaction between light and matter through the charges.

The Hamiltonian, Eq. (5.1.1), thus governs the dynamics of the electromagnetic field interacting with dipoles embedded in a dielectric material treated macroscopically through $\varepsilon(\mathbf{r})$ which is assumed local in time and space. It is thus able to treat the dynamics of light-matter interaction in

systems such as quantum dots in photonic crystals, nitrogen vacancy centers in diamond, and clouds of atoms alike.

We will spend the next section on simplifying the interaction term before we write up the equations of motion for the field and solve them in terms of the dipole operators.

### 5.1.1 Interaction Hamiltonian

We will now discuss the interaction Hamiltonian for a while in order to try to slightly demystify it. We will introduce the dipole approximation and show two typical simplifications made in the literature; a linearization and a multipolar expansion. This will be useful for deriving dynamic equations for the field operators in the Heisenberg picture and solve these in terms of the atomic operators in Sec. 5.2. Furthermore, it will make it possible to derive the fluorescence spectrum of a cloud of atoms in the next chapter.

First of all, we notice that $\hat{\mathbf{A}}(\hat{\mathbf{q}}_m, t)$ depends on the dipole position operator, $\hat{\mathbf{q}}_m$, and thus does not in general commute with the momentum operator, $\hat{\mathbf{p}}_m$. Often the dipoles such as atoms or molecules are much smaller than the wavelength of the electric field and thus the vector potential does not vary much over their size. It is then valid to replace the position operator, $\hat{\mathbf{q}}_m(t)$, with its classical averaged value, i.e. $\hat{\mathbf{A}}(\hat{\mathbf{q}}_m, t) \approx \hat{\mathbf{A}}(\mathbf{R}_m, t)$ with $\langle \hat{\mathbf{q}}_m \rangle = \mathbf{R}_m$. This is known as the dipole approximation after which the vector potential and the momentum operator do commute. We further assume that the averaged positions $\mathbf{R}_m$ are constant, thereby describing stationary dipoles. This leads us to the minimum-coupling interaction Hamiltonian

$$\mathcal{H}_{\mathrm{I}}^{\mathrm{min}} = -\sum_m \left[ \dot{\hat{\boldsymbol{\mu}}}_m(t) \cdot \hat{\mathbf{A}}(\mathbf{R}_m, t) - \frac{e^2}{2m_e} \hat{\mathbf{A}}^2(\mathbf{R}_m, t) \right], \tag{5.1.2}$$

where we have defined the dipole moment operator $\hat{\boldsymbol{\mu}}_m(t) = e\hat{\mathbf{q}}_m(t)$ such that $\hat{\mathbf{p}}_m(t) = m_e \dot{\hat{\boldsymbol{\mu}}}_m(t)$. The dipole approximation is usually quite good when dealing with atoms, but has recently been shown to be inadequate when dealing with large quantum dots close to metallic interfaces [47]. The assumption of stationary dipoles perfectly describes solid-state systems. Furthermore, in atomic systems, which we consider in the next chapter, laser cooling can eliminate Doppler effects such that the stationary description is valid [12].

Usually $\mathcal{H}_{\mathrm{I}}^{\mathrm{min}}$ is simplified before carrying out calculations. There are two simplifications which are often used. In one of them, the $\hat{\mathbf{A}}^2(\mathbf{R}_m, t)$ term is considered much smaller than the $\dot{\hat{\boldsymbol{\mu}}}_m(t) \cdot \hat{\mathbf{A}}(\mathbf{R}_m, t)$ term and the Hamiltonian is simplified by linearizing it in the field operator giving the so-called $\mathbf{p} \cdot \mathbf{A}$

Hamiltonian

$$\mathcal{H}_{\mathrm{I}}^{\mathrm{pA}} = -\sum_m \dot{\hat{\boldsymbol{\mu}}}_m(t) \cdot \hat{\mathbf{A}}(\mathbf{R}_m, t). \tag{5.1.3}$$

Another way of simplifying the minimal-coupling Hamiltonian is to invoke a unitary transformation $\hat{U} = \exp\left[-\frac{i}{\hbar}\hat{\mathbf{q}}_m \cdot \hat{\mathbf{A}}(\mathbf{R}_m, t)\right]$ giving the multipolar or Power–Zienau–Woolley Hamiltonian [48, 49]. Neglecting all terms except the dominant one gives the electric-dipole Hamiltonian

$$\mathcal{H}_{\mathrm{I}}^{\mathrm{Ed}} = -\sum_m \hat{\boldsymbol{\mu}}_m(t) \cdot \hat{\mathbf{E}}(\mathbf{R}_m, t), \tag{5.1.4}$$

which is known as the electric-dipole approximation.

There has been some controversy on which of the Hamiltonians would give the correct physics, see eg. [12]. The controversy seems to have settled with the preferred use of the electric-dipole Hamiltonian since it not only allows coupling to transverse modes. In the present chapter we will investigate the properties of both the full minimal-coupling Hamiltonian, Eq. (5.1.2), and the electric-dipole Hamiltonian, Eq. (5.1.4), to pinpoint the differences between the two.

## 5.2 Field Operator Evolution

We will now find the exact evolution of the field operators in the Heisenberg picture in terms of the dipole operators without assuming any particular model for the dipoles. In Sec. 5.3 we will choose to investigate the two-level model for the atoms, which we will use in Chap. 6 to describe a cloud of atoms. We thus write the total Hamiltonian $\mathcal{H} = \mathcal{H}_{\mathrm{R}} + \mathcal{H}_{\mathrm{A}} + \mathcal{H}_{\mathrm{I}}$ with the noninteracting field Hamiltonian written as, recall Eq. (2.3.8),

$$\mathcal{H}_{\mathrm{R}} = \sum_\lambda \hbar\omega_\lambda \left[\hat{a}_\lambda^\dagger(t)\hat{a}_\lambda(t) + \frac{1}{2}\right]. \tag{5.2.1}$$

For the interaction Hamiltonian, $\mathcal{H}_{\mathrm{I}}$, we will compare the minimal coupling interaction, Eq. (5.1.2), with the electric-dipole interaction, Eq. (5.1.4).

### 5.2.1 Field Evolution with the Electric-Dipole Hamiltonian

We will now use the electric-dipole Hamiltonian, Eq. (5.1.4), to derive the evolution of the field operators in the Heisenberg picture. This is a generalization of the results of Ref. [50], where a harmonic oscillator model is used

for the dipoles. Later on in Sec. 5.3.1 we will use the results derived here to find the dynamic equations for a two-level model for the dipoles.

As in Chap. 2.4, we write the electric-field operator as an expansion in the generalized transverse modes, see Eq. (2.3.10),

$$\hat{\mathbf{E}}(\mathbf{r},t) = i\sum_{\lambda}\sqrt{\frac{\hbar\omega_\lambda}{2\varepsilon_0}}\left[\hat{a}_\lambda(t)\mathbf{f}_\lambda(\mathbf{r}) - \hat{a}^\dagger_\lambda(t)\mathbf{f}^*_\lambda(\mathbf{r})\right], \tag{5.2.2}$$

where the time-evolution of the creation and annihilation operators is no longer harmonic. Using the equal-time commutation relation for the mode creation and annihilation operators, $[\hat{a}_\lambda(t);\hat{a}^\dagger_{\lambda'}(t)] = \delta_{\lambda,\lambda'}$, we get

$$[\hat{a}_\lambda(t);\mathcal{H}_\mathrm{R}] = \hbar\omega_\lambda\hat{a}_\lambda(t), \tag{5.2.3a}$$

$$[\hat{a}_\lambda(t);\mathcal{H}^{\mathrm{Ed}}_\mathrm{I}] = i\sqrt{\frac{\hbar\omega_\lambda}{2\varepsilon_0}}\sum_m \mathbf{f}^*_\lambda(\mathbf{R}_m)\cdot\hat{\boldsymbol{\mu}}_m(t), \tag{5.2.3b}$$

and we can then write the Heisenberg equations of motion

$$\dot{\hat{a}}_\lambda(t) = -i\omega_\lambda\hat{a}_\lambda(t) + \sqrt{\frac{\omega_\lambda}{2\hbar\varepsilon_0}}\sum_m \mathbf{f}^*_\lambda(\mathbf{R}_m)\cdot\hat{\boldsymbol{\mu}}_m(t), \tag{5.2.4a}$$

$$\dot{\hat{a}}^\dagger_\lambda(t) = i\omega_\lambda\hat{a}^\dagger_\lambda(t) + \sqrt{\frac{\omega_\lambda}{2\hbar\varepsilon_0}}\sum_m \mathbf{f}_\lambda(\mathbf{R}_m)\cdot\hat{\boldsymbol{\mu}}_m(t). \tag{5.2.4b}$$

We now introduce the Laplace transform

$$\mathcal{L}\left\{g(t)\right\}(\omega) = g(\omega) = \int_0^\infty \mathrm{d}t\; e^{i\omega t}g(t), \tag{5.2.5}$$

where $\omega$ contains an infinitesimal positive imaginary part which ensures that the transform is well defined. Using this we get

$$\hat{a}_\lambda(\omega) = \frac{i\hat{a}_\lambda(0)}{\omega-\omega_\lambda} + \frac{i}{\omega-\omega_\lambda}\sqrt{\frac{\omega_\lambda}{2\hbar\varepsilon_0}}\sum_m \mathbf{f}^*_\lambda(\mathbf{R}_m)\cdot\hat{\boldsymbol{\mu}}_m(\omega), \tag{5.2.6a}$$

$$\hat{a}^\dagger_\lambda(\omega) = \frac{i\hat{a}^\dagger_\lambda(0)}{\omega+\omega_\lambda} + \frac{i}{\omega+\omega_\lambda}\sqrt{\frac{\omega_\lambda}{2\hbar\varepsilon_0}}\sum_m \mathbf{f}_\lambda(\mathbf{R}_m)\cdot\hat{\boldsymbol{\mu}}_m(\omega), \tag{5.2.6b}$$

with the notation $\hat{a}_\lambda(0) = \hat{a}_\lambda(t=0)$ has been used for brevity. Notice that due to the one-sidedness of the Laplace transform $[\hat{a}_\lambda(\omega)]^\dagger \neq \hat{a}^\dagger_\lambda(\omega)$. By inserting Eqs. (5.2.6) into the positive- and negative-frequency components

of the electric field, we get

$$\hat{\mathbf{E}}^{(+)}(\mathbf{r},\omega) = -\sum_{\lambda}\sqrt{\frac{\hbar\omega_\lambda}{2\varepsilon_0}}\frac{\hat{a}_\lambda(0)}{\omega-\omega_\lambda}\mathbf{f}_\lambda(\mathbf{r}) - \frac{1}{2\varepsilon_0}\sum_{m\lambda}\frac{\omega_\lambda \mathbf{f}_\lambda(\mathbf{r})\otimes\mathbf{f}_\lambda^*(\mathbf{R}_m)}{\omega-\omega_\lambda}\cdot\hat{\boldsymbol{\mu}}_m(\omega) \tag{5.2.7a}$$

$$\hat{\mathbf{E}}^{(-)}(\mathbf{r},\omega) = \sum_{\lambda}\sqrt{\frac{\hbar\omega_\lambda}{2\varepsilon_0}}\frac{\hat{a}_\lambda^\dagger(0)}{\omega+\omega_\lambda}\mathbf{f}_\lambda(\mathbf{r}) + \frac{1}{2\varepsilon_0}\sum_{m\lambda}\frac{\omega_\lambda \mathbf{f}_\lambda^*(\mathbf{r})\otimes\mathbf{f}_\lambda(\mathbf{R}_m)}{\omega+\omega_\lambda}\cdot\hat{\boldsymbol{\mu}}_m(\omega). \tag{5.2.7b}$$

We thus see that, very similar to the classical Green function approach of point scattering in Sec. 2.2.1, the field consists of a free field and a scattered field component. This is even more apparent when we write the total field, $\hat{\mathbf{E}}(\mathbf{r},\omega) = \hat{\mathbf{E}}^{(+)}(\mathbf{r},\omega) + \hat{\mathbf{E}}^{(-)}(\mathbf{r},\omega)$, giving

$$\hat{\mathbf{E}}(\mathbf{r},\omega) = \hat{\mathbf{E}}_{(0)}(\mathbf{r},\omega) - \mu_0\omega^2\sum_m \mathbf{K}(\mathbf{r},\mathbf{R}_m,\omega)\cdot\hat{\boldsymbol{\mu}}_m(\omega). \tag{5.2.8}$$

Here, $\hat{\mathbf{E}}_{(0)}(\mathbf{r},\omega) = \hat{\mathbf{E}}^{(+)}_{(0)}(\mathbf{r},\omega) + \hat{\mathbf{E}}^{(-)}_{(0)}(\mathbf{r},\omega)$ is the free-field component, $c_0^{-2} = \mu_0\varepsilon_0$, and the kernel $\mathbf{K}(\mathbf{r},\mathbf{r}',\omega)$ is defined by

$$\mathbf{K}(\mathbf{r},\mathbf{r}',\omega) = c_0^2\sum_\lambda \frac{\omega_\lambda^2}{\omega^2}\frac{\mathbf{f}_\lambda(\mathbf{r})\otimes\mathbf{f}_\lambda^*(\mathbf{r}')}{\omega^2-\omega_\lambda^2} \tag{5.2.9a}$$

$$= \mathbf{G}^{\mathrm{T}}(\mathbf{r},\mathbf{r}',\omega) - \frac{c_0^2}{\varepsilon(\mathbf{r})\omega^2}[\boldsymbol{\delta}_{\boldsymbol{\epsilon}}^{\mathbf{T}}(\mathbf{r}',\mathbf{r})]^\dagger \tag{5.2.9b}$$

$$= \mathbf{G}^{+}(\mathbf{r},\mathbf{r}',\omega) - \frac{c_0^2}{\varepsilon(\mathbf{r})\omega^2}\delta(\mathbf{r}-\mathbf{r}')\mathbf{I}. \tag{5.2.9c}$$

The dyadic kernel $\mathbf{K}(\mathbf{r},\mathbf{r}',\omega)$ is thus related to the retarded Green function $\mathbf{G}^{+}(\mathbf{r},\mathbf{r}',\omega)$ or the retarded transverse Green function $\mathbf{G}^{\mathrm{T}}(\mathbf{r},\mathbf{r}',\omega)$ also found in classical theory of point scatterers [51]. The obvious and intuitive physical significance of Eq. (5.2.8) is that the field $\hat{\mathbf{E}}(\mathbf{r},\omega)$ is given by the field in absence of atoms, $\hat{\mathbf{E}}_0(\mathbf{r},\omega)$, plus the light emitted by the atoms at $\mathbf{R}_m$ and arriving at $\mathbf{r}$. The difference between classical scattering on points and quantum scattering on dipoles is though that the two interact. We will see in Chap. 6 that the quantum treatment gives rise to nonlinear phenomena which for example can be seen in the spectrum. Notice that up until now the derivation is exact since we have not made use of any approximations besides

the electric-dipole approximation. An often used approximation is to remove terms with phases which rotate with much higher frequencies than those of the phenomena of interest. This is known as the rotating-wave approximation (RWA). It is sometimes used at the initial Hamiltonian, but this would not lead to a kernel related to the classical Green function that we found above in Eq. (5.2.8). To obtain the expression Eq. (5.2.9a) for the kernel $\mathbf{K}(\mathbf{r}, \mathbf{r}', \omega)$, we rewrote the scattering term of $\hat{\mathbf{E}}^{(-)}(\mathbf{r}, \omega)$ in Eq. (5.2.7b), see App. B.1 for details.

The expression, Eq. (5.2.8), has previously been found for the specific model in which the dipoles are treated as quantum harmonic oscillators [50]. It should be noted that with our new treatment, the current expression is independent of the chosen model for the dipoles. Our formalism can thus describe the light-matter interaction of cold atoms in vacuum, quantum dots in photonic crystals, and nitrogen vacancy centers in diamond alike. In the latter two cases atom-phonon interaction could also be taken into account in the present formalism by including these in the atomic Hamiltonian.

The evolution of the field operators can now be found by an inverse Laplace transform. Let us do so.

First of all, the free field positive- and negative-frequency components, $\hat{\mathbf{E}}^{(\pm)}_{(0)}(\mathbf{r}, \omega)$, become

$$\hat{\mathbf{E}}^{(+)}_{(0)}(\mathbf{r}, t) = i \sum_{\lambda} \sqrt{\frac{\hbar\omega_\lambda}{2\varepsilon_0}} \hat{a}_\lambda(0) e^{-i\omega_\lambda t} \mathbf{f}_\lambda(\mathbf{r}), \tag{5.2.10a}$$

$$\hat{\mathbf{E}}^{(-)}_{(0)}(\mathbf{r}, t) = -i \sum_{\lambda} \sqrt{\frac{\hbar\omega_\lambda}{2\varepsilon_0}} \hat{a}^\dagger_\lambda(0) e^{i\omega_\lambda t} \mathbf{f}^*_\lambda(\mathbf{r}). \tag{5.2.10b}$$

This describe the harmonic time-evolution of the eigenmodes in the dielectric structure in the absence of dipoles as we found in Sec. 2.3.2, Eqs. (2.3.11). It should be noted that since we work in the Heisenberg picture the initial operators are considered known quantities and thus Eqs. (5.2.10) are in principle known if we can calculate the classical field modes.

Using the convolution theorem, $\mathcal{L}^{-1}\{f(\omega)g(\omega)\} = \int_0^t \mathrm{d}\tau f(\tau)g(t-\tau)$, for the Laplace transform defined in Eq. (5.2.5), the inverse Laplace transform of the second part of $\hat{\mathbf{E}}^{(\pm)}(\mathbf{r}, \omega)$, corresponding to the scattering part, $\hat{\mathbf{E}}^{(\pm)}_{\mathrm{Scat}}(\mathbf{r}, t)$, is given by

$$\hat{\mathbf{E}}^{(\pm)}_{\mathrm{Scat}}(\mathbf{r}, t) = \pm \frac{i}{2\varepsilon_0} \sum_m \sum_\lambda \omega_\lambda \mathbf{f}_\lambda(\mathbf{r}) \otimes \mathbf{f}^*_\lambda(\mathbf{R}_m) \cdot \int_0^t \mathrm{d}\tau \hat{\boldsymbol{\mu}}_m(\tau) e^{\mp i\omega_\lambda(t-\tau)}. \tag{5.2.11}$$

The expression has an intuitive physical structure which is most easily seen by rearranging the expression a bit in order to write the integrand as

$$\hat{\mathbf{E}}^{(\pm)}_{\mathrm{Scat}}(\mathbf{r},t) = \pm\frac{i}{2\varepsilon_0}\sum_m\sum_\lambda \omega_\lambda \mathbf{f}_\lambda(\mathbf{r})e^{\mp i\omega_\lambda t} \otimes \int_0^t \mathrm{d}\tau \mathbf{f}^*_\lambda(\mathbf{R}_m)e^{\pm i\omega_\lambda \tau}\cdot\hat{\boldsymbol{\mu}}_m(\tau). \tag{5.2.12}$$

The terms $\mathbf{f}^*_\lambda(\mathbf{R}_m)e^{\pm i\omega_\lambda\tau}$ and $\mathbf{f}_\lambda(\mathbf{r})e^{\mp i\omega_\lambda t}$ corresponds to the noninteracting harmonic field evolution at the position of the dipole at $\mathbf{R}_m$ at time $\tau$ and at position $\mathbf{r}$ at time $t$ respectively. By reading Eq. (5.2.12) from right to left we have that the evolution of the field at position $\mathbf{r}$ at time $t$ is given by the dynamics of the dipoles $\hat{\boldsymbol{\mu}}_m(\tau)$ at previous times $\tau$. The field then evolve harmonically from the dipole positions, $\mathbf{R}_m$, at the previous time $\tau$ to the point $\mathbf{r}$ at the present time $t$.

The found expressions for the field are exact, but depend on the time-evolution of dipole operators, $\hat{\boldsymbol{\mu}}_m(t)$. The evolution of the dipole operators in turn depend on the evolution of the field and therefore the found field evolution is in fact an implicit equation. The scattered field is thus not explicitly known, but governed by the evolution of $\hat{\boldsymbol{\mu}}_m(t)$ which we will investigate in Sec. 5.3.1. But let us just make a fruitful comparison with the field evolution with the minimal-coupling Hamiltonian.

### 5.2.2 Field Evolution with the Minimal-Coupling Hamiltonian

We will now in a similar fashion as above find the field operator for the full minimal-coupling Hamiltonian. We will find that the coupling between light and atoms will be different than for the electric-dipole coupling and furthermore we will identify the effect of linearizing the Hamiltonian with respect to the vector potential.

Using the generalized transverse mode expansion of the vector potential we get the commutation relation

$$[\hat{a}_\lambda(t);\hat{\mathbf{A}}(\mathbf{r},t)] = \sqrt{\frac{\hbar}{2\varepsilon_0\omega_\lambda}}\mathbf{f}_\lambda(\mathbf{r}). \tag{5.2.13}$$

This gives us

$$[\hat{a}_\lambda(t);\mathcal{H}_{\mathrm{I}}^{\mathrm{min}}] = -\sqrt{\frac{\hbar}{2\varepsilon_0\omega_\lambda}}\sum_m \mathbf{f}^*_\lambda(\mathbf{R}_m)\cdot\left[\dot{\hat{\boldsymbol{\mu}}}_m(t) - \frac{e^2}{m_e}\hat{\mathbf{A}}(\mathbf{R}_m,t)\right], \tag{5.2.14}$$

where the last term in the square brackets is due to the nonlinear term in the Hamiltonian, $\hat{\mathbf{A}}^2$. The square bracket equals $\frac{e}{m_e}$ times the kinetic

momentum operator which is Hermitian and thus we will write $\hat{\mathbf{k}}_m(t)$ for brevity, but remember that it involves the Hilbert spaces of both the field and the dipoles.

With this we get

$$\dot{\hat{a}}_\lambda(t) = -i\omega_\lambda \hat{a}_\lambda(t) + \frac{i}{\sqrt{2\varepsilon_0 \hbar \omega_\lambda}} \sum_m \mathbf{f}_\lambda^*(\mathbf{R}_m) \cdot \left[ \frac{e}{m_e} \hat{\mathbf{k}}_m(t) \right], \tag{5.2.15a}$$

$$\dot{\hat{a}}_\lambda^\dagger(t) = i\omega_\lambda \hat{a}_\lambda^\dagger(t) - \frac{i}{\sqrt{2\varepsilon_0 \hbar \omega_\lambda}} \sum_m \mathbf{f}_\lambda(\mathbf{R}_m) \cdot \left[ \frac{e}{m_e} \hat{\mathbf{k}}_m(t) \right], \tag{5.2.15b}$$

which, using the Laplace transform and insertion in the electric field positive and negative frequency mode expansion, gives

$$\hat{\mathbf{E}}^{(+)}(\mathbf{r},\omega) = \hat{\mathbf{E}}_{(0)}^{(+)}(\mathbf{r},\omega) - \frac{i}{2\varepsilon_0} \sum_m \sum_\lambda \frac{\mathbf{f}_\lambda(\mathbf{r}) \otimes \mathbf{f}_\lambda^*(\mathbf{R}_m)}{\omega - \omega_\lambda} \cdot \left[ \frac{e}{m_e} \hat{\mathbf{k}}_m(\omega) \right], \tag{5.2.16a}$$

$$\hat{\mathbf{E}}^{(-)}(\mathbf{r},\omega) = \hat{\mathbf{E}}_{(0)}^{(-)}(\mathbf{r},\omega) - \frac{i}{2\varepsilon_0} \sum_m \sum_\lambda \frac{\mathbf{f}_\lambda^*(\mathbf{r}) \otimes \mathbf{f}_\lambda(\mathbf{R}_m)}{\omega + \omega_\lambda} \cdot \left[ \frac{e}{m_e} \hat{\mathbf{k}}_m(\omega) \right]. \tag{5.2.16b}$$

The total electric-field operator is then given by

$$\begin{aligned} \hat{\mathbf{E}}(\mathbf{r},\omega) = \hat{\mathbf{E}}_{(0)}(\mathbf{r},\omega) &- i\omega\mu_0 \sum_m \mathbf{G}^{\mathrm{T}}(\mathbf{r},\mathbf{R}_m,\omega) \cdot \mathcal{L}\left\{ \dot{\hat{\boldsymbol{\mu}}}_m(t) \right\}(\omega) \\ &+ \frac{e^2\mu_0}{m_e} \sum_m \mathbf{G}^{\mathrm{T}}(\mathbf{r},\mathbf{R}_m,\omega) \cdot [i\omega \hat{\mathbf{A}}(\mathbf{R}_m,\omega)], \end{aligned} \tag{5.2.17}$$

where we have explicitly written scattering terms due to the linear and quadratic nonlinear parts of the interaction Hamiltonian in the first and the second line, respectively. Let us describe the two different scattering terms separately.

First, let us neglect the term in the second line, i.e. corresponding to having linearized the Hamiltonian. The form of the electric field operator resembles that found in the previous section, Eq. (5.2.8), but there is a subtle difference. The dipole couples only to the generalized transverse modes of the electric field through the transverse Green function $\mathbf{G}^{\mathrm{T}}(\mathbf{r},\mathbf{r}',\omega)$ independent of the model for the dipoles. This is know from classical electromagnetic propagation not to be true and is thus a strong argument against the use of the linearized minimal-coupling Hamiltonian, since it does not reduce to the classical counterpart. Further arguments and discussions on the dispute on which type of interaction Hamiltonian to use can be found in Ref. [52].

Next, let us neglect the first scattering term of Eq. (5.2.17) and take a look at the equation with only the scattering term from the nonlinear part of the Hamiltonian. This corresponds to a far off-resonant illumination of the dipoles. With this term, the equation is seen to be an implicit equation in the field, which becomes most apparent by noticing that $i\omega\hat{\mathbf{A}}(\mathbf{R}_m,\omega) \sim \hat{\mathbf{E}}(\mathbf{r},\omega)$. Furthermore, we see that the scattering is the same as for classical point scattering using Green functions shown in Sec. 2.2.1. Linearizing the Hamiltonian thus corresponds to neglecting non-resonant elastic scattering on the dipoles and thus also corresponds to neglecting the scattering renormalization of the Green function. Since the decay rate and Lamb shift depend on the imaginary and real parts of the Green function the renormalization thus have implications on the on-resonant dipole dynamics.

In conclusion, the linearized minimal-coupling Hamiltonian does not reduce to the classical propagation of the field and it thus does not seem to describe the evolution of the field correctly. The full minimal-coupling Hamiltonian would be preferred for the calculations since it is exact, but the implicitness of the field evolution in Eq. (5.2.17) complicate further calculations. Since we are interested in the inelastic scattering we thus settle with the electric-dipole Hamiltonian for the further calculations of the dipole dynamics under the two-level model since it give the correct coupling to both longitudinal and transverse modes.

## 5.3 Dipole Operator Evolution

In the present section we will investigate the evolution of the operators governing the dipoles. We will introduce the two-level model for the previous unspecified internal dynamics of the dipoles and derive the equations of motion using the electric-dipole Hamiltonian. This will enable us to derive the fluorescence spectrum of a cloud of atoms in the next chapter.

### 5.3.1 Two-Level Dipole Equations of Motion

Let us look at the dynamics of dipoles under the assumption that they can be described by only two energy levels. Such models are much used in the literature due to the simplicity and ability to give qualitatively as well as quantitatively good results [12]. We will go into the details of the derivation of the equations of motion for the dipole operators since it is the simplest model containing saturation effects. The resulting equations of motion will be solved in the next chapter for a dilute cloud of atoms as an example of the use of the formalism derived in this chapter.

In the two-level model, the dipole moment operator, $\hat{\boldsymbol{\mu}}_m(t)$, can be expanded as

$$\hat{\boldsymbol{\mu}}_m(t) = \boldsymbol{\mu}_m \hat{b}_m(t) + \boldsymbol{\mu}_m^* \hat{b}_m^\dagger(t) \tag{5.3.1}$$

where $\boldsymbol{\mu}_m = \langle g_m | \hat{\boldsymbol{\mu}}_m | e_m \rangle$ is the diagonal element of the projection of the $m$'th dipole onto its eigenstates and $\hat{b}_m = |g_m\rangle \langle e_m|$ and $\hat{b}_m^\dagger = |e_m\rangle \langle g_m|$ are the excited-state annihilation and creation operators with $|e_m\rangle$ and $|g_m\rangle$ being the excited and ground states of the $m$'th atom respectively. Note that the dipole moment operator $\hat{\boldsymbol{\mu}}_m(t)$ is Hermitian, $\hat{\boldsymbol{\mu}}_m(t) = \hat{\boldsymbol{\mu}}_m^\dagger(t)$. Thereby the interaction Hamiltonian becomes

$$\mathcal{H}_{\mathrm{I}} = -\sum_m \left[ \boldsymbol{\mu}_m \hat{b}_m(t) + \boldsymbol{\mu}_m^* \hat{b}_m^\dagger(t) \right] \cdot \hat{\mathbf{E}}(\mathbf{R}_m, t). \tag{5.3.2}$$

Furthermore, the free-atom Hamiltonian is given by [12]

$$\mathcal{H}_{\mathrm{A}} = \sum_m \hbar\omega_m \left[ \hat{\sigma}_m(t) + \frac{1}{2} \right] \tag{5.3.3}$$

where $\hat{\sigma}_m = \frac{1}{2}(|e_m\rangle \langle e_m| - |g_m\rangle \langle g_m|)$ is the atomic occupation operator and $\hbar\omega_m$ is the energy difference of the excited and ground states of the $m$'th dipole. The operators have the equal-time commutation relations

$$[\hat{b}_m(t); \hat{\sigma}_{m'}(t)] = \hat{b}_m(t)\delta_{mm'}, \tag{5.3.4a}$$

$$[\hat{b}_m(t); \hat{b}_{m'}^\dagger(t)] = -2\hat{\sigma}_m(t)\delta_{mm'}, \tag{5.3.4b}$$

such that

$$[\hat{\sigma}_m(t); \mathcal{H}_{\mathrm{A}}] = 0, \tag{5.3.5a}$$

$$[\hat{\sigma}_m(t); \mathcal{H}_{\mathrm{I}}^{\mathrm{Ed}}] = \left[ \boldsymbol{\mu}_m \hat{b}_m(t) - \boldsymbol{\mu}_m^* \hat{b}_m^\dagger(t) \right] \cdot \hat{\mathbf{E}}(\mathbf{R}_m, t), \tag{5.3.5b}$$

and

$$[\hat{b}_m(t); \mathcal{H}_{\mathrm{A}}] = \hbar\omega_m \hat{b}_m(t), \tag{5.3.6a}$$

$$[\hat{b}_m(t); \mathcal{H}_{\mathrm{I}}^{\mathrm{Ed}}] = 2\hat{\sigma}_m(t)\boldsymbol{\mu}_m^* \cdot \hat{\mathbf{E}}(\mathbf{R}_m, t). \tag{5.3.6b}$$

We thus get the exact Heisenberg equations of motion

$$\dot{\hat{b}}_m(t) = -i\omega_m \hat{b}_m(t) - 2\frac{i}{\hbar}\hat{\sigma}_m(t)\boldsymbol{\mu}_m^* \cdot \hat{\mathbf{E}}(\mathbf{R}_m, t), \tag{5.3.7a}$$

$$\dot{\hat{\sigma}}_m(t) = \frac{i}{\hbar}\hat{b}_m^\dagger(t)\boldsymbol{\mu}_m^* \cdot \hat{\mathbf{E}}(\mathbf{R}_m, t) + h.c., \tag{5.3.7b}$$

with *h.c.* denoting Hermitian conjugation. As we can see, the evolution of the dipoles depends on the field at the position of the dipole. While the fields in turn depend on the evolution of the dipoles as were found in Sec. 5.2.1. This give our indirect dipole-dipole coupling mediated by the radiative field.

### 5.3.2 The First Approximations

Up until now the derivation has been exact, but we are about to make the first approximations. After carrying out any approximations the field and dipole operators will in general not necessarily commute. We thus reorder the operators such that the electric-field operators are normally ordered. This we do because we shortly assume that the field is in a coherent state and integrate out the initial field operators by taking the expectation value with respect to the Hilbert space of the field. When doing this, it is important that the positive-frequency electric field operators is the first that "meet" the expectation values at the right since the coherent state is a eigenstate of the *positive*-frequency electric field operator. Similar the negative-frequency operators need to be on the left side. As we found in Sec. 5.2 the positive- and negative-frequency field components can be written as a free-field contribution plus a scattering contribution and we thus write

$$\begin{aligned}\dot{\hat{b}}_m(t) = &-i\omega_m\hat{b}_m(t) - 2\frac{i}{\hbar}\hat{\sigma}_m(t)\boldsymbol{\mu}_m^*\cdot\hat{\mathbf{E}}_{(0)}^{(+)}(\mathbf{R}_m,t) - 2\frac{i}{\hbar}\boldsymbol{\mu}_m^*\cdot\hat{\mathbf{E}}_{(0)}^{(-)}(\mathbf{R}_m,t)\hat{\sigma}_m(t)\\ &- 2\frac{i}{\hbar}\hat{\sigma}_m(t)\boldsymbol{\mu}_m^*\cdot\hat{\mathbf{E}}_{\mathrm{Scat}}^{(+)}(\mathbf{R}_m,t) - 2\frac{i}{\hbar}\boldsymbol{\mu}_m^*\cdot\hat{\mathbf{E}}_{\mathrm{Scat}}^{(-)}(\mathbf{R}_m,t)\hat{\sigma}_m(t),\end{aligned} \tag{5.3.8a}$$

$$\begin{aligned}\dot{\hat{\sigma}}_m(t) = &\frac{i}{\hbar}\hat{b}_m^\dagger(t)\boldsymbol{\mu}_m^*\cdot\hat{\mathbf{E}}_{(0)}^{(+)}(\mathbf{R}_m,t) + \frac{i}{\hbar}\boldsymbol{\mu}_m^*\cdot\hat{\mathbf{E}}_{(0)}^{(-)}(\mathbf{R}_m,t)\hat{b}_m^\dagger(t)\\ &+ \frac{i}{\hbar}\hat{b}_m^\dagger(t)\boldsymbol{\mu}_m^*\cdot\hat{\mathbf{E}}_{\mathrm{Scat}}^{(+)}(\mathbf{R}_m,t) + \frac{i}{\hbar}\boldsymbol{\mu}_m^*\cdot\hat{\mathbf{E}}_{\mathrm{Scat}}^{(-)}(\mathbf{R}_m,t)\hat{b}_m^\dagger(t) + h.c.\end{aligned} \tag{5.3.8b}$$

We will perform two approximations, the Born–Markov approximation (BMA) and the RWA. The order at which the approximations are carried out is important for the physics of the system. We will do the BMA first followed by the RWA since this will give us that the interaction between the dipoles is governed by the Green function of the electric field while the reverse would not.

The scattered field for the electric-dipole Hamiltonian was found to be, see Eq. (5.2.11),

$$\hat{\mathbf{E}}_{\mathrm{Scat}}^{(\pm)}(\mathbf{r},t) = \pm\frac{i}{2\varepsilon_0}\sum_m\sum_\lambda\omega_\lambda\mathbf{f}_\lambda(\mathbf{r})\otimes\mathbf{f}_\lambda^*(\mathbf{R}_m)\cdot\int_0^t\mathrm{d}\tau\hat{\boldsymbol{\mu}}_m(\tau)e^{\mp i\omega_\lambda(t-\tau)}. \tag{5.3.9}$$

We are about to perform the BMA which is well known in the theory of light-matter interaction, see eg. [12] or any other textbook on the subject. It is a way of performing a no-memory approximation, known as a Markov approximation, but doing it in a consistent way in which only first-order

interactions are taken into account, corresponding to a first-order Born approximation. The assumption of no memory allows us to simplify the time integral in Eq. (5.3.9). Specifically we write

$$\begin{aligned}\int_0^t \mathrm{d}\tau \hat{\boldsymbol{\mu}}_m(\tau) e^{\mp i\omega_\lambda(t-\tau)} &= \int_0^t \mathrm{d}\tau \left[\boldsymbol{\mu}_m \hat{b}_m(\tau) + h.c\right] e^{\mp i\omega_\lambda(t-\tau)} \\ &= \int_0^t \mathrm{d}\tau \left[\boldsymbol{\mu}_m \hat{b}_{mr}(\tau) e^{-i\omega_m\tau} + h.c.\right] e^{\mp i\omega_\lambda(t-\tau)} \\ &\approx \int_0^t \mathrm{d}\tau \left[\boldsymbol{\mu}_m \hat{b}_{mr}(t) e^{-i\omega_m\tau} + h.c.\right] e^{\mp i\omega_\lambda(t-\tau)} \\ &= \int_0^t \mathrm{d}\tau \left[\boldsymbol{\mu}_m \hat{b}_m(t) e^{i\omega_m(t-\tau)} + h.c.\right] e^{\mp i\omega_\lambda(t-\tau)}, \quad (5.3.10)\end{aligned}$$

where in the second line we introduce the dipole annihilation operator rotating in the frame of reference of a non-interacting dipole, $\hat{b}_{mr}(t) = \hat{b}_m(t)e^{i\omega_m t}$. In the transition from the second to the third line we notice that the scattering field is itself a first-order interaction term and thus we find the time-evolution of the rotating operator, $\hat{b}_{mr}(t-\tau)$, to zeroth-order in the interaction. Because we have moved to a rotating frame we see that the time-derivative of $\hat{b}_{mr}(t)$ is indeed proportional to the interaction and thus to zeroth-order we have $\hat{b}_{mr}(t-\tau) \approx \hat{b}_{mr}(t)$. Notice that, in case we had performed the no-memory approximation without going to the rotating frame we would have thrown away terms even of zeroth order in an uncontrolled way. The BMA is thus more controlled than a simple no-memory approximation.

An important question is of course the validity of the approximation. Since it is a first-order approximation of the interaction between the light and matter it is not valid in cases where any of the field modes of the underlying dielectric material are in resonance with the dipoles such as quantum dots in especially designed resonant nano-cavities. The BMA in connection with the two-level model has however predicted phenomena such as the single-dipole Mollow spectrum [53], experimentally verified for hot atoms in Ref. [54] and quantum dots in micro-pillars in Ref. [55] or photon anti-bunching of light emission from single atom proposed and demonstrated in Ref. [56]. In the next chapter we will investigate the fluorescence spectrum of a dilute cloud of cold atoms. We will do this in the dilute cloud limit in which the interaction between the atoms is weak and thus consistent with the BMA.

Let us continue the derivation of the equations of motion within the BMA and RWA. By the change of variables $\tau' = t - \tau$ we have that in the long-time limit

$$i\int_0^t \mathrm{d}\tau e^{i(\omega_m \mp \omega_\lambda)\tau'} \approx i\int_0^\infty \mathrm{d}\tau e^{i(\omega_m \mp \omega_\lambda)\tau'} = -\frac{1}{\omega_m \mp \omega_\lambda} \qquad (5.3.11)$$

such that the scattered electric field can be written as

$$\begin{aligned}\hat{\mathbf{E}}^{(\pm)}_{\mathrm{Scat}}(\mathbf{R}_m,t) &\approx \mp\frac{1}{2\varepsilon_0}\sum_n \hat{b}_n(t)\sum_\lambda \frac{\omega_\lambda \mathbf{f}_\lambda(\mathbf{R}_m)\otimes\mathbf{f}^*_\lambda(\mathbf{R}_n)\cdot\boldsymbol{\mu}_n}{\omega_n \mp \omega_\lambda} \\ &\quad \mp \frac{1}{2\varepsilon_0}\sum_n \hat{b}^\dagger_n(t)\sum_\lambda \frac{\omega_\lambda \mathbf{f}_\lambda(\mathbf{R}_m)\otimes\mathbf{f}^*_\lambda(\mathbf{R}_n)\cdot\boldsymbol{\mu}^*_n}{-\omega_n \mp \omega_\lambda} \\ &= \sum_n \hat{b}_n(t)\mathbf{U}^{(\pm)}_{mn}\cdot\boldsymbol{\mu}^*_n + \sum_n \hat{b}^\dagger_n(t)\mathbf{V}^{(\pm)}_{mn}\cdot\boldsymbol{\mu}^*_n, \end{aligned} \tag{5.3.12}$$

where, for convenience, we have defined $\mathbf{U}^{(\pm)}_{mn}$ and $\mathbf{V}^{(\pm)}_{mn}$, which are related through $[\mathbf{U}^{(\pm)}_{mn}]^* = \mathbf{V}^{(\mp)}_{mn}$, see App. B.2, and to the kernel of the electric field $\mathbf{K}(\mathbf{r},\mathbf{r}',\omega)$, Eq. (5.2.9), through $\mathbf{U}^{(+)}_{mn} + \mathbf{U}^{(-)}_{mn} = -\mu_0\omega_n^2\mathbf{K}(\mathbf{R}_m,\mathbf{R}_n,\omega_n)$.

We are now able to calculate the scattering field terms for $\hat{b}_m(t)$ and $\hat{\sigma}_m(t)$ in Eqs. (5.3.8), see App. B.2. To do this we use the equal-time relations $\hat{b}^\dagger_m(t)\hat{b}_m(t) = \hat{\sigma}_m + \frac{1}{2}$, $\hat{b}^\dagger_m(t)\hat{\sigma}_m(t) = -\frac{1}{2}\hat{b}^\dagger_m(t)$ and $\hat{b}_m(t)\hat{\sigma}_m(t) = \frac{1}{2}\hat{b}_m(t)$ and their Hermitian conjugates. Furthermore, we use the RWA giving

$$\begin{aligned}\dot{\hat{b}}_m(t) &= (-\beta_m - i\omega_m + i\gamma_m)\hat{b}_m(t) - 2\frac{i}{\hbar}\hat{\sigma}_m(t)\boldsymbol{\mu}^*_m\cdot\hat{\mathbf{E}}^{(+)}_{(0)}(\mathbf{R}_m,t) \\ &\quad + 2i\sum_{n\neq m}\hat{\sigma}_m(t)\hat{b}_n(t)\frac{\mu_0\omega_n^2}{\hbar}\boldsymbol{\mu}^*_m\cdot\mathbf{K}(\mathbf{R}_m,\mathbf{R}_n,\omega_n)\cdot\boldsymbol{\mu}_n, \end{aligned} \tag{5.3.13a}$$

$$\begin{aligned}\dot{\hat{\sigma}}_m(t) &= -2\beta_m\left[\hat{\sigma}_m(t) + \frac{1}{2}\right] + \left[\frac{i}{\hbar}\hat{b}^\dagger_m(t)\boldsymbol{\mu}^*_m\cdot\hat{\mathbf{E}}^{(+)}_{(0)}(\mathbf{R}_m,t) + h.c.\right] \\ &\quad - i\sum_{n\neq m}\hat{b}^\dagger_m(t)\hat{b}_n(t)\frac{\mu_0\omega_n^2}{\hbar}\boldsymbol{\mu}^*_m\cdot\mathbf{K}(\mathbf{R}_m,\mathbf{R}_n,\omega_n)\cdot\boldsymbol{\mu}_n \\ &\quad + i\sum_{n\neq m}\hat{b}^\dagger_n(t)\hat{b}_m(t)\left[\frac{\mu_0\omega_n^2}{\hbar}\boldsymbol{\mu}^*_m\cdot\mathbf{K}(\mathbf{R}_m,\mathbf{R}_n,\omega_n)\cdot\boldsymbol{\mu}_n\right]^*. \end{aligned} \tag{5.3.13b}$$

Here, the decay rate, $\beta_m$, and Lamb shift, $\gamma_m$, have been identified as

$$\beta_m = -\frac{\mu_0\omega_m^2}{\hbar}\mathrm{Im}\left\{\boldsymbol{\mu}^*_m\cdot\mathbf{K}(\mathbf{R}_m,\mathbf{R}_m,\omega_m)\cdot\boldsymbol{\mu}_m\right\}, \tag{5.3.14a}$$

$$\gamma_m = \frac{1}{\hbar}\mathrm{Re}\left\{\boldsymbol{\mu}^*_m\cdot\left[\mathbf{U}^{(+)}_{mm}(t) - \mathbf{U}^{(-)}_{mm}(t)\right]\cdot\boldsymbol{\mu}_m\right\}. \tag{5.3.14b}$$

With the most cumbersome calculations done, it is about time for some physics.

We will start by discussing the parts of the equations that are only governed by local operators, i.e. the diagonal terms. First of all, we notice that

$\beta_m$ is proportional to the imaginary part of the kernel $\mathbf{K}(\mathbf{R}_m, \mathbf{R}_m, \omega_m)$ which is equal to the imaginary part of the retarded Green function, see Eq. (5.2.9). The decay rate of the dipole is thus proportional to the density of optical states projected onto the direction of the dipole moment as we would also expect, e.g. from Fermi's Golden Rule. By changing the density of states it is thus possible to change the decay dynamics. This has been experimentally observed eg. for quantum dots in photonic crystals [57, 58]. Furthermore, we see that the Lamb shift is related to the real part of the kernel $\mathbf{K}(\mathbf{R}_m, \mathbf{R}_m, \omega)$. Interestingly, the real part of $\mathbf{K}(\mathbf{r}, \mathbf{r}', \omega)$ is known to diverge as $\mathbf{r}$ and $\mathbf{r}'$ approach each other. This gives the well-known property that the Lamb shift seems to be infinite. This divergence is though sometimes attributed to lack of inclusion of relativistic effects, see eg. Ref. [12], which would indeed avoid the infinity. From our treatment it is though seen that the divergence could instead be removed by including a finite size of the dipole, e.g. using the regularization procedure of the theory of point scattering, see Ref. [51]. In free space it is well known that such regularization only changes the real part of the Green function and not the imaginary part. It is thus clear that the dynamics of the dipole depends strongly on the possibility of coupling to the surrounding photonic environment.

Next, let us take a look at the coupling of the $m$'th atom to the field and the other atoms in Eq. (5.3.13). The light couples to the dipole $m$ by its initial field operators. The coupling of the free field to $\hat{b}_m$ depends on the excitation $\hat{\sigma}_m$ of the dipole. The coupling to $\hat{\sigma}_m$ on the other hand depends on both $\hat{b}_m$ and $\hat{b}_m^\dagger$. This coupling can be understood by noticing that $\hat{\mathbf{E}}_{(0)}^{(+)}$ is a composition of photon annihilation operators and thus the term $\hat{b}_m^\dagger(t)\boldsymbol{\mu}_m^* \cdot \hat{\mathbf{E}}_{(0)}^{(+)}(\mathbf{R}_m, t)$ corresponds to the annihilation of a photon and excitation of the dipole and vice versa for its hermitian conjugate. At last, the coupling amongst the dipoles is seen to occur through the radiation field via the kernel $\mathbf{K}(\mathbf{R}_m, \mathbf{R}_n, \omega_n)$. This kernel is equal to the retarded Green function for $\mathbf{R}_m \neq \mathbf{R}_n$ and thus the scattering among the dipoles occurs through the same propagator as is found by classical point scattering. It should be noticed that if we had used the RWA at any point before this we would not obtain that the interaction was mediated by the usual classical field Green function, but instead some less physical kernel.

In the next chapter we will investigate the fluorescence spectrum of a driven cloud of cold atoms and we will thus simplify the Eqs. (5.3.13) by assuming identical atoms in vacuum. Furthermore, we will assume a homogeneous coherent driving field such that

$$\hat{\mathbf{E}}_{(0)}^{(+)}(\mathbf{R}_m, t)\,|\psi_{\text{in}}\rangle = \frac{1}{2}\mathbf{E}_0 e^{i\mathbf{k}_0\cdot\mathbf{R}_m - i\omega_0 t}\,|\psi_{\text{in}}\rangle\,, \tag{5.3.15}$$

where $\mathbf{E}_0$ is the electric field amplitude, $\mathbf{k}_0$ is the wave-vector of the incoming field and $\omega_0$ its frequency. It is at this point that we use that the equations of motion are normal ordered with respect to the field operators. We now use this to define the electric field fluctuation operator $\delta\hat{\mathbf{E}}^{(\pm)}_{(0)}(\mathbf{r},t) = \hat{\mathbf{E}}^{(\pm)}_{(0)}(\mathbf{r},t) - \left\langle \hat{\mathbf{E}}^{(\pm)}_{(0)}(\mathbf{r},t) \right\rangle$. We further define the Rabi frequency $\Omega_{\mathrm{R}} = \frac{|\boldsymbol{\mu}\cdot\mathbf{E}_0|}{\hbar\beta}$, the propagator

$$G_{mn} = -\frac{\mu_0\omega_a^2}{\beta\hbar}\boldsymbol{\mu}_m^* \cdot \mathbf{K}(\mathbf{R}_m,\mathbf{R}_n,\omega_a)\cdot\boldsymbol{\mu}_n e^{-i\mathbf{k}_0\cdot(\mathbf{R}_m-\mathbf{R}_n)}, \tag{5.3.16}$$

and the detuning $\Delta = \frac{\omega_0-\omega_a+\gamma}{\beta}$ all normalized with respect to $\beta$ which in vacuum is

$$\beta = \frac{2}{3}\frac{\mu_0\mu_a^2\omega_a^3}{4\pi\hbar c}, \tag{5.3.17}$$

where $\mu_s$ is the magnitude of the dipole moments, $\boldsymbol{\mu}_m$. Notice that $\beta$ is half the so-called Einstein $A$-coefficient or spontaneous-decay rate. Finally, we define the atomic annihilation operator rotating in the frame of the applied field

$$\hat{b}_{mr'}(t) = \hat{b}_m(t)e^{-i\mathbf{k}_0\cdot\mathbf{R}_m+i\omega_0 t}. \tag{5.3.18}$$

Notice that this is not the same rotating frame as in Eq. (5.3.10) hence the subscript $r'$ instead of $r$. With this we get the set of coupled nonlinear differential equations for the atomic operators

$$\begin{aligned}\frac{1}{\beta}\dot{\hat{b}}_{mr'}(t) = &-(1-i\Delta)\hat{b}_{mr'}(t) - i\Omega_{\mathrm{R}}\hat{\sigma}_m(t) + \hat{F}^{(+)}_m(t)\\ &- 2i\sum_{n\neq m}\hat{\sigma}_m(t)\hat{b}_{nr'}(t)G_{mn},\end{aligned} \tag{5.3.19a}$$

$$\begin{aligned}\frac{1}{\beta}\dot{\hat{\sigma}}_m(t) = &-2\left[\hat{\sigma}_m(t)+\frac{1}{2}\right] + \frac{i}{2}\Omega_{\mathrm{R}}\hat{b}^\dagger_{mr'}(t) - \frac{i}{2}\Omega_{\mathrm{R}}\hat{b}_{mr'}(t) + \hat{F}^{(z)}_m(t)\\ &+ i\sum_{n\neq m}\hat{b}^\dagger_{mr'}(t)\hat{b}_{nr'}(t)G_{mn} - i\sum_{n\neq m}\hat{b}^\dagger_{nr'}(t)\hat{b}_{mr'}(t)G^*_{mn},\end{aligned} \tag{5.3.19b}$$

where $\hat{F}^{(+)}_m(t)$ and $\hat{F}^{(z)}_m(t)$ are Langevin noise terms containing combinations of atomic operators and electric field fluctuation operators. These noise terms were suggested by K. Mølmer during the defence of this thesis. They are shown in a future publication not to contribute to the cases studied in the next chapter, but should in general be included.

This is the main result of this section. In the next chapter we will solve this set of equations to find the fluorescent spectrum of a cloud of atoms. We will omit the subscript $r'$ for brevity, but remember that we are rotating with the frame of the driving field. Furthermore we will use the normalized time $t' = t\beta$ and the normalized energies $\omega/\beta$.

## 5.4 Chapter Summary

In this chapter we introduce inelastic scattering by considering light scattered off point-dipoles embedded in an arbitrary dielectric structure. The quantum mechanical description of the interaction between the light and the dipoles through the minimal-coupling and electric-dipole interaction Hamiltonians was stated and briefly discussed.

Using these the Heisenberg equations of motion for the electric field were derived and exact relations between the electric field and dipole operators were found. These relations of the field evolution upon scattering on dipoles showed similarities with classical point scattering and both interaction Hamiltonians gave rise to a free-field evolution and a scattering contribution while the latter included different physics. The scattered field using electric-dipole interaction Hamiltonian consisted of the propagation from the different dipoles through a dyadic kernel which, except for a delta-function contribution, was equal to the full Green function known from classical light propagation. On the other hand, the scattered field in the minimal-coupling Hamiltonian had two contributions, one consisted of the propagation of light emitted from the dipole through the *transverse* Green function. The other term is the elastic scattering of the light on the dipoles. The minimal-coupling Hamiltonian is often linearized in the literature. We found that this corresponds to to neglecting the elastic-scattering component. The elastic-scattering component of the minimal-couping Hamiltonian would complicate further calculations and thus, since the focus of the chapter is on inelastic scattering, we chose to use the electric-dipole interaction Hamiltonian.

We then turned our attention to the evolution of the dipoles by using a two-level model. With this model we found the Heisenberg equations of motion of the dipole operators. In deriving the equations of motion we used the Born–Markov approximation and the rotating-wave approximation. By postponing the use of the rotating-wave approximation to the very end, we found that the interaction amongst the dipoles is governed by the Green function known from classical light propagation. Furthermore, we found that the decay rate of the dipoles is proportional to the imaginary part of the Green function, while the Lamb shift is related to the real part of the

Green function. The equations of motion will be used in the next chapter to explore a driven cloud of cold atoms.

The treatment of the chapter is a generalization to the nonlinear regime of the work of Ref. [50] considering scattering of quantized light on harmonic atoms.

# 6

# Fluorescence Spectrum of a Dilute Cloud of Atoms

In this chapter, we explore the steady-state properties of two-level atoms. We find the fluorescence spectrum of a cloud of cold atoms in a dilute limit for which we predict collective phenomena in the spectrum that depend on the angle of detection.

We begin the chapter in Sec. 6.1 by reviewing the driven single atom where we find the steady-state population and fluorescence spectrum. The spectrum is divided into the elastic and inelastic parts, where the inelastic part reveals the well-known Mollow triplet. We do this in order to be able to distinguish single-atom properties from $N$-atom properties. Next, in Sec. 6.2, we revisit the Heisenberg equations of motions for $N$ coupled two-level atoms, which we found in the previous chapter. After this, in Sec. 6.3 we find the impact on the atomic population of having more than one atom. Then, in Sec. 6.4 we derive the fluorescence spectrum of a dilute cloud of cold atoms which have similarities with the single-atom spectrum, but with distinct differences, some of which are attributed to collective atomic effects. Finally, we summarize the findings of the chapter in Sec. 6.5.

## 6.1 The Single Two-Level Atom

Let us have a look at the properties of a single atom in vacuum modeled as having only a ground and an excited state, $|g\rangle$ and $|e\rangle$, with an energy difference $\hbar\omega_a$. Similar to Refs. [12, 53, 59] we conduct the calculations in the Heisenberg picture. While these references only consider a single atom we will expand the method to $N$ atoms later on, but at this point we perform the calculations for a single atom. The atom is assumed driven by a coherent laser field of frequency $\omega_0$ and wave vector $\mathbf{k}_0$. As described in Sec. 5.3.1 of the previous chapter, the atom is characterized by the population inversion

operator $\hat{\sigma}(t) = \frac{1}{2}(|e\rangle\langle e| - |g\rangle\langle g|)$ and the lowering operator in the frame rotating with the field

$$\hat{b}(t) = |g\rangle\langle e| \exp(i\omega_0 t - i\mathbf{k}_0 \cdot \mathbf{R}), \tag{6.1.1}$$

along with its hermitian conjugate, where $\mathbf{R}$ is the position of the atom. For such a system the equations of motion are, see Eq. (5.3.19),

$$\dot{\hat{b}}(t) = -(1 - i\Delta)\hat{b}(t) - i\Omega_{\mathrm{R}}\hat{\sigma}(t), \tag{6.1.2a}$$

$$\dot{\hat{\sigma}}(t) = -2\left[\hat{\sigma}(t) + \frac{1}{2}\right] + \frac{i}{2}\Omega_{\mathrm{R}}\hat{b}^\dagger(t) - \frac{i}{2}\Omega_{\mathrm{R}}\hat{b}(t), \tag{6.1.2b}$$

which are normalized with respect to the free-space decay rate

$$\beta = \frac{2}{3}\frac{\mu_0|\boldsymbol{\mu}|^2\omega_a^3}{4\pi\hbar c}, \tag{6.1.3}$$

where $\boldsymbol{\mu}$ is the dipole moment of the atom. The parameters of the atomic evolution are the normalized Rabi frequency $\Omega_{\mathrm{R}}$ and detuning $\Delta$.

By defining the vector $\hat{\mathbf{x}}(t) = [\hat{b}^\dagger(t), \hat{b}(t), \hat{\sigma}(t)]$ we then get

$$\dot{\hat{\mathbf{x}}}(t) = -\mathbf{M}\hat{\mathbf{x}}(t) - \mathbf{e}_3, \tag{6.1.4}$$

where we have defined the vector $\mathbf{e}_3 = [0, 0, 1]$ and the matrix

$$\mathbf{M} = \begin{bmatrix} 1 + i\Delta & 0 & -i\Omega_{\mathrm{R}} \\ 0 & 1 - i\Delta & i\Omega_{\mathrm{R}} \\ -\frac{i\Omega_{\mathrm{R}}}{2} & \frac{i\Omega_{\mathrm{R}}}{2} & 2 \end{bmatrix}. \tag{6.1.5}$$

With this it is easy to find the dynamics of the system.

### 6.1.1 Steady-State Population of a Single Atom

First, let us calculate the steady-state population of the atom. The population is given by $\left\langle \hat{b}^\dagger(t)\hat{b}(t) \right\rangle = \langle\hat{\sigma}(t)\rangle + \frac{1}{2}$. By defining $\mathbf{x}(t) = \langle\hat{\mathbf{x}}(t)\rangle$ we have that

$$\mathbf{x}(\infty) = \langle\hat{\mathbf{x}}\rangle_{ss} = -\mathbf{M}^{-1}\mathbf{e}_3 \tag{6.1.6}$$

where $\langle : \rangle_{ss}$ denote the steady state expectation value such that eg. $\langle\hat{\sigma}\rangle_{ss} = \mathbf{e}_3 \cdot \mathbf{x}(\infty) = -\mathbf{e}_3 \cdot \mathbf{M}^{-1}\mathbf{e}_3$. Thereby the steady-state atomic population is

$$\left\langle \hat{b}^\dagger\hat{b} \right\rangle_{ss} = \frac{\Omega_{\mathrm{R}}^2}{2(2 + 2\Delta^2 + \Omega_{\mathrm{R}}^2)} = \frac{\tilde{\Omega}_R^2}{2(1 + \tilde{\Omega}_R^2)}, \tag{6.1.7}$$

where we have defined the effective Rabi frequency $\tilde{\Omega}_R^2 = \frac{\Omega_{\rm R}^2}{2(1+\Delta^2)}$, sometimes known as the saturation parameter. This quantity describes that as the driving field is detuned from the atomic transition, i.e. for large $\Delta^2$, the atom will not be affected as much by the intensity of the driving field, i.e. $\Omega_{\rm R}^2$. We notice that the population only depends on this effective intensity of the incident field, $\tilde{\Omega}_R^2$, and as we increase this the population increases, but saturates at a maximum of $\frac{1}{2}$. This is shown in the upper plot of Fig. 6.1. Notice that the dependence of the population, Eq. 6.1.7, is symmetric in the detuning, $\Delta$.

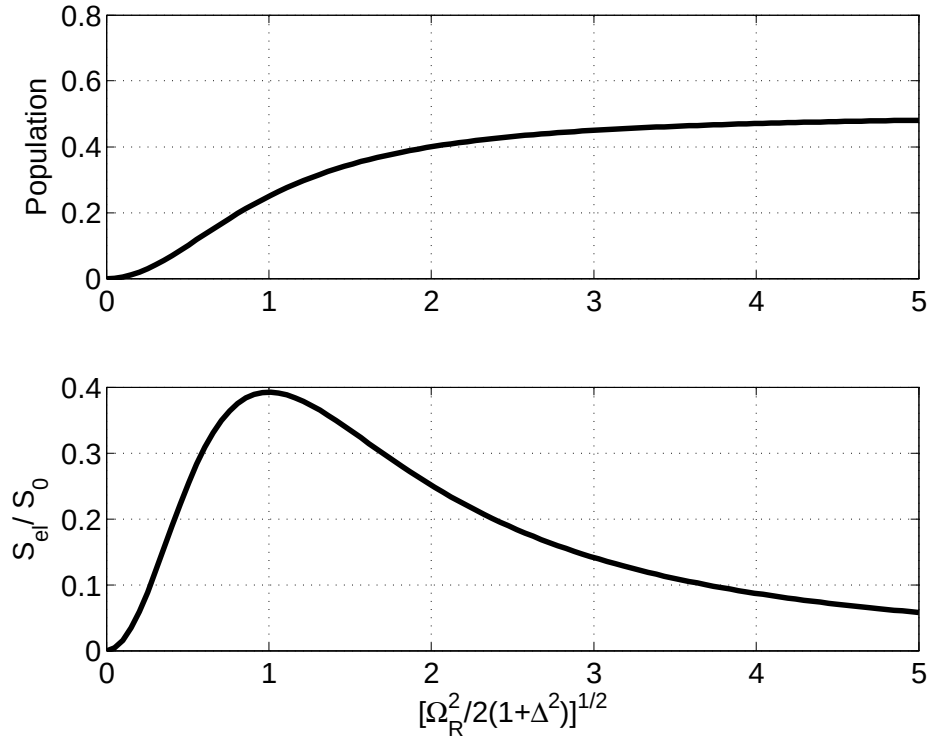


**Figure 6.1** (Top) The single atom population versus effective Rabi frequency, $\tilde{\Omega}_R = \sqrt{\Omega_{\rm R}^2/2(1+\Delta^2)}$. (Bottom) The elastic spectrum of a single atom versus effective Rabi frequency.

### 6.1.2 Fluorescence Spectrum of a Single Atom

Next, we find the steady-state fluorescence spectrum which is defined as, eg. see Ref. [12],

$$S(\mathbf{r},\omega') = \mathrm{Re}\left\{\lim_{t\to\infty}\int_0^\infty \mathrm{d}\tau e^{i\omega'\tau}\left\langle \hat{\mathbf{E}}^{(-)}(\mathbf{r},t)\cdot\hat{\mathbf{E}}^{(+)}(\mathbf{r},t+\tau)\right\rangle\right\}, \qquad (6.1.8)$$

where $\mathbf{r}$ is the position of the detector. We know from Sec. 5.2.1 of the last chapter that the field operators may be written as a free field plus a scattering field. In the far field and using the RWA we have [11]

$$\hat{\mathbf{E}}^{(+)}_{\mathrm{Scat}}(\mathbf{r},t) = -\frac{k_0^2|\boldsymbol{\mu}|\sin\theta\hat{\mathbf{r}}_d}{4\pi\epsilon_0 r}\hat{b}\left(t-\frac{r}{c}\right)e^{-i\omega_0\left(t-\frac{r}{c}\right)+i\mathbf{k}_0\cdot\mathbf{R}}e^{-i\mathbf{k}_d\cdot\mathbf{R}}, \tag{6.1.9}$$

where $\theta$ is the angle between the dipole moment and the vector from the atom to the detector, $\mathbf{k}_d = k_0\hat{\mathbf{r}}_d$, and $\hat{\mathbf{r}}_d$ being the unit vector pointing from the atom to the detector. For simplicity we will assume that we can filter out the free field, eg. by measuring in a direction away from the incident light, and will omit the $r/c$ time contribution in the operator since we are taking the long-time limit anyway. We then get

$$S(\mathbf{r},\omega) = S_0\mathrm{Re}\left\{\lim_{t\to\infty}\int_0^\infty \mathrm{d}\tau e^{i\omega\tau}\left\langle\hat{b}^\dagger(t)\hat{b}(t+\tau)\right\rangle\right\}, \tag{6.1.10}$$

where we have defined the frequency centered around the frequency of the driving field $\omega = \omega' - \omega_0$ and the prefactor of the spectrum

$$S_0 = \left(\frac{k_0^2|\boldsymbol{\mu}|\sin\theta}{4\pi\epsilon_0 r}\right)^2. \tag{6.1.11}$$

In order to calculate the spectrum we thus need to find the Laplace transform of $\left\langle\hat{b}^\dagger(t)\mathbf{e}_2\cdot\hat{\mathbf{x}}(t+\tau)\right\rangle$ with respect to $\tau$, where $\mathbf{e}_2 = [0,1,0]$, and subsequently take the long-time limit of time $t$. Proceeding with the Laplace transform with respect to $\tau$ of $\hat{\mathbf{x}}(t+\tau)$, Eq. (6.1.4), we get

$$\hat{\mathbf{x}}(\omega) = (\mathbf{M} - i\omega\mathbf{I})^{-1}\left[\hat{\mathbf{x}}(t) - \frac{i}{\omega}\mathbf{e}_3\right], \tag{6.1.12}$$

where $\mathbf{I}$ is the unit matrix. From the equal-time operator relations $\hat{b}^\dagger(t)\hat{b}^\dagger(t) = 0$, $\hat{b}^\dagger(t)\hat{b}(t) = \hat{\sigma}(t) + \frac{1}{2}$, and $\hat{b}^\dagger(t)\hat{\sigma}(t) = -\frac{1}{2}\hat{b}^\dagger(t)$ we have that

$$\hat{b}^\dagger(t)\left[\hat{\mathbf{x}}(t) - \frac{i}{\omega}\mathbf{e}_3\right] = \left(\mathbf{U} - \frac{i}{\omega}\mathbf{V}\right)\hat{\mathbf{x}}(t) + \frac{1}{2}\mathbf{e}_2, \tag{6.1.13}$$

with the matrices

$$\mathbf{U} = \begin{bmatrix} 0 & 0 & 0 \\ 0 & 0 & 1 \\ -\frac{1}{2} & 0 & 0 \end{bmatrix}, \qquad \mathbf{V} = \begin{bmatrix} 0 & 0 & 0 \\ 0 & 0 & 0 \\ 1 & 0 & 0 \end{bmatrix}. \tag{6.1.14}$$

With this we get that

$$\left\langle \hat{b}^\dagger(t)\mathbf{e}_2 \cdot \hat{\mathbf{x}}(\omega) \right\rangle_{ss} = \mathbf{e}_2 \cdot (\mathbf{M} - i\omega\mathbf{I})^{-1} \left[ \left( \frac{i}{\omega}\mathbf{V} - \mathbf{U} \right) \mathbf{M}^{-1}\mathbf{e}_3 + \frac{1}{2}\mathbf{e}_2 \right]. \tag{6.1.15}$$

Using the small positive imaginary part of $\omega$ in the definition of the Laplace transform we recognize that $\omega^{-1} = P(\omega^{-1}) - i\pi\delta(\omega)$, and from physical considerations we identify the delta function contribution as the elastic part of the spectrum. That is, the elastic spectrum is given by

$$\begin{aligned} \frac{S_{\mathrm{el}}(\mathbf{r},\omega)}{S_0} &= \pi \mathbf{e}_2 \cdot \mathbf{M}^{-1}\mathbf{V}\mathbf{M}^{-1}\mathbf{e}_3 \delta(\omega) \\ &= \frac{\pi\tilde{\Omega}_R^2}{2\left(1+\tilde{\Omega}_R^2\right)^2}\delta(\omega) = \frac{\pi\delta(\omega)}{1+\tilde{\Omega}_R^2}\left\langle \hat{b}^\dagger\hat{b} \right\rangle_{ss}, \end{aligned} \tag{6.1.16}$$

where the subscript el indicates the elastic part of the spectrum and we have identified the steady-state population, Eq. (6.1.7). The elastic spectrum is shown in the lower plot of Fig. 6.1 versus $\tilde{\Omega}_R$. As we increase the effective intensity, $\tilde{\Omega}_R^2$, the magnitude of the elastically scattered spectrum increases until $\tilde{\Omega}_R^2 = 1$ after which the scattering decreases. This is because as we increase the intensity the population increases and thus the light will increasingly interact with the atoms and thus scatter inelastically. This brings us to the inelastic spectrum which is given by

$$\begin{aligned} \frac{S_{\mathrm{in}}(\mathbf{r},\omega)}{S_0} &= \mathrm{Re}\left\{ \mathbf{e}_2 \cdot (\mathbf{M} - i\omega)^{-1} \left[ \left( \frac{i}{\omega}\mathbf{V} - \mathbf{U} \right) \mathbf{M}^{-1}\mathbf{e}_3 + \frac{1}{2}\mathbf{e}_2 \right] \right\} \\ &= \mathrm{Re}\left\{ \frac{i\omega\Omega_{\mathrm{R}}^2 - 2(2-i\omega)\left[\Delta^2 + (1-i\omega)^2\right]}{2i\omega(2-i\omega)\left[\Delta^2 + (1-i\omega)^2\right] + 2i\omega(1-i\omega)\Omega_{\mathrm{R}}^2} \right\} \frac{\left\langle \hat{b}^\dagger\hat{b} \right\rangle_{ss}}{2}. \end{aligned} \tag{6.1.17}$$

By partial-fraction decomposition this can be written as a sum of three Lorentzian terms. These correspond to three spectral components, the center and the two sidebands of the well-known Mollow triplet [53]. Physically, the three components are caused by the hybridization of the combined atomic and the electromagnetic field states which occur when the atom is driven sufficiently strong.

The general decomposed expression of Eq. (6.1.17) is rather long and will not be stated here. In the case of zero detuning, $\Delta = 0$, the sidebands occur when $\Omega_{\mathrm{R}} > \frac{1}{2}$ and are located at the frequencies $\pm\sqrt{\Omega_{\mathrm{R}}^2 - \frac{1}{4}}$ symmetrically

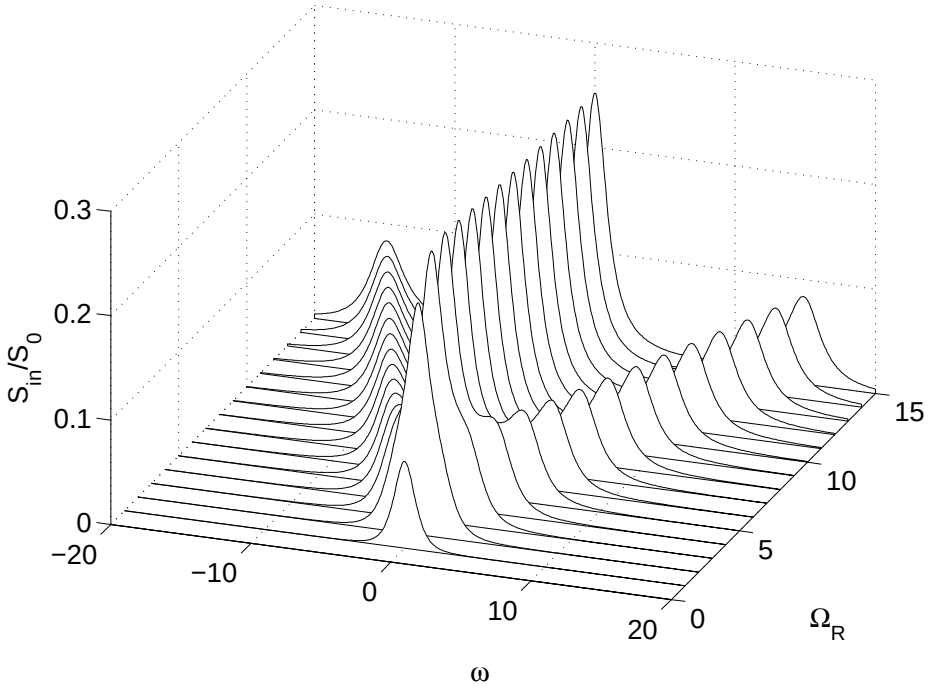


**Figure 6.2** The single-atom inelastic spectrum, $S_{\rm in}$, versus Rabi frequency, $\Omega_{\rm R}$, for zero detuning, $\Delta = 0$.

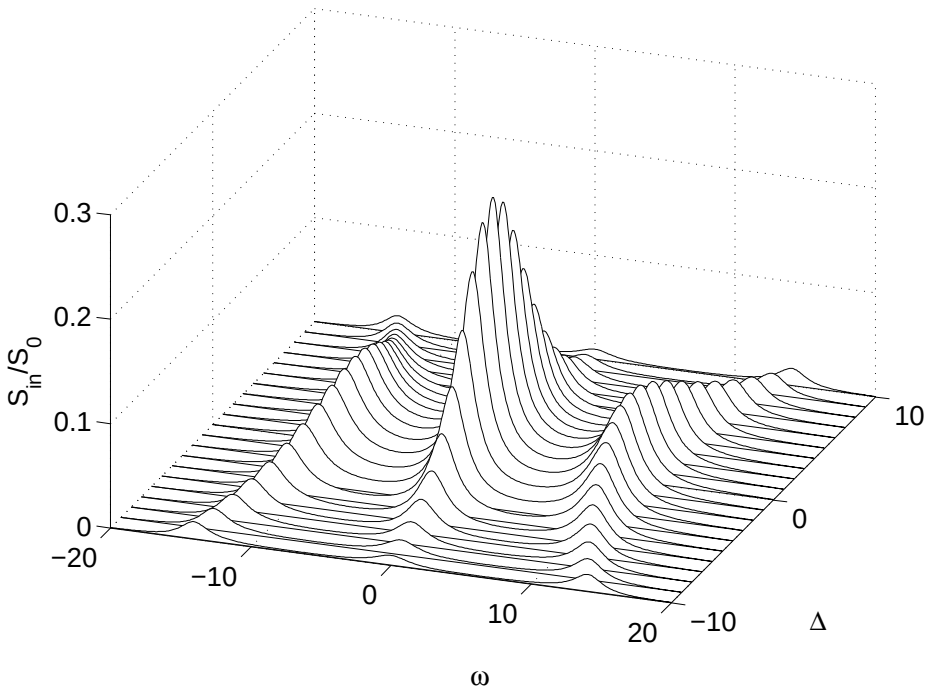


**Figure 6.3** The single-atom inelastic spectrum, $S_{\rm in}$, versus detuning, $\Delta$, for a Rabi frequency of $\Omega_{\rm R} = 10$.

around the central peak. In the general case there are three things that should be noted. Although difficult to see from Eq. (6.1.17) i) the single atom spectrum is symmetric around the central peak for all values of detuning $\Delta$ and Rabi frequency $\Omega_{\mathrm{R}}$, ii) the position of the two sidebands depends on $\Omega_{\mathrm{R}}$ and $\Delta$, and iii) the magnitude of all three peaks decreases when $|\Delta|$ is increased independent of the sign of $\Delta$. These features can be seen in Figs. 6.2 and 6.3. Here, Fig. 6.2 shows the inelastic spectrum versus Rabi frequency, $\Omega_{\mathrm{R}}$, for zero detuning, $\Delta = 0$, illustrating the splitting into the three peaks. In Fig. 6.3 the spectrum versus the detuning, $\Delta$, for a Rabi frequency of $\Omega_{\mathrm{R}} = 10$ is shown. As the driving field is detuned from the atomic transition, the strength of the spectral peaks decrease symmetrically. With this we will end the discussion of the single-atom fluorescence spectrum while we are about to investigate a cloud of atoms. We should though keep the single-atom properties in mind in order to compare with those of the atomic cloud.

## 6.2 The Dilute Atomic Cloud

We now turn our attention to the cloud of $N$ identical atoms. In this section we will describe the equations of motion that we will use to find the steady-state population in Sec. 6.3 and the fluorescence spectrum in Sec. 6.4.

The equations of motion for the $N$ two-level atoms was found in the previous chapter, Eq. (5.3.19), to be

$$\dot{\hat{b}}_m(t) = -(1 - i\Delta)\hat{b}_m(t) - i\Omega_{\mathrm{R}}\hat{\sigma}_m(t) - 2i\sum_{n\neq m}\hat{\sigma}_m(t)\hat{b}_n(t)G_{mn}, \tag{6.2.1a}$$

$$\dot{\hat{\sigma}}_m(t) = -2\left[\hat{\sigma}_m(t) + \frac{1}{2}\right] + \frac{i}{2}\Omega_{\mathrm{R}}\hat{b}_m^\dagger(t) - \frac{i}{2}\Omega_{\mathrm{R}}\hat{b}_m(t) + i\sum_{n\neq m}\hat{b}_m^\dagger(t)\hat{b}_n(t)G_{mn} - i\sum_{n\neq m}\hat{b}_n^\dagger(t)\hat{b}_m(t)G_{mn}^*, \tag{6.2.1b}$$

where, like in the single atom case, $\Omega_{\mathrm{R}}$ is the Rabi frequency, $\Delta$ is the detuning, and we have neglected the Langevin terms. Furthermore, when more than one atom is present, the atoms will couple by a dipole-dipole interaction via the electric field through $G_{mn}$. We found in the previous chapter that this inter-atomic coupling is proportional to the Green function known from classical scattering of electromagnetic waves. As we learned in Sec. 2.2.1 of Chap. 2 the Green function describes the probability amplitude of propagation from one point to another and $G_{mn}$ is thus related to the probability of light emitted at one atom to arrive at the other. The Green function for light propagation in vacuum can be found analytically, see eg.

Ref. [51], such that if we assume that the dipoles are randomly oriented, we have, see App. C.1,

$$G_{mn} = \frac{e^{ik_a R_{mn}}}{k_a R_{mn}} e^{-i\mathbf{k}_0 \cdot \mathbf{R}_{mn}} \tag{6.2.2}$$

where $k_a = \frac{\omega_a}{c}$, $R_{mn} = |\mathbf{R}_{mn}| = |\mathbf{R}_m - \mathbf{R}_n|$ is the length between the $m$'th and the $n$'th atom, and $\mathbf{k}_0$ is the wave vector of the driving field. The assumption of randomly oriented dipoles corresponds to using the far field part of the Green function which is justified below.

It is of course not feasible to exactly solve the dynamics of the atoms under general conditions, since an experiment considering clouds of atoms often contains large numbers of atoms, eg. the number of atoms is $N \sim 10^7 - 10^9$ in Ref. [60]. Previous investigations have thus considered limiting cases such as assuming extremely dilute clouds, $G_{mn} = 0$, [61], linearizing the atomic operator equations by assuming weakly driven atoms, i.e. $\hat{\sigma}_m = -\frac{1}{2}$, [60, 62, 63], or having only few atoms, $N \sim 2 - 5$, [64, 65, 66, 67]. In the following we will do a combination which go beyond the three in that we will look at a dilute cloud, where interactions small, but not zero as Ref. [61] take them. Thereby we are able to observe changes in the spectrum similar to those for two atoms of Refs. [64, 66] while keeping the cooperative interference effects that exist in large clouds as considered in Refs. [61, 63]. We thus assume that the atoms are far apart, justifying the use of the far field Green function, and only take terms to first order in $G_{mn}$ into account corresponding to a single-scattering approximation.

Using the same approach as in the previous section we write up the equations of motion in matrix form

$$\dot{\hat{\mathbf{x}}}_m(t) = -\mathbf{M}\hat{\mathbf{x}}_m(t) - \mathbf{e}_3 - \sum_{n \neq m} \left( i\mathbf{Q}G_{mn} - i\tilde{\mathbf{Q}}G^*_{mn} \right) \hat{\mathbf{y}}_{mn}(t), \tag{6.2.3a}$$

$$\dot{\hat{\mathbf{y}}}_{mn}(t) = -\mathbf{A}\hat{\mathbf{y}}_{mn}(t) - \mathbf{B}\hat{\mathbf{x}}_m(t) - \tilde{\mathbf{B}}\hat{\mathbf{x}}_n(t) + \mathcal{O}(G_{mn}), \tag{6.2.3b}$$

where $\hat{\mathbf{x}}_m(t)$ like for the single atom case is a vector containing the three operators of the $m$'th atom, while $\hat{\mathbf{y}}_{mn}(t)$ is a vector which contains the 9 combinations of the operator products of the $m$'th and $n$'th atomic operators with $m \neq n$, e.g. the first component of $\hat{\mathbf{y}}_{mn}(t)$ is $\hat{b}^\dagger_m(t)\hat{b}_n(t)$. The equation for $\hat{\mathbf{y}}_{mn}(t)$ is to zeroth order in the interaction $G_{mn}$ according to our single scattering approximation since solving for $\hat{\mathbf{y}}_{mn}$ and insertion in the equation for $\hat{\mathbf{x}}_m$ gives to $\hat{\mathbf{x}}_m(t)$ to first order. By writing the products of the different operators as a new operator we include inter-atomic coherences. The matrix $\mathbf{M}$ governs the evolution of the atom due to the driving and is the same as in the single atom case. Similar to $\mathbf{M}$ for $\hat{\mathbf{x}}_m(t)$, the matrix $\mathbf{A}$ govern

the evolution of $\hat{\mathbf{y}}_{mn}(t)$ due to the driving. The matrices $\mathbf{Q}$ and $\tilde{\mathbf{Q}}$ couple $\hat{\mathbf{x}}_m(t)$ to $\hat{\mathbf{y}}_{mn}(t)$ due to the dipole interaction while $\mathbf{B}$ and $\tilde{\mathbf{B}}$ couple $\hat{\mathbf{y}}_{mn}(t)$ to $\hat{\mathbf{x}}_m(t)$ and $\hat{\mathbf{x}}_n(t)$. In case the field was not isotropic the matrices $\mathbf{M}$ and $\mathbf{A}$ would depend on the specific atoms, i.e. $\mathbf{M} \to \mathbf{M}_m$ and $\mathbf{A} \to \mathbf{A}_{mn}$. In case the atoms were fluorescent nanospheres embedded in a random dielectric structure, such as in the experiment of Ref. [68], all the matrices would depend on the emission properties of the specific emitter. The matrices are written out in App. C.5.

We will use the coupled set of equations to find the same steady-state population and fluorescence spectrum of the cloud of atoms as we did for the single atom. We begin with the steady-state population.

## 6.3 Steady-State Population of a Cloud of $N$ Atoms

Similar to the procedure of the single atom we now determine the steady-state population. We write the derivation in some detail since the calculations will give us some insight in the validity of the single-scattering approximation. We define the expectation values of $\mathbf{x}_m(t) = \langle \hat{\mathbf{x}}_m(t) \rangle$ and $\mathbf{y}_{mn}(t) = \langle \hat{\mathbf{y}}_{mn}(t) \rangle$ and use the term "local" for the atom $m$. In steady state we get

$$\begin{aligned} \mathbf{0} = &-\mathbf{M}\mathbf{x}_m(\infty) - \mathbf{e}_3 \\ &+ \left( i\mathbf{Q}G_m - i\tilde{\mathbf{Q}}G_m^* \right) \mathbf{A}^{-1}\mathbf{B}\mathbf{x}_m(\infty) \\ &+ \sum_{n \neq m} \left( i\mathbf{Q}G_{mn} - i\tilde{\mathbf{Q}}G_{mn}^* \right) \mathbf{A}^{-1}\tilde{\mathbf{B}}\mathbf{x}_n(\infty), \end{aligned} \quad (6.3.1)$$

where

$$G_m = \sum_{n \neq m} G_{mn} \quad (6.3.2)$$

has been defined. The quantity $G_m$ concerns the total probability amplitude of light emitted from any of the other atoms to arrive at the atom $m$ and vice versa for the complex conjugate. We see that the local properties of the atom are given by two contributions, a single-atom contribution (the first line) and a correction term due to the change in the electromagnetic environment caused by the presence of all the other atoms (the second line). Furthermore, the local properties of the atom depend on the properties of all the other atoms coupled through the electromagnetic field (the third line).

Now, let us write Eq. (6.3.1) as a $3N \times 3N$ matrix equation. We do this by defining the block-diagonal matrices $\mathbf{M}^{(N)}$ and $\mathbf{\Lambda}$ and the block-off-diagonal block matrix $\mathbf{\Pi}$. The block-matrix elements of $\mathbf{M}^{(N)}$ are the

single-atom matrices $\mathbf{M}$ while the block elements of the matrices $\mathbf{\Lambda}$ and $\mathbf{\Pi}$ are the diagonal and off-diagonal interaction corrections respectively, i.e.

$$\{\mathbf{M}^{(N)}\}_{mn} = \mathbf{M}\delta_{mn}, \tag{6.3.3a}$$

$$\{\mathbf{\Lambda}\}_{mn} = \left(i\mathbf{Q}G_m - i\tilde{\mathbf{Q}}G_m^*\right)\mathbf{A}^{-1}\mathbf{B}\delta_{mn}, \tag{6.3.3b}$$

$$\{\mathbf{\Pi}\}_{mn} = \left(i\mathbf{Q}G_{mn} - i\tilde{\mathbf{Q}}G_{mn}^*\right)\mathbf{A}^{-1}\tilde{\mathbf{B}}(1-\delta_{mn}). \tag{6.3.3c}$$

Furthermore, we write the length-$3N$ vectors $\mathbf{X}(\infty)$ and $\mathbf{C}$ having the elements $\{\mathbf{X}(\infty)\}_m = \mathbf{x}_m(\infty)$ and $\{\mathbf{C}\}_m = \mathbf{e}_3$. With this we can write Eq. (6.3.1) as

$$\mathbf{X}(\infty) = -\left[\mathbf{M}^{(N)} - \mathbf{\Lambda} - \mathbf{\Pi}\right]^{-1}\mathbf{C}. \tag{6.3.4}$$

We will now make use of the fact that we are dealing with a dilute cloud such that the scattering is weak, and we only aim to find the population to first order in the scattering. We do this by writing $\left[\mathbf{M}^{(N)} - \mathbf{\Lambda} - \mathbf{\Pi}\right]^{-1}$ as a geometric series and taking only the first term into account, i.e.

$$\begin{aligned}
[\mathbf{M}^{(N)} - \mathbf{\Lambda} - \mathbf{\Pi}]^{-1} &= \{\mathbf{I} - [\mathbf{M}^{(N)}]^{-1}(\mathbf{\Lambda} + \mathbf{\Pi})\}^{-1}[\mathbf{M}^{(N)}]^{-1} \\
&= \sum_n \{[\mathbf{M}^{(N)}]^{-1}(\mathbf{\Lambda} + \mathbf{\Pi})\}^n [\mathbf{M}^{(N)}]^{-1} \\
&\approx \{\mathbf{I} + [\mathbf{M}^{(N)}]^{-1}(\mathbf{\Lambda} + \mathbf{\Pi})\}[\mathbf{M}^{(N)}]^{-1}.
\end{aligned} \tag{6.3.5}$$

This is actually equivalent to making the first order Born-approximation and is thus consistent with the use of the Born–Markov approximation as explained in Sec. 5.3.1 of the previous chapter. This is e.g. opposed to the treatments of the fluorescence spectrum of two atoms in Refs. [64, 66] where, under the same approximations as here (the BMA and RWA), it is assumed valid to take all orders of the inter-atomic scattering into account. The beauty of our formulation of the approximation as a cut-off in the geometric series, is that we directly obtain a criterion of its validity, i.e.

$$||\mathbf{\Lambda} + \mathbf{\Pi}|| \ll ||\mathbf{M}^{(N)}||, \tag{6.3.6}$$

where $||:||$ is the matrix infinity norm. We will go further into the details of this validity criterion shortly, but let us first complete the calculations of the steady-state population.

We notice that, since all the block vector elements of $[\mathbf{M}^{(N)}]^{-1}\mathbf{C}$ are equal, we get

$$\left\{\mathbf{\Pi}[\mathbf{M}^{(N)}]^{-1}\mathbf{C}\right\}_m = \left(i\mathbf{Q}G_m - i\tilde{\mathbf{Q}}G_m^*\right)\mathbf{A}^{-1}\tilde{\mathbf{B}}\mathbf{M}^{-1}\mathbf{e}_3. \tag{6.3.7}$$

We thus have that the steady-state operators of the $m$'th atom can be written as a zeroth- and a first-order contribution, i.e. $\mathbf{x}_m(\infty) \approx \mathbf{x}_m^{(0)}(\infty) + \mathbf{x}_m^{(1)}(\infty)$, with

$$\mathbf{x}_m^{(0)}(\infty) = -\mathbf{M}^{-1}\mathbf{e}_3, \tag{6.3.8a}$$

$$\mathbf{x}_m^{(1)}(\infty) = -\mathbf{M}^{-1}\left(i\mathbf{Q}G_m - i\tilde{\mathbf{Q}}G_m^*\right)\mathbf{A}^{-1}(\mathbf{B}+\tilde{\mathbf{B}})\mathbf{M}^{-1}\mathbf{e}_3. \tag{6.3.8b}$$

That is, the steady-state population is given by a zeroth-order term which equals the single-atom population found in the previous section

$$\left\langle \hat{b}_m^\dagger \hat{b}_m \right\rangle_{ss}^{(0)} = \frac{\tilde{\Omega}_R^2}{2(1+\tilde{\Omega}_R^2)}, \tag{6.3.9}$$

plus the first-order correction given by

$$\left\langle \hat{b}_m^\dagger \hat{b}_m \right\rangle_{ss}^{(1)} = -\frac{(\mathrm{Im}\{G_m\} + \mathrm{Re}\{G_m\}\,\Delta)\tilde{\Omega}_R^2}{(1+\Delta^2)\left(1+\tilde{\Omega}_R^2\right)^3}. \tag{6.3.10}$$

First, as would be expected when including interactions, the population depends on the actual position of the atom. This occurs through $G_m$, Eq (6.3.2), and thus the correction to the specific atom depends on the probability for light from the other atoms to actually arrive at this atom. Second, different from the single-atom case, the correction term *does* depend on the sign of the detuning, $\Delta$. Specifically, the term concerning the real part of $G_m$ is asymmetric in $\Delta$ and gives rise to a a shift in value of the detuning at which maximal population is obtained. This is consistent with $G_m$ being related to the change in the photonic environment due to the appearance of all the other atoms and the real part of $G_m$ thus gives the corresponding change in the Lamb shift. The imaginary part of $G_m$ then corresponds to the change in the decay rate and thus changes the width of the excitation peak.

In Figs. 6.4 and 6.5 we treat $G_m$ as a parameter to show these behaviors. The effect of $\mathrm{Re}\{G_m\}$ is shown in Fig. 6.4 for $G_m$ purely real-valued in the range $G_m \in [-\frac{1}{2}; \frac{1}{2}]$ while the effect of the imaginary part is shown in Fig. 6.5 with $G_m$ purely imaginary in the range $G_m \in [-\frac{i}{2}; \frac{i}{2}]$. Both plots are with $\Omega_\mathrm{R} = 1$ and as the Rabi frequency increases the effect of the interaction decreases (not shown). As we will see, these used values of $G_m$ are exaggerated and the validity of the approximation for these values is questionable, but we use these values for the purpose of illustration. Before we move on to derive the fluorescence spectrum, we investigate realistic values of $G_m$ by ensemble averaging with respect to position and use this to discuss the range of validity of the single-scattering approximation.

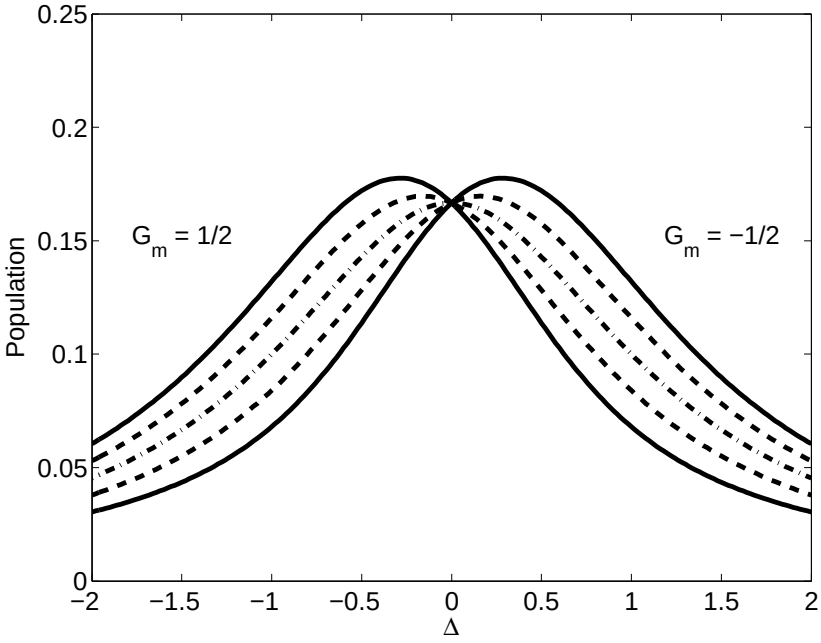


**Figure 6.4** The population versus detuning, $\Delta$, for various real values of $G_m$ in the range $G_m \in [-\frac{1}{2};\frac{1}{2}]$ and a fixed Rabi frequency of $\Omega_{\rm R} = 1$. The solid lines correspond to $G_m = \pm\frac{1}{2}$, the dashed lines to $G_m = \pm\frac{1}{4}$, and the dash-dotted line to the noninteracting case $G_m = 0$.

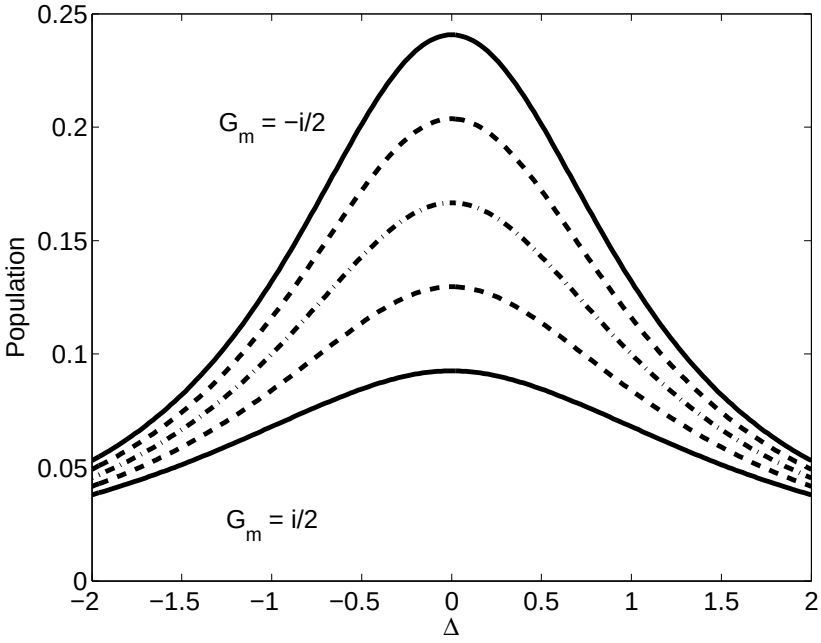


**Figure 6.5** The population versus detuning, $\Delta$, for various imaginary values of $G_m$ in the range $G_m \in [-\frac{i}{2};\frac{i}{2}]$ and a fixed Rabi frequency of $\Omega_{\rm R} = 1$. The solid lines correspond to $G_m = \pm\frac{i}{2}$, the dashed lines to $G_m = \pm\frac{i}{4}$, and the dash-dotted line to the noninteracting case $G_m = 0$.

### 6.3.1 Ensemble-Averaged Interaction

In an actual experiment the position of the individual atoms is most often random and unknown and thus only the averaged properties can be predicted. We therefore determine the value of $G_{mn}$ averaged with respect to the positions of the $m$'th and $n$'th atoms. With the expression for $G_{mn}$, Eq. (6.2.2), the ensemble average over the atomic positions can be written as

$$\overline{G_{mn}} = \int \mathrm{d}\mathbf{r} n(\mathbf{r}) \int \mathrm{d}\mathbf{r}' n(\mathbf{r}') \frac{e^{i[k_a|\mathbf{r}-\mathbf{r}'|-\mathbf{k}_0\cdot(\mathbf{r}-\mathbf{r}')]}}{k_a|\mathbf{r}-\mathbf{r}'|}, \tag{6.3.11}$$

where $n(\mathbf{r})$ is the distribution of atomic positions and since $m \neq n$ in $G_{mn}$ the positions $\mathbf{r}$ and $\mathbf{r}'$ are uncorrelated. We will assume that the cloud has Gaussian shape with thickness $\tilde{\rho}$, i.e.

$$n(\mathbf{r}) = \frac{1}{\sqrt{(2\pi\tilde{\rho}^2)^3}} \exp\left(-\frac{r^2}{2\tilde{\rho}^2}\right). \tag{6.3.12}$$

The assumption of a Gaussian shaped cloud corresponds to the use of harmonic potentials in the magnetic traps that often hold the atomic cloud. Furthermore, assuming this particular distribution makes it possible to split the multidimensional integrals in the average into two independent ones. In this way we get, see App. C.1.2,

$$\overline{G_{mn}} = \frac{1}{(2\rho)^2}\left[e^{-4\rho^2}\mathrm{Erfi}(2\rho) + i\left(1 - e^{-4\rho^2}\right)\right], \tag{6.3.13}$$

where $\rho = k_a\tilde{\rho}$ is the cloud size normalized with the atomic wavenumber and $\mathrm{Erfi}(x)$ is the imaginary error function which is related to the usual error function, $\mathrm{Erf}(x)$, through $\mathrm{Erfi}(x) = -i\mathrm{Erf}(ix)$. For large clouds ($\rho > 5$) this further simplifies to

$$\overline{G_{mn}} \approx \frac{1}{(2\rho)^2}\left[\frac{1}{2\sqrt{\pi}\rho} + i\right]. \tag{6.3.14}$$

For a cloud of thickness $\rho = 5000$ and with $N = 10^8$ atoms [60] we have that $\overline{G_m} = N\overline{G_{mn}} \approx 10^{-4} + i$ and thus for large clouds $\overline{G_{mn}}$ is almost purely imaginary. By comparison, the values of Fig. 6.4 are thus exaggerated, but still serve as a nice illustration of the real part of the interaction.

We now introduce the off-resonance optical thickness $b(\Delta) = b_0/(1+\Delta^2)$, with $b_0 = 3N/\rho^2$ being the on-resonance optical thickness for a Gaussian shaped cloud, see eg. Ref. [63]. The off-resonance optical thickness is a

measure of how dense the atomic cloud is for the driving field. That is, if the driving field is detuned from the atomic transition, it will experience less scattering and the cloud is effectively less dense. With this we obtain that, for large $\rho$ and $N$, the average correction to the population of one of the atoms, Eq. (6.3.10), is

$$\overline{\left\langle \hat{b}_m^\dagger \hat{b}_m \right\rangle_{ss}^{(1)}} = -\frac{b(\Delta)\tilde{\Omega}_R^2}{12\left(1+\tilde{\Omega}_R^2\right)^3}, \tag{6.3.15}$$

by using that $\overline{G_m} = N\overline{G_{mn}} \approx i\frac{b_0}{12}$. This correction to the population due to the interaction with the other atoms increases as the effective thickness of the cloud, $b(\Delta)$, increases. Furthermore, when the effective intensity, $\tilde{\Omega}_R^2$, is increased, the effect of the correction decreases. This can be understood by noticing that the effect on the $m$'th atom due to the dipole-dipole interaction, $G_{mn}$ terms in Eq. (6.2.1), will become relatively smaller than the effect of the driving field, $\Omega_{\mathrm{R}}$.

We will now asses the range of validity of our single scattering approximation. The validity criterion for the single-scattering approximation given by Eq. (6.3.6), can be written into a form where the parameters of the driving field, $\Omega_{\mathrm{R}}$ and $\Delta$, and those of the atomic cloud, $G_{mn}$ and $N$, are separated, see App. C.4. There are three criteria depending on the relative magnitude of $\Omega_{\mathrm{R}}$ and $\Delta$, see Eqs. (C.4.7) to (C.4.9), and they can be written as

$$\frac{\sum_m |\sum_{n\neq m} G_{mn}|}{N} \ll \begin{cases} 2\Omega_{\mathrm{R}}, & 2\sqrt{1+\Delta^2} < \Omega_{\mathrm{R}} \\ 2\sqrt{1+\Delta^2}+\Omega_{\mathrm{R}}, & 2 < \Omega_{\mathrm{R}} < 2\sqrt{1+\Delta^2} \\ 2(1+\sqrt{1+\Delta^2}), & \Omega_{\mathrm{R}} < 2 \end{cases} . \tag{6.3.16}$$

In order to get an analytical expression so that we can get a physical intuition of this we further use $|\sum_{n\neq m} G_{mn}| \leq \sum_{n\neq m} |G_{mn}|$, giving

$$\frac{\sum_m \sum_{n\neq m} |G_{mn}|}{N} \ll \begin{cases} 2\Omega_{\mathrm{R}}, & 2\sqrt{1+\Delta^2} < \Omega_{\mathrm{R}} \\ 2\sqrt{1+\Delta^2}+\Omega_{\mathrm{R}}, & 2 < \Omega_{\mathrm{R}} < 2\sqrt{1+\Delta^2} \\ 2(1+\sqrt{1+\Delta^2}), & \Omega_{\mathrm{R}} < 2 \end{cases} . \tag{6.3.17}$$

The average of $|G_{mn}|$ is $\overline{|G_{mn}|} = (\sqrt{\pi}\rho)$ such that, assuming that there are much more than one atom, $N \gg 1$, we get the averaged validity criterieon

$$\frac{N-1}{\sqrt{\pi}\rho} = \sqrt{\frac{Nb_0}{3\pi}} \ll \begin{cases} 2\Omega_{\mathrm{R}}, & 2\sqrt{1+\Delta^2} < \Omega_{\mathrm{R}} \\ 2\sqrt{1+\Delta^2}+\Omega_{\mathrm{R}}, & 2 < \Omega_{\mathrm{R}} < 2\sqrt{1+\Delta^2} \\ 2(1+\sqrt{1+\Delta^2}), & \Omega_{\mathrm{R}} < 2 \end{cases} . \tag{6.3.18}$$

This signifies that the correction to the atomic population, Eq. (6.3.10), is valid when the optical thickness *times the number of atoms* is much smaller than the intensity and/or the detuning. The validity estimate seem quite difficult to obtain with realistic experimental values since values such as $N = 10^8$ and $\rho = 5000$ [60] gives $b_0 \approx 10$ and thus $\sqrt{Nb_0/3\pi} \approx 10^4$, which are orders of magnitude larger larger than the paramters of the driving field in most experimental situations. The values used in Figs. 6.4 and 6.5 thus correspond to a regime where our approximation does not seem to be valid. Thus, either the inter-atomic interaction are not negligible in usual atom experiments or the restriction $|\sum_{n\neq m} G_{mn}| \leq \sum_{n\neq m} |G_{mn}|$ is too crude. Using $|\sum_{n\neq m} G_{mn}| \leq \sum_{n\neq m} |G_{mn}|$ to calculate the validity criterion is certainly giving a high estimate of $\sum_m |\sum_{n\neq m} G_{mn}|$ since it neglect all phase contributions for the scattered light, i.e. neglect interferences.

We note that the validity criterion for the single-scattering approximation when deriving the fluorescence spectrum is the same as the above, see App. C.4. In the following we will obey the strict validity criterion, Eq. (6.3.18), for plotting.

## 6.4 Fluorescence Spectrum of a Cloud of $N$ Atoms

We now determine the fluorescence spectrum of a dilute cloud of atoms. Since we are dealing with more than one atom, the scattered field is a sum over the contributions from all the atoms and we thus get the spectrum to be

$$\frac{S(\mathbf{r},\omega)}{S_0} = \sum_{m,n} \mathrm{Re}\left\{ \lim_{t\to\infty} \int_0^\infty \mathrm{d}\tau e^{i\omega\tau} \left\langle \hat{b}_m^\dagger(t+\tau)\hat{b}_n(t)\right\rangle e^{i(\mathbf{k}_0-\mathbf{k}_d)\cdot(\mathbf{R}_m-\mathbf{R}_n)} \right\}, \tag{6.4.1}$$

where $\mathbf{k}_0$ is the wave vector of the driving field, $\mathbf{k}_d = k_0\hat{\mathbf{r}}_d$ and $\hat{\mathbf{r}}_d$ is the unit vector directed from the center of the cloud towards the detector. We will find that the spectrum depends on the angle between $\mathbf{k}_0$ and $\mathbf{k}_d$ which we will dub the detection angle $\theta_d$ and write $S(\theta_d,\omega)$ instead of $S(\mathbf{r},\omega)$. For simplicity, we have again assumed that we can filter out the free field and have omitted the $r/c$ delay-time contribution in the operator since we are taking the long time limit. We will split the spectrum up in two parts: a sum over the same atomic indices, let us call it the local part, and a double

sum over different atomic indices, which we call the interference part, i.e.

$$\frac{S_{\rm loc}(\theta_d,\omega)}{S_0} = \sum_m {\rm Re}\left\{\lim_{t\to\infty}\int_0^\infty {\rm d}\tau e^{i\omega\tau}\left\langle \hat{b}_m^\dagger(t+\tau)\hat{b}_m(t)\right\rangle\right\}, \tag{6.4.2a}$$

$$\frac{S_{\rm int}(\theta_d,\omega)}{S_0} = \sum_{m,n\neq m} {\rm Re}\left\{\lim_{t\to\infty}\int_0^\infty {\rm d}\tau e^{i\omega\tau}\left\langle \hat{b}_m^\dagger(t+\tau)\hat{b}_n(t)\right\rangle e^{i\delta\mathbf{k}\cdot\mathbf{R}_{mn}}\right\}, \tag{6.4.2b}$$

where $\delta\mathbf{k} = \mathbf{k}_0 - \mathbf{k}_d$ and $\mathbf{R}_{mn} = \mathbf{R}_m - \mathbf{R}_n$. The local part of the spectrum is a sum over intensity contributions from the different atoms, while the interference part is the interference amongst field amplitude contributions emitted from the $N$ different atoms. Like with the atomic population for $N$ atoms in Sec. 6.3 we will write the local and interference parts of the spectrum as a zeroth-order term and a first-order correction, i.e. $S_{\rm loc} \approx S_{\rm loc}^{(0)} + S_{\rm loc}^{(1)}$ and $S_{\rm int} \approx S_{\rm int}^{(0)} + S_{\rm int}^{(1)}$. In the following we will first investigate the elastic spectrum, where reasonably simple analytic expressions can be obtained, and then look into the effects of the inter-atomic interaction on the inelastic part of the spectrum. Details of the calculations can be found in App. C.2.

### 6.4.1 Elastic Spectrum

We now show the effect of atomic interactions on the elastic spectrum by investigating the zeroth- and first-order terms separately. The different parts of the elastic spectrum contain similar types of interaction terms as the inelastic spectrum and can thus give us some insight in the more complicated inelastic spectrum.

#### Zeroth-order elastic spectrum

Let us begin with the ensemble-averaged zeroth-order terms of the elastic spectrum. These correspond to the very dilute limit used in Ref. [61] which consider spatial photon correlations from a driven atomic cloud. The average contribution to the zeroth-order spectrum from the local part is given by $N$ times the elastic spectrum of a single atom, i.e.

$$\overline{\frac{S_{{\rm loc},el}^{(0)}(\theta_d,\omega)}{NS_0}} = \frac{\pi\tilde{\Omega}_R^2}{2\left(1+\tilde{\Omega}_R^2\right)^2}\delta(\omega) = \frac{\pi\delta(\omega)}{1+\tilde{\Omega}_R^2}\left\langle \hat{b}^\dagger\hat{b}\right\rangle_{ss}^{(0)}, \tag{6.4.3}$$

where $\left\langle \hat{b}^\dagger\hat{b}\right\rangle_{ss}^{(0)}$ is the single-atom population, Eq. (6.1.7). This corresponds to the intensity of the driving field being isotropically scattered on the atoms.

The interference part is on the other hand given by

$$\frac{\overline{S^{(0)}_{\mathrm{int},el}(\theta_d,\omega)}}{NS_0} = (N-1)f^2(\delta\mathbf{k})\frac{\pi\delta(\omega)}{1+\tilde{\Omega}_R^2}\left\langle \hat{b}^\dagger\hat{b}\right\rangle^{(0)}_{ss}. \tag{6.4.4}$$

Here, the function $f(\delta\mathbf{k})$ is the ensemble average of $e^{-i\delta\mathbf{k}\cdot\mathbf{R}_m}$ which for our Gaussian cloud we find in App. C.3, Eq. (C.3.13), to be

$$f(\delta\mathbf{k}) = \exp\left[-\rho^2\sin^2\left(\frac{\theta_d}{2}\right)\right]. \tag{6.4.5}$$

At first sight Eq. (6.4.4) might look as if it is a cooperative phenomenon since it has a term which is $N$ times larger than the single-atom case. This again would seem strange since it is the spectral contribution from non-interacting atoms which are expected to be mutually incoherent. The coherence amongst the atoms is of course irrelevant when dealing with the elastic spectrum, since this has to do with the coherence of the driving field and not the atomic coherences. The factor of $N$ thus derives from the interferences of the elastically scattered driving field. The function $f(\delta\mathbf{k})$ is the scattering amplitude of Rayleigh–Gans scattering [69]. The regime of Rayleigh–Gans scattering corresponds to weak scattering off a scatterer which is larger than the wavelength of the scattered light. We are considering point scatterers, which of course are not larger than the wavelength of the light. In our case it is thus not the individual scatterers, but the *averaged* properties which is considered. Thus, *on average*, the atomic cloud is considered a single weakly scattering object by the light of size $\rho$. This is also known from ensemble-averaged elastic scattering of light on classical point scatterers [69].

Rayleigh–Gans scattering gives rise to strong forward-directed scattering, with a shape which is increasingly narrow as the size of the cloud increases. Specifically, we have that the contribution from Eq. (6.4.4) becomes important when $f(\delta\mathbf{k}) > N^{-1}$. For large clouds this corresponds to an effect only for small $\theta_d$ such that we can write $f(\delta\mathbf{k}) > N^{-1}$ with Eq. (6.4.5), as

$$\exp\left[-\left(\frac{\rho\theta_d}{2}\right)^2\right] > N^{-1}, \tag{6.4.6}$$

which corresponds to $\rho|\theta_d| < 2\sqrt{\ln(N)}$. Thus, $N = 10^8$ and $\rho = 5000$ give $|\theta_d| < 10^{-3}$, i.e. very close to the direct forward direction. We should remember that our analysis is not valid in the exact forward direction since we excluded the free driving field from the spectrum Eq. (6.4.1). It is nevertheless in principle possible to get arbitrarily close to the forward direction.

Therefore, we will keep all directions in our discussions while considering the problem of filtering out the free field as a challenge for the experimentalists.

In summary, the zeroth-order elastic spectrum shows a strong forward-directed contribution due to interference. Based on considerations concerning elastic scattering this was found to be not very surprising, but it will prove interesting now that we will include effects of the inter atomic dipole-dipole interaction.

### First-order correction to the elastic spectrum

The first-order correction to the local spectrum is, Eq. (C.2.17b),

$$\overline{\frac{S^{(1)}_{\mathrm{loc},el}(\theta_d,\omega)}{NS_0}} = \pi\delta(\omega)\frac{1-\tilde{\Omega}_R^2}{1+\tilde{\Omega}_R^2}\overline{\left\langle \hat{b}_m^\dagger \hat{b}_m \right\rangle^{(1)}_{ss}}, \tag{6.4.7}$$

where we have inserted the averaged correction to the steady-state population found in Eq. (6.3.10). The correction changes sign as $\tilde{\Omega}_R^2$ goes from $\tilde{\Omega}_R^2 < 1$ to $\tilde{\Omega}_R^2 > 1$. As we found for the single-atom case the value $\tilde{\Omega}_R = 1$ correspond to the transition from elastic to inelastic scattering due to saturation of the atomic population. The effect of the inter atomic interaction is thus the least as scattering changes from being primarily elastic to being increasingly inelastic. This is also found in the interference part of the elastic spectrum which is a bit more complicated than the other terms. It is given by, Eq. (C.2.17b),

$$\begin{aligned}
&\overline{\frac{S^{(1)}_{\mathrm{int},el}(\theta_d,\omega)}{NS_0}} = \\
&-(N-1)(N-2)f(\delta\mathbf{k})\frac{\pi\left[\mathrm{Im}\left\{g(\delta\mathbf{k},\mathbf{0})\right\}+\mathrm{Re}\left\{g(\delta\mathbf{k},\mathbf{0})\right\}\Delta\right]\tilde{\Omega}_R^2\left(1-\tilde{\Omega}_R^2\right)}{2\left(1+\Delta^2\right)\left(1+\tilde{\Omega}_R^2\right)^4}\delta(\omega) \\
&-(N-1)\frac{\pi\left[\mathrm{Im}\left\{g(\delta\mathbf{k},\delta\mathbf{k})\right\}+\mathrm{Re}\left\{g(\delta\mathbf{k},\delta\mathbf{k})\right\}\Delta\right]\tilde{\Omega}_R^2\left(1-\tilde{\Omega}_R^2\right)}{2\left(1+\Delta^2\right)\left(1+\tilde{\Omega}_R^2\right)^4}\delta(\omega).
\end{aligned} \tag{6.4.8}$$

Here we have defined the a function

$$g(\mathbf{k},\mathbf{k}') = G(\mathbf{k},\mathbf{k}') + G(-\mathbf{k},-\mathbf{k}'), \tag{6.4.9}$$

where $G(\mathbf{k},\mathbf{k}')$ is the ensemble average of $e^{i\mathbf{k}\cdot\mathbf{R}_m}e^{-i\mathbf{k}'\cdot\mathbf{R}_n}G_{mn}$. Remember that $G_{mn}$ is the inter atomic interaction through the electric field and thus

$e^{i\mathbf{k}\cdot\mathbf{R}_m}e^{-i\mathbf{k}'\cdot\mathbf{R}_n}G_{mn}$ corresponds to the interference of the incident light with the inter atomic radiation. The function $G(\mathbf{k},\mathbf{k}')$ can be calculated to be, see Eq. (C.3.11),

$$\begin{aligned} G(\mathbf{k},\mathbf{k}') = &-\frac{1}{d(2\rho)^2}e^{-[b^2+(1-d)^2]\rho^2}\mathrm{Erfi}[(1-d)\rho] \\ &+\frac{1}{d(2\rho)^2}e^{-[b^2+(1+d)^2]\rho^2}\mathrm{Erfi}[(1+d)\rho] \\ &+i\frac{1}{d(2\rho)^2}e^{-[b^2+(1-d)^2]\rho^2}\left(1-e^{-4d\rho^2}\right), \end{aligned} \tag{6.4.10}$$

with $b=|\mathbf{k}-\mathbf{k}'|/2k_a$, $d=|2\mathbf{k}_0-\mathbf{k}-\mathbf{k}'|/2k_a$.

In the direct forward direction, $\theta=0$, the difference $\delta\mathbf{k}=\mathbf{0}$ such that $G(\mathbf{0},\mathbf{0})=\overline{G_{mn}}$ and $f(\mathbf{0})=1$. Thereby we get

$$\overline{\frac{S^{(1)}_{\mathrm{int},el}(0,\omega)}{NS_0}} = (N-1)\pi\delta(\omega)\frac{1-\tilde{\Omega}_R^2}{1+\tilde{\Omega}_R^2}\overline{\left\langle \hat{b}_m^\dagger\hat{b}_m\right\rangle^{(1)}_{ss}}. \tag{6.4.11}$$

That is, the interaction between the different atoms is enhanced due to the Rayleigh–Gans interference and thereby enhancing the interaction by a factor of $N-1$ in the forward direction! We identify this as a cooperative effect since it is an enhancement of the interaction which depend on the number of atoms. Interestingly, this cooperative effect is also visible in the inelastic spectrum as we will now see.

### 6.4.2 Inelastic Spectrum

Even though the finding of the cooperative effect is indeed intriguing such effects in the elastic spectrum can equally well be found in a linearized theory for weakly-driven atoms in the harmonic limit [62] even though it would not include the found saturation effects. Here we will show cooperative effects in the inelastic spectrum. These effects could not have been found in a linearized treatment since such cannot explain the inelastic scattering which is only present in models with saturation effects. Here in the main text we will not show any lengthy expressions since they do not give further insight. Instead, we show the inelastic spectrum and discuss the physical properties. The details of the calculations can be found in App. C.2 and are summarized in Eqs. (C.2.16) and (C.2.18).

First, the local zeroth-order inelastic spectrum is simply given by $N$ times the single-atom spectrum and thus gives the usual Mollow triplet. The zeroth-order interference part should on the other hand be strictly zero since the noninteracting atoms are not mutually coherent. We indeed find that this

contribution vanish, which is a nontrivial check on our calculations so far. The first-order correction to the inelastic spectrum has similar ensemble-averaged contributions as arising in the elastic spectrum. Specifically the interference part of the spectrum has a similar strong forward-directed contribution. This is shown in Fig. 6.6 where the average inelastic fluorescence spectrum per atom is plotted as a function of $\rho\theta_d$ for a cloud of size $\rho = 5000$ and $N = 25000$ atoms driven by a field which is detuned by $\Delta = 5$ at a Rabi frequency of $\Omega_{\mathrm{R}} = 10$. We use the product $\rho\theta_d$ since we found, Eq. (6.4.6), that the spectra become more forward peaked as the size of the cloud, $\rho$, increase. Three things should be noticed in from Fig. 6.6. First, for $|\rho\theta| > 2$ the spectrum look like the normal single atom Mollow triplet. Second, as we go closer to the exact forward direction we see that the spectrum deviates from the usual single-atom spectrum. This is caused by the cooperative enhancement of the interaction due to the interference from Rayleigh–Gans scattering. Lastly, we see that as the interaction become important the spectrum become asymmetric, see inset. Such behavior was also found in Ref. [66] for the fluorescence spectrum of two atoms where it was also identified as a cooperative effect.

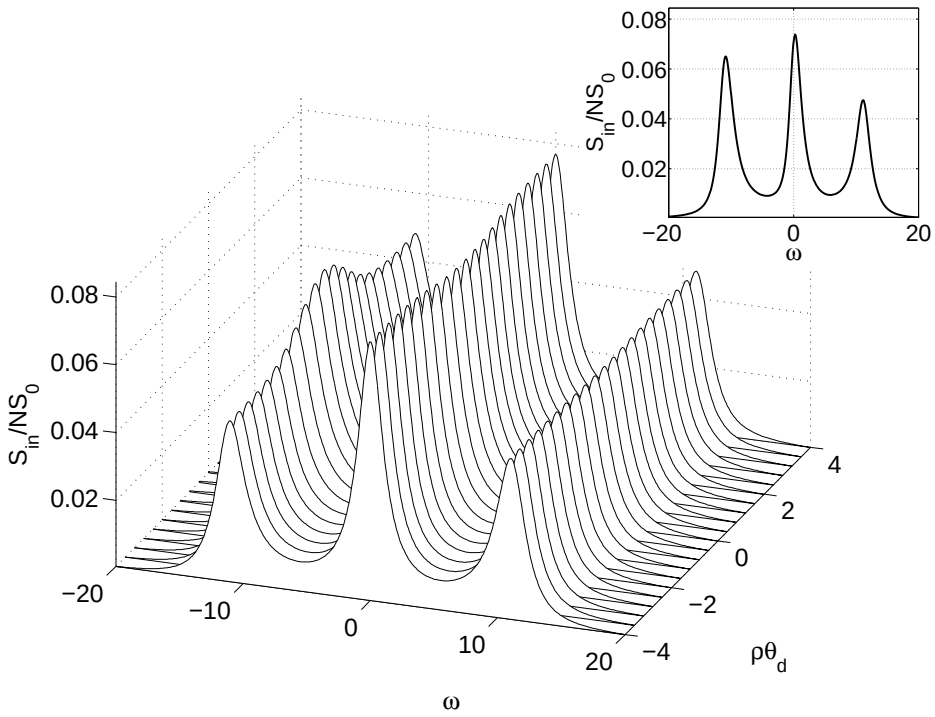


**Figure 6.6** The average inelastic fluorescence spectrum per atom as a function of normalized detection angle, $\rho\theta_d$, for $N = 25000$ and $\rho = 5000$ such that $N/\rho = 5$. The detuning is $\Delta = 5$ and the Rabi frequency is $\Omega_{\rm R} = 10$. The inset show the asymmetric spectrum at the exact forward direction.

## 6.5 Chapter Summary

In this chapter we examined the steady-state properties of driven two-level atoms. We first considered a single two-level atom. We found that non negligible steady-state exited-atom population influences the properties of the elastic fluorescence spectrum. As the population increased the interaction between the driving field and the atom increased. This gave rise to an inelastic spectrum which showed the three-peaked spectrum known as the Mollow triplet. This spectrum is symmetric around the frequency of the driving field independent of the detuning and Rabi frequency.

We then considered a cloud of atoms using the Heisenberg equations of motion for $N$ two-level atoms derived in the previous chapter. By assuming the cloud of atoms to be dilute, we found a simple analytical expression for the first-order correction to the atomic population. From this we identified that the interaction amongst the atoms gives rise to a change in the resonance frequency and an alteration of the decay properties through the real and imaginary parts of the dipole-dipole interaction respectively. Through the analysis, a criterion for the importance of taking atomic interactions into account naturally appeared. Although our criterion for the validity of the first-order scattering is sufficient, but not necessary, we have indications that the interactions should be considered in many atomic experiments.

After this we found the elastic spectrum of the atoms. This showed sign of Rayleigh–Gans scattering even without interaction due to the interference of the elastically scattered light. This interference was further found to increase the interaction between the atoms showing a cooperative enhancement of the interaction in the exact forward direction. The analysis included the effects of saturation which cannot be taken into account in the usual linearized treatment.

Finally, the inelastic spectrum was calculated, for which an analytic but not simple expression was found. The inelastic spectrum showed the same cooperative effect of the enhanced dipole-dipole interaction in the forward direction. This gives rise to asymmetric spectra which could otherwise not occur in the single-atom case. The asymmetries in the inelastic spectra are a clear indication that interactions amongst the atoms takes place. We thus suggest experimentalist to look for cooperativity in the forward direction where it show angle dependence of the inelastic fluorescence spectrum.

# 7

# Summary and Outlook

In this thesis we have quantum mechanically investigated multiple scattering of light. The investigation was split into two parts; one concerning elastic multiple scattering while the other concerned inelastic scattering.

## 7.1 Part I

First, in Chap. 2 we introduced some background theory in order to prepare the reader for following chapters. Initially, the classical theory of elastic multiple scattering was discussed in order to get an intuitive feeling for the subject. There, the intensity transmission correlation function was introduced as a measure of the averaged intensity correlations for waves passing through a multiple scattering medium. After this the quantization of the electromagnetic field was reviewed and it was found that the mode of the quantized electromagnetic field is the same as the classical electromagnetic field. Then, two quantities were introduced, the photon correlation function and the degree of quadrature entanglement. These quantities were finally illustrated by one of the simplest scatterers imaginable, the beam splitter. While the beam splitter is a very common element in most optical setups, and its classical optical functionality is well understood, in a quantum context the response remain intriguing. With this it was shown, using the photon correlation function, that quantum interference already occurs in the simple interference scheme of a beam splitter. Furthermore, interfering two squeezed beams on the beam splitter illustrated the possibility of inducing quadrature entanglement between the two quantum states of the output ports, through scattering.

Next, in Chap. 3, effects of interfering quantum states of light on a multiple scattering medium was explored. Using the finding of the previous chapter that the quantum optical modes are the same as the classical for elastic scattering, allowed us to relate the quantum optical propagation to

the classical. This made it possible to investigate the possibility of inducing quantum entanglement by multiple scattering and the strength of quantum interference after multiple scattering. Specifically two settings were explored; the propagation through a single realization of a scattering medium and the ensemble-averaged transport properties of the quantum states after being multiply scattered. In the investigation of the single realization of a scattering medium, it was found that entanglement between two output modes can be induced by interfering two squeezed beams. This induced entanglement is directly analogous to interfering two squeezed beams on a beam splitter. Furthermore, it was found that quantum interference between two or more input beams gave rise to large fluctuations in the photon correlations between different outputs after multiple scattering. Interestingly, this effect of quantum interference, which is sometimes thought to be feeble, even survived ensemble averaging. This might seem surprising since a multiple scattering process could naively be considered a randomization of the phase and thus eliminating all interference effects. The survival of the interference is due to the constructive interference of certain propagation paths through the scattering medium. The effect of quantum interference was found to have an increasing effect on the correlations between different output directions as the amount of scattering increased, while saturating in the localized regime. Lastly, it was found that the induced quadrature entanglement would not survive ensemble averaging.

Then, in Chap. 4, the theoretical treatment of a quantum optical multiple scattering experiment was derived. The experiment aims to measure the existence of photon correlations between two output modes of a multiple scattering medium illuminated by a quantum optical state. In order to describe the experimental scheme, the formalism of Chap. 3 was modified by introducing a continuous-mode theory with time-dependent operators. Using this, the photon correlation function between two different output modes was related to the photon statistics of the total transmitted and reflected light, which was then related to the power noise spectrum measured in the experiment. It was found that, unlike classical elastic multiple scattering, it was possible to deterministically and continuously alter the average intensity correlations by changing the photon statistics of the incident light beam. Thereby it was possible to achieve both positive and negative correlations between two output modes even in the diffusive regime, where output modes are uncorrelated in the case of classical scattering.

As possible theoretical continuations of the work presented in the first part, it could be interesting to consider the inclusion of the time dependence of the operators in the case of interference between multiple beams. This has been considered in Ref. [70] for the interference of two entangled

single-photon states, and it was found that the quantum interference properties depended on the typical time it takes to propagate through a random medium. Furthermore, it could be exciting to investigate the properties of the reflected light in more details. In classical wave scattering, strong negative correlations are found in this direction [19], which could result in the possibility to on average create entangled states by multiple scattering. Another similar exploration would be to investigate the higher order-moments of the degree of entanglement to see how probable it is to find entangled states.

It would also be interesting to try to observe the quantum interference predicted in Chap. 3. In order to do that, it would be preferable to use a disordered waveguide which only supports a few modes, since this make it easier to reach the strong scattering regime where the signs of the quantum interference are strongest. Here, a disordered photonic crystal waveguide seems an optimal candidate since it would makes it possible to tune the scattering mean free path by changing the wavelength of the light source due to the dispersive properties of the medium. Another suggestion would be to develop a multi-mode beam splitter, where the mutual entanglement between output ports could be chosen by changing the squeezing parameters of the input beams.

## 7.2 Part II

In the second part of the thesis, inelastic effects were included in the scattering processes. This was done in Chap. 5, where the inelastic scattering was introduced by quantum mechanically treating scattering of light on point dipoles embedded in an arbitrary dielectric structure. The interaction was described using two different interaction Hamiltonians, known as the electric-dipole and the minimal-coupling Hamiltonians. Using these, a formalism was derived in the Heisenberg picture focusing on the evolution of the electric field operators rather than the dipole operators. We found exact relations between the electric field and the dipole operators for both types of interaction Hamiltonians, while keeping the model of the dipoles arbitrary. The differences between using the two Hamiltonians could then be compared. This comparison showed that the linearization of the field in the minimal-coupling interaction Hamiltonian, which is sometimes used in the literature, leads to that light scattered from the dipole couple only to the transverse modes of the field. The electric-dipole interaction Hamiltonian on the other hand coupled the scattered light to both the longitudinal and transverse modes of the field. Lastly, an example of the use of the formalism is presented by deriving the equations of motion of $N$ two-level dipoles.

Finally, in Chap. 6 we investigated the steady-state properties of two-level atoms. We began by reviewing the single-atom fluorescence which gave rise to the well-known three-peaked inelastic spectrum known as the Mollow triplet. Then we demonstrated the possibilities of the formalism of Chap. 5 by using the derived equations of motion for $N$ two-level dipoles to calculate the fluorescence spectrum of a cloud of $N$ two-level atoms. These equations of motion contain a coupling term, the dipole-dipole coupling, between the different atoms which is mediated by the electric field. Using the physical intuition from elastic scattering we simplified the calculations for dilute clouds. With such simplification we derived analytical expressions for the steady-state atomic population and fluorescence spectrum. The investigation of the atomic population gave simple intuitive explanations of the effect of the interaction as a change in the photonic environment. The fluorescence spectrum consists of an elastic and an inelastic part. Due to the interaction amongst the atoms the elastic part of the spectrum contains a cooperative effect which we identified as being caused by interference effects of a Rayleigh–Gans type of scattering. Such interference effects were furthermore found to result in cooperative contributions to the inelastic spectrum as well.

Future possibilities of theoretical explorations of the topics considered in this part could be to investigate coupling of quantum dots in photonic environments, e.g. for quantum information protocols. Furthermore, it could be interesting to use the hydrogen model for the dipoles since it is exactly solvable even when the dipole is considered having a finite size. This could make it possible to investigate theoretically the size effects of quantum dots in photonic environments as was done experimentally in Ref. [47].

As a suggestion for the experimentalists it would be very interesting to see the cooperative effects in the inelastic spectrum, which is most visible in a forward detection scheme. In hot atomic vapors the atomic coherences is probably absent, so for observation of the cooperative effects predicted here, we need clouds that are both dilute and cold.

# A

# Details for Chapter 2

## A.1 Quadrature entanglement

The difference $\hat{X}_3 - \hat{X}_4$ can be written as

$$\begin{aligned}\hat{X}_3 - \hat{X}_4 &= \frac{1}{\sqrt{2}}\left(\hat{a}_3^\dagger + \hat{a}_3 - \hat{a}_4^\dagger - \hat{a}_4\right) \\ &= \frac{1}{\sqrt{2}}\left(-\alpha_+\hat{a}_1^\dagger - \alpha_+^*\hat{a}_1 + \alpha_-^*\hat{a}_2^\dagger + \alpha_-\hat{a}_2\right) \\ &= -\hat{\tilde{X}}_1 + \hat{\tilde{X}}_2 \qquad \text{(A.1.1)}\end{aligned}$$

with the rescaled operators $\hat{\tilde{X}}_1 = \frac{1}{\sqrt{2}}(\alpha_+\hat{a}_1^\dagger + \alpha_+^*\hat{a}_1)$ and $\hat{\tilde{X}}_2 = \frac{1}{\sqrt{2}}(\alpha_-^*\hat{a}_2^\dagger + \alpha_-\hat{a}_2)$ having the scaling constants

$$\alpha_\pm = \sqrt{\mathcal{R}}e^{-i\phi_I} \pm \sqrt{\mathcal{T}}e^{i\phi_I}, \qquad \text{(A.1.2)}$$

(A.1.3)

so that

$$\Delta(\hat{X}_3 - \hat{X}_4)^2 = \Delta\hat{\tilde{X}}_1^2 + \Delta\hat{\tilde{X}}_2^2 - 2\Delta\hat{\tilde{X}}_1\hat{\tilde{X}}_2. \qquad \text{(A.1.4)}$$

If we assume initially uncorrelated beams we have $\Delta\hat{\tilde{X}}_1\hat{\tilde{X}}_2 = 0$ while

$$\Delta\hat{\tilde{X}}_1 = \frac{1}{2}\left[\Delta(\alpha_+^*\hat{a}_1)^2 + \Delta(\alpha_+\hat{a}_1^\dagger)^2 + 2|\alpha_+|^2\Delta\hat{a}_1^\dagger\hat{a}_1 + |\alpha_+|^2\right], \qquad \text{(A.1.5a)}$$

$$\Delta\hat{\tilde{X}}_2 = \frac{1}{2}\left[\Delta(\alpha_-\hat{a}_2)^2 + \Delta(\alpha_-^*\hat{a}_2^\dagger)^2 + 2|\alpha_-|^2\Delta\hat{a}_2^\dagger\hat{a}_2 + |\alpha_-|^2\right], \qquad \text{(A.1.5b)}$$

and similar

$$\Delta(\hat{Y}_3 + \hat{Y}_4)^2 = \Delta\hat{\tilde{Y}}_1^2 + \Delta\hat{\tilde{Y}}_2^2 + 2\Delta\hat{\tilde{Y}}_1\hat{\tilde{Y}}_2, \qquad \text{(A.1.6)}$$

with $\hat{\tilde{Y}}_1 = \frac{i}{\sqrt{2}}(\alpha_-^* \hat{a}_1^\dagger - \alpha_- \hat{a}_1)$ and $\hat{\tilde{Y}}_2 = \frac{i}{\sqrt{2}}(\alpha_+ \hat{a}_2^\dagger + \alpha_+^* \hat{a}_2)$ and

$$\Delta\hat{\tilde{Y}}_1 = -\frac{1}{2}\left[\Delta(\alpha_- \hat{a}_1)^2 + \Delta(\alpha_-^* \hat{a}_1^\dagger)^2 - 2|\alpha_-|^2 \Delta\hat{a}_1^\dagger \hat{a}_1 - |\alpha_-|^2\right], \tag{A.1.7a}$$

$$\Delta\hat{\tilde{Y}}_2 = -\frac{1}{2}\left[\Delta(\alpha_+^* \hat{a}_2)^2 + \Delta(\alpha_+ \hat{a}_2^\dagger)^2 - 2|\alpha_+|^2 \Delta\hat{a}_2^\dagger \hat{a}_2 - |\alpha_+|^2\right]. \tag{A.1.7b}$$

For coherent states then $\Delta\hat{\tilde{X}}_1 = |\alpha_+|^2/2 = \Delta\hat{\tilde{Y}}_2$ and $\Delta\hat{\tilde{X}}_2 = |\alpha_-|^2/2 = \Delta\hat{\tilde{Y}}_1$ such that, since $|\alpha_\pm|^2 = 1 \pm 2\sqrt{\mathcal{RT}}\cos(\phi_\pm)$, we get

$$\Delta(\hat{X}_3 - \hat{X}_4)^2 = \Delta(\hat{Y}_3 + \hat{Y}_4)^2 = 1. \tag{A.1.8}$$

For a squeezed state with squeezing parameter $s_i$ and squeezing phase $\theta_i$ we have

$$\langle \hat{a}_i \rangle = 0, \tag{A.1.9a}$$

$$\left\langle \hat{a}_i^\dagger \hat{a}_i \right\rangle = \sinh^2(s_i), \tag{A.1.9b}$$

$$\langle \hat{a}_i \hat{a}_i \rangle = -e^{i\theta_i} \sinh(s_i)\cosh(s_i), \tag{A.1.9c}$$

such that

$$\begin{aligned}\Delta\hat{\tilde{X}}_1 &= \frac{1}{2}\left\{-\left[(\alpha_+^*)^2 e^{i\theta_1} + \alpha_+^2 e^{-i\theta_i}\right]\cosh(s_1)\sinh(s_1) + |\alpha_+|^2\left[2\sinh^2(s_1) + 1\right]\right\} \\ &= \frac{|\alpha_+|^2}{2}\left[-\cos(\theta_1 - \phi_+)\sinh(2s_1) + \cosh(2s_1)\right],\end{aligned} \tag{A.1.10}$$

$$\Delta\hat{\tilde{X}}_2 = \frac{|\alpha_-|^2}{2}\left[-\cos(\theta_2 + \phi_-)\sinh(2s_2) + \cosh(2s_2)\right], \tag{A.1.11}$$

and similarly

$$\Delta\hat{\tilde{Y}}_1 = \frac{|\alpha_-|^2}{2}\left[\cos(\theta_1 + \phi_-)\sinh(2s_1) + \cosh(2s_1)\right], \tag{A.1.12}$$

$$\Delta\hat{\tilde{Y}}_2 = \frac{|\alpha_+|^2}{2}\left[\cos(\theta_2 - \phi_+)\sinh(2s_2) + \cosh(2s_2)\right], \tag{A.1.13}$$

where $\phi_i$ is defined from $\alpha_i^2 = |\alpha_i|^2 e^{i\phi_i}$. For a symmetric, phase-less BS, $|\alpha_\pm|^2 = 1 \pm 1$, we thus get

$$\Delta(\hat{X}_3 - \hat{X}_4)^2 = -\cos(\theta_1)\sinh(2s_1) + \cosh(2s_1), \tag{A.1.14a}$$

$$\Delta(\hat{Y}_3 + \hat{Y}_4)^2 = \cos(\theta_2)\sinh(2s_2) + \cosh(2s_2), \tag{A.1.14b}$$

or, using $\frac{1}{2}[1 + \cos(2\theta)] = \cos^2(\theta)$ and $\frac{1}{2}[1 - \cos(2\theta)] = \sin^2(\theta)$,

$$\Delta(\hat{X}_3 - \hat{X}_4)^2 = \sin^2\left(\frac{\theta_1}{2}\right)e^{2s_1} + \cos^2\left(\frac{\theta_1}{2}\right)e^{-2s_1}, \tag{A.1.15a}$$

$$\Delta(\hat{Y}_3 + \hat{Y}_4)^2 = \cos^2\left(\frac{\theta_2}{2}\right)e^{2s_2} + \sin^2\left(\frac{\theta_2}{2}\right)e^{-2s_2}. \tag{A.1.15b}$$

# B

# Details for Chapter 5

## B.1 Green function reordering

I will use the asterisk $^*$ for complex conjugation and the dagger $^\dagger$ for hermitian conjugation, i.e. complex conjugation and a transpose. Thus, in space coordinates the state $|\mathbf{g}_\lambda\rangle$ is the vector function $\langle \mathbf{r}\,|\mathbf{g}_\lambda\rangle = \mathbf{g}_\lambda(\mathbf{r})$ while the bra is $\mathbf{g}_\lambda^\dagger(\mathbf{r})$. With this notation we have that an inner product of two states $|\mathbf{g}_\lambda\rangle$ and $|\mathbf{g}_\mu\rangle$ will be written such that

$$\begin{aligned}\langle \mathbf{g}_\lambda\,|\mathbf{g}_\mu\rangle &= \left\langle \mathbf{g}_\lambda \left| \int \mathrm{d}\mathbf{r}\,|\mathbf{r}\rangle\,\langle\mathbf{r}| \right| \mathbf{g}_\mu \right\rangle \\ &= \int \mathrm{d}\mathbf{r}\mathbf{g}_\lambda^\dagger(\mathbf{r})\mathbf{g}_\mu(\mathbf{r}) \\ &= \int \mathrm{d}\mathbf{r}\mathbf{g}_\lambda^*(\mathbf{r})\cdot\mathbf{g}_\mu(\mathbf{r}). \end{aligned} \tag{B.1.1}$$

This distinction makes it possible for us to write the outer product $\mathbf{g}_\lambda(\mathbf{r})\otimes\mathbf{g}_\mu^*(\mathbf{r}')$ *and* $\mathbf{g}_\lambda^*(\mathbf{r})\otimes\mathbf{g}_\mu(\mathbf{r}')$ with the latter being

$$\begin{aligned}\mathbf{g}_\lambda^*(\mathbf{r})\otimes\mathbf{g}_\mu(\mathbf{r}') &= \mathbf{g}_\lambda^*(\mathbf{r})[\mathbf{g}_\mu^*(\mathbf{r}')]^\dagger \\ &= \langle\mathbf{r}||\mathbf{g}_\lambda^*\rangle\,\langle\mathbf{g}_\mu^*||\mathbf{r}'\rangle. \end{aligned} \tag{B.1.2}$$

Let us considering the eigenvalue problem

$$\frac{1}{\sqrt{\epsilon(\mathbf{r})}}\nabla\times\nabla\times\left[\frac{1}{\sqrt{\epsilon(\mathbf{r})}}\mathbf{g}_\lambda(\mathbf{r})\right] - \frac{\omega_\lambda^2}{c^2}\mathbf{g}_\lambda(\mathbf{r}) = 0 \tag{B.1.3}$$

where $\epsilon(\mathbf{r})$ is real and non-zero which, if we choose proper boundary conditions such that the operator is self-adjoint, has the orthogonality relation

$$(\omega_\lambda^2-\omega_\mu^2)\int \mathrm{d}\mathbf{r}\mathbf{g}_\lambda^*(\mathbf{r})\cdot\mathbf{g}_\mu(\mathbf{r}) = 0, \tag{B.1.4}$$

and the eigenvalues $(\omega_\lambda/c)^2$ are real and positive. With this we define another basis set of complex functions $\{\mathbf{f}_\lambda(\mathbf{r})\}$ given by $\mathbf{f}_\lambda(\mathbf{r}) = \mathbf{g}_\lambda(\mathbf{r})/\sqrt{\epsilon(\mathbf{r})}$ which is the solution to

$$\nabla \times \nabla \times \mathbf{f}_\lambda(\mathbf{r}) - \frac{\epsilon(\mathbf{r})\omega_\lambda^2}{c^2}\mathbf{f}_\lambda(\mathbf{r}) = 0 \tag{B.1.5}$$

and obey

$$(\omega_\lambda^2 - \omega_\mu^2) \int \mathrm{d}\mathbf{r}\epsilon(\mathbf{r})\mathbf{f}_\lambda^*(\mathbf{r}) \cdot \mathbf{f}_\mu(\mathbf{r}) = 0. \tag{B.1.6}$$

We now want to know if we can somehow write the tensor

$$\mathbf{T}(\mathbf{r}, \mathbf{r}') = \sum_\lambda p(\omega, \omega_\lambda)\mathbf{f}_\lambda^*(\mathbf{r}) \otimes \mathbf{f}_\lambda(\mathbf{r}') \tag{B.1.7}$$

as

$$\sum_\lambda q(\omega, \omega_\lambda)\mathbf{f}_\lambda(\mathbf{r}) \otimes \mathbf{f}_\lambda^*(\mathbf{r}'), \tag{B.1.8}$$

where $p$ and $q$ are complex valued functions of $\omega$ and $\omega_\lambda$. In order to do so, let us make a basis set of real valued vector functions $\mathbf{h}_\lambda(\mathbf{r})$. Since both $|\mathbf{f}_\lambda\rangle$ and $|\mathbf{h}_\lambda\rangle$ are complete and normalized sets of eigenvectors there is a unitary transformation between the two sets given by

$$|\mathbf{f}_\lambda\rangle = \sum_\mu |\mathbf{h}_\mu\rangle \langle \mathbf{g}_\mu| \, |\mathbf{f}_\lambda\rangle = \sum_\mu U_{\lambda\mu}^* \mathbf{h}_\mu. \tag{B.1.9}$$

From the orthogonality relation Eq. (B.1.6) we have that $U_{\lambda\mu}^*$ is zero *unless* $\omega_\lambda^2 = \omega_\mu^2$! We can thus write $U_{\lambda\mu}^* = U_{\lambda\mu}^* \delta_{\omega_\lambda^2 \omega_\mu^2}$ with $\delta_{ij}$ being the Kronecker delta function. If we expand the $|\mathbf{f}_\lambda\rangle$'s of $\mathbf{T}(\mathbf{r}, \mathbf{r}')$ in the $|\mathbf{h}_\mu\rangle$ set we get

$$\begin{aligned}
\mathbf{T}(\mathbf{r}, \mathbf{r}') &= \sum_\lambda p(\omega, \omega_\lambda)\mathbf{f}_\lambda^*(\mathbf{r}) \otimes \mathbf{f}_\lambda(\mathbf{r}') \\
&= \sum_\lambda p(\omega, \omega_\lambda) \langle \mathbf{r}| \left[\sum_\mu U_{\lambda\mu} |\mathbf{h}_\mu\rangle\right] \left[\sum_\nu U_{\lambda\nu} |\mathbf{h}_\nu\rangle\right]^\dagger |\mathbf{r}'\rangle \\
&= \sum_{\lambda\mu\nu} p(\omega, \omega_\lambda) U_{\lambda\mu} U_{\lambda\nu}^* \langle \mathbf{r} |\mathbf{h}_\mu\rangle \langle \mathbf{h}_\nu |\mathbf{r}'\rangle \\
&= \sum_{\lambda\mu\nu} p(\omega, \omega_\lambda) U_{\lambda\mu} \delta_{\omega_\lambda^2 \omega_\mu^2} U_{\lambda\nu}^* \langle \mathbf{r} |\mathbf{h}_\mu\rangle \langle \mathbf{h}_\nu |\mathbf{r}'\rangle
\end{aligned} \tag{B.1.10}$$

which, *if* $p(\omega,\omega_\lambda) = P(\omega,\omega_\lambda^2)$ *is a function of* $\omega_\lambda^2$, can be written as

$$\begin{aligned}\mathbf{T}(\mathbf{r},\mathbf{r}') &= \sum_{\mu\nu} P(\omega,\omega_\nu^2) \sum_{\lambda} U_{\lambda\mu} U_{\lambda\nu}^* \left\langle \mathbf{r} \right| \left. \mathbf{h}_\mu \right\rangle \left\langle \mathbf{h}_\nu \right| \left. \mathbf{r}' \right\rangle \\ &= \sum_{\nu} p(\omega,\omega_\nu) \mathbf{h}_\nu(\mathbf{r}) \otimes \mathbf{h}_\nu(\mathbf{r}'). \end{aligned} \tag{B.1.11}$$

In our case the eigenfrequencies $\omega_\lambda$ are real-valued and nonnegative. The spectrum is consequently nonnegative. We need a unique label for that. As far as the labeling is concerned, either one uses $\omega_\lambda^2$, or one uses $\omega_\lambda$, but then one should choose all $\omega_\lambda$'s positive or all of them negative to keep the labeling unique. But $\omega_\lambda$ is not just a label, it is also the energy of a photon in that mode. That energy is positive for passive systems therefore the physical choice for the labeling is by the nonnegative $\omega_\lambda$.

We are thus able to rewrite the sum

$$\begin{aligned}\mathbf{T}(\mathbf{r},\mathbf{r}') &= \sum_{\lambda} p(\omega,\omega_\lambda) \mathbf{f}_\lambda^*(\mathbf{r}) \otimes \mathbf{f}_\lambda(\mathbf{r}') \\ &= \sum_{\nu} p(\omega,\omega_\nu) \mathbf{h}_\nu(\mathbf{r}) \otimes \mathbf{h}_\nu(\mathbf{r}') \\ &= \sum_{\mu} p(\omega,\omega_\mu) \mathbf{f}_\mu(\mathbf{r}) \otimes \mathbf{f}_\mu^*(\mathbf{r}'). \end{aligned} \tag{B.1.12}$$

The indices $\lambda$, $\nu$, and $\mu$ are simply labellings for the sums over the same amount of eigenfrequencies and thus we have that

$$\mathbf{T}(\mathbf{r},\mathbf{r}') = \sum_{\lambda} p(\omega,\omega_\lambda) \mathbf{f}_\lambda(\mathbf{r}) \otimes \mathbf{f}_\lambda^*(\mathbf{r}'). \tag{B.1.13}$$

Notice that it is the sums that are equal while in general $\mathbf{f}_\lambda^*(\mathbf{r}) \otimes \mathbf{f}_\lambda(\mathbf{r}') \neq \mathbf{f}_\lambda(\mathbf{r}) \otimes \mathbf{f}_\lambda^*(\mathbf{r}')$.

## B.2 Details in two-level atom equations of motion derivation

In Sec. 5.3.1 of Chap. 5 we find, Eq. (5.3.12), that we can write the scattered electric field as

$$\hat{\mathbf{E}}^{(\pm)}_{\mathrm{Scat}}(\mathbf{R}_m,t)=\sum_n \hat{b}_n(t)\mathbf{U}^{(\pm)}_{mn}\cdot\boldsymbol{\mu}^*_n+\sum_n \hat{b}^\dagger_n(t)\mathbf{V}^{(\pm)}_{mn}\cdot\boldsymbol{\mu}^*_n, \tag{B.2.1}$$

where we have defined

$$\mathbf{U}^{(\pm)}_{mn}=\mp\frac{1}{2\epsilon_0}\sum_\lambda \frac{\omega_\lambda \mathbf{f}_\lambda(\mathbf{R}_m)\otimes\mathbf{f}^*_\lambda(\mathbf{R}_n)}{\omega_n\mp\omega_\lambda}, \tag{B.2.2}$$

$$\mathbf{V}^{(\pm)}_{mn}=\mp\frac{1}{2\epsilon_0}\sum_\lambda \frac{\omega_\lambda \mathbf{f}_\lambda(\mathbf{R}_m)\otimes\mathbf{f}^*_\lambda(\mathbf{R}_n)}{-\omega_n\mp\omega_\lambda}. \tag{B.2.3}$$

Using App. B.1, these are related through

$$\begin{aligned}[\mathbf{U}^{(\pm)}_{mn}]^*&=\mp\frac{1}{2\epsilon_0}\sum_\lambda \frac{\omega_\lambda \mathbf{f}^*_\lambda(\mathbf{r}_m)\otimes\mathbf{f}_\lambda(\mathbf{R}_n)}{\omega_n\mp\omega_\lambda}=\pm\frac{1}{2\epsilon_0}\sum_\lambda \frac{\omega_\lambda \mathbf{f}_\lambda(\mathbf{r}_m)\otimes\mathbf{f}^*_\lambda(\mathbf{R}_n)}{-\omega_n\pm\omega_\lambda}\\&=\mathbf{V}^{(\mp)}_{mn}.\end{aligned} \tag{B.2.4}$$

Furthermore, they are related to the kernel of the electric field $\mathbf{K}(\mathbf{r},\mathbf{r}',\omega)$, Eq. (5.2.9), through $\mathbf{U}^{(+)}_{mn}+\mathbf{U}^{(-)}_{mn}=-\mu_0\omega_n^2\mathbf{K}(\mathbf{R}_m,\mathbf{R}_n,\omega_n)$.

We are now able to calculate the scattering field term for the equation of motion for $\hat{b}_m(t)$, Eq. (5.3.8a). To do this we use the equal-time operator relations $\hat{b}^\dagger_m(t)\hat{\sigma}_m(t)=-\frac{1}{2}\hat{b}^\dagger_m(t)$ and $\hat{b}_m(t)\hat{\sigma}_m(t)=\frac{1}{2}\hat{b}_m(t)$ and their Hermitian conjugates, giving

$$\begin{aligned}&-2\frac{i}{\hbar}\left[\hat{\sigma}_m(t)\boldsymbol{\mu}^*_m\cdot\hat{\mathbf{E}}^{(+)}_{\mathrm{Scat}}(\mathbf{R}_m,t)+\boldsymbol{\mu}^*_m\cdot\hat{\mathbf{E}}^{(-)}_{\mathrm{Scat}}(\mathbf{R}_m,t)\hat{\sigma}_m(t)\right]\\
&=\frac{i}{\hbar}\hat{b}_m(t)\boldsymbol{\mu}^*_m\cdot\left[\mathbf{U}^{(+)}_{mm}(t)-\mathbf{U}^{(-)}_{mm}(t)\right]\cdot\boldsymbol{\mu}_m\\
&\qquad\qquad-\frac{i}{\hbar}\hat{b}^\dagger_m(t)\boldsymbol{\mu}^*_m\cdot\left[\mathbf{V}^{(+)}_{mm}(t)-\mathbf{V}^{(-)}_{mm}(t)\right]\cdot\boldsymbol{\mu}^*_m\\
&\quad-2\frac{i}{\hbar}\sum_{n\neq m}\hat{\sigma}_m(t)\hat{b}_n(t)\boldsymbol{\mu}^*_m\cdot\left[\mathbf{U}^{(+)}_{mn}(t)+\mathbf{U}^{(-)}_{mn}(t)\right]\cdot\boldsymbol{\mu}_n\\
&\qquad\qquad-2\frac{i}{\hbar}\sum_{n\neq m}\hat{b}^\dagger_n(t)\hat{\sigma}_m(t)\boldsymbol{\mu}^*_m\cdot\left[\mathbf{V}^{(+)}_{mn}(t)+\mathbf{V}^{(-)}_{mn}(t)\right]\cdot\boldsymbol{\mu}^*_n\\
&\quad\approx\frac{i}{\hbar}\hat{b}_m(t)\boldsymbol{\mu}^*_m\cdot\left[\mathbf{U}^{(+)}_{mm}(t)-\mathbf{U}^{(-)}_{mm}(t)\right]\cdot\boldsymbol{\mu}_m\\
&\qquad-2\frac{i}{\hbar}\sum_{n\neq m}\hat{\sigma}_m(t)\hat{b}_n(t)\boldsymbol{\mu}^*_m\cdot\left[\mathbf{U}^{(+)}_{mn}(t)+\mathbf{U}^{(-)}_{mn}(t)\right]\cdot\boldsymbol{\mu}_n.\end{aligned} \tag{B.2.5}$$

where in the last equality we have performed the RWA by noticing that $\hat{b}_m$ and $\hat{b}_m^\dagger$ rotate at frequencies $2\omega_n$ apart. It should be noticed that the matrices with superscript $(-)$ would not be there if we had used the RWA at any earlier point and would therefore not give a dipole-dipole coupling through the kernel of the classical field.

For the scattering field term for $\hat{\sigma}_m(t)$ in Eq. (5.3.8b) we get

$$\begin{aligned}
&\frac{i}{\hbar}\Big[\hat{b}_m^\dagger(t)\boldsymbol{\mu}_m^*\cdot\hat{\mathbf{E}}_{\text{Scat}}^{(+)}(\mathbf{R}_m,t)+\boldsymbol{\mu}_m^*\cdot\hat{\mathbf{E}}_{\text{Scat}}^{(-)}(\mathbf{R}_m,t)\hat{b}_m^\dagger(t)\\
&\qquad\qquad -\hat{b}_m(t)\boldsymbol{\mu}_m\cdot\hat{\mathbf{E}}_{\text{Scat}}^{(+)}(\mathbf{R}_m,t)-\boldsymbol{\mu}_m\cdot\hat{\mathbf{E}}_{\text{Scat}}^{(-)}(\mathbf{R}_m,t)\hat{b}_m(t)\Big]\\
&=\frac{i}{\hbar}\hat{b}_m^\dagger(t)\hat{b}_m(t)\left[\boldsymbol{\mu}_m^*\cdot\mathbf{U}_{mm}^{(+)}\cdot\boldsymbol{\mu}_m-\boldsymbol{\mu}_m\cdot\mathbf{V}_{mm}^{(-)}\cdot\boldsymbol{\mu}_m^*\right]\\
&\qquad\qquad +\frac{i}{\hbar}\hat{b}_m(t)\hat{b}_m^\dagger(t)\left[\boldsymbol{\mu}_m^*\cdot\mathbf{U}_{mm}^{(-)}\cdot\boldsymbol{\mu}_m-\boldsymbol{\mu}_m\cdot\mathbf{V}_{mm}^{(+)}\cdot\boldsymbol{\mu}_m^*\right]\\
&\quad+\frac{i}{\hbar}\sum_{n\neq m}\hat{b}_m^\dagger(t)\hat{b}_n(t)\boldsymbol{\mu}_m^*\cdot\left[\mathbf{U}_{mn}^{(+)}+\mathbf{U}_{mn}^{(-)}\right]\cdot\boldsymbol{\mu}_n\\
&\qquad\qquad +\frac{i}{\hbar}\sum_{n\neq m}\hat{b}_m^\dagger(t)\hat{b}_n^\dagger(t)\boldsymbol{\mu}_m^*\cdot\left[\mathbf{V}_{mn}^{(+)}+\mathbf{V}_{mn}^{(-)}\right]\cdot\boldsymbol{\mu}_n^*\\
&\quad-\frac{i}{\hbar}\sum_{n\neq m}\hat{b}_m(t)\hat{b}_n(t)\boldsymbol{\mu}_m\cdot\left[\mathbf{U}_{mn}^{(+)}+\mathbf{U}_{mn}^{(-)}\right]\cdot\boldsymbol{\mu}_n\\
&\qquad\qquad -\frac{i}{\hbar}\sum_{n\neq m}\hat{b}_n^\dagger(t)\hat{b}_m(t)\boldsymbol{\mu}_m\cdot\left[\mathbf{V}_{mn}^{(+)}+\mathbf{V}_{mn}^{(-)}\right]\cdot\boldsymbol{\mu}_n^*. \qquad \text{(B.2.6)}
\end{aligned}$$

At this point it is relevant to point out that

$$\begin{aligned}
\mathbf{U}_{mm}^{(-)}&=\frac{1}{2\epsilon_0}\sum_\lambda\frac{\omega_\lambda\mathbf{f}_\lambda(\mathbf{R}_m)\otimes\mathbf{f}_\lambda^*(\mathbf{R}_m)}{\omega_m+\omega_\lambda}\\
&=\frac{1}{2\epsilon_0}\sum_\lambda\omega_\lambda\mathbf{f}_\lambda(\mathbf{R}_m)\otimes\mathbf{f}_\lambda^*(\mathbf{R}_m)\left[P\left(\frac{1}{\omega_m+\omega_\lambda}\right)-i\pi\delta(\omega_m+\omega_\lambda)\right]
\end{aligned} \qquad \text{(B.2.7)}$$

where the $P$ stands for principal value and the infinitely small positive imaginary part from the Laplace transform has been used. Since both $\omega_m$ and $\omega_\lambda$ are positive we get $\text{Im}\left\{\boldsymbol{\mu}_m^*\cdot\mathbf{U}_{mm}^{(-)}\cdot\boldsymbol{\mu}_m\right\}=0$. This along with the RWA

gives

$$\begin{aligned}
&\frac{i}{\hbar}\Big[\hat{b}_m^\dagger(t)\boldsymbol{\mu}_m^*\cdot\hat{\mathbf{E}}_{\mathrm{Scat}}^{(+)}(\mathbf{R}_m,t)+\boldsymbol{\mu}_m^*\cdot\hat{\mathbf{E}}_{\mathrm{Scat}}^{(-)}(\mathbf{R}_m,t)\hat{b}_m^\dagger(t)\\
&\qquad\qquad -\hat{b}_m(t)\boldsymbol{\mu}_m\cdot\hat{\mathbf{E}}_{\mathrm{Scat}}^{(+)}(\mathbf{R}_m,t)-\boldsymbol{\mu}_m\cdot\hat{\mathbf{E}}_{\mathrm{Scat}}^{(-)}(\mathbf{R}_m,t)\hat{b}_m(t)\Big]\\
&\approx\frac{i}{\hbar}\hat{b}_m^\dagger(t)\hat{b}_m(t)\left[\boldsymbol{\mu}_m^*\cdot\mathbf{U}_{mm}^{(+)}\cdot\boldsymbol{\mu}_m-c.c.\right]\\
&\qquad+\frac{i}{\hbar}\sum_{n\neq m}\hat{b}_m^\dagger(t)\hat{b}_n(t)\boldsymbol{\mu}_m^*\cdot\left[\mathbf{U}_{mn}^{(+)}+\mathbf{U}_{mn}^{(-)}\right]\cdot\boldsymbol{\mu}_n\\
&\qquad\qquad-\frac{i}{\hbar}\sum_{n\neq m}\hat{b}_n^\dagger(t)\hat{b}_m(t)\boldsymbol{\mu}_m\cdot\left[\mathbf{V}_{mn}^{(+)}+\mathbf{V}_{mn}^{(-)}\right]\cdot\boldsymbol{\mu}_n^*. \qquad \text{(B.2.8)}
\end{aligned}$$

Therefore we have

$$\begin{aligned}
&-2\frac{i}{\hbar}\Big[\hat{\sigma}_m(t)\boldsymbol{\mu}_m^*\cdot\hat{\mathbf{E}}_{\mathrm{Scat}}^{(+)}(\mathbf{R}_m,t)+\boldsymbol{\mu}_m^*\cdot\hat{\mathbf{E}}_{\mathrm{Scat}}^{(-)}(\mathbf{R}_m,t)\hat{\sigma}_m(t)\Big]\\
&\qquad=\frac{i}{\hbar}\hat{b}_m(t)\boldsymbol{\mu}_m^*\cdot\left[\mathbf{U}_{mm}^{(+)}(t)-\mathbf{U}_{mm}^{(-)}(t)\right]\cdot\boldsymbol{\mu}_m\\
&\qquad\qquad+2i\sum_{n\neq m}\hat{\sigma}_m(t)\hat{b}_n(t)\frac{\mu_0\omega_n^2}{\hbar}\boldsymbol{\mu}_m^*\cdot\mathbf{K}(\mathbf{R}_m,\mathbf{R}_n,\omega_n)\cdot\boldsymbol{\mu}_n \qquad \text{(B.2.9)}
\end{aligned}$$

and

$$\begin{aligned}
&\frac{i}{\hbar}\Big[\hat{b}_m^\dagger(t)\boldsymbol{\mu}_m^*\cdot\hat{\mathbf{E}}_{\mathrm{Scat}}^{(+)}(\mathbf{R}_m,t)+\boldsymbol{\mu}_m^*\cdot\hat{\mathbf{E}}_{\mathrm{Scat}}^{(-)}(\mathbf{R}_m,t)\hat{b}_m^\dagger(t)\\
&\qquad\qquad -\hat{b}_m(t)\boldsymbol{\mu}_m\cdot\hat{\mathbf{E}}_{\mathrm{Scat}}^{(+)}(\mathbf{R}_m,t)-\boldsymbol{\mu}_m\cdot\hat{\mathbf{E}}_{\mathrm{Scat}}^{(-)}(\mathbf{R}_m,t)\hat{b}_m(t)\Big]\\
&=2\hat{b}_m^\dagger(t)\hat{b}_m(t)\frac{\mu_0\omega_m^2}{\hbar}\mathrm{Im}\left\{\boldsymbol{\mu}_m^*\cdot\mathbf{K}(\mathbf{R}_m,\mathbf{R}_m,\omega_m)\cdot\boldsymbol{\mu}_m\right\}\\
&\qquad-i\sum_{n\neq m}\hat{b}_m^\dagger(t)\hat{b}_n(t)\frac{\mu_0\omega_n^2}{\hbar}\boldsymbol{\mu}_m^*\cdot\mathbf{K}(\mathbf{R}_m,\mathbf{R}_n,\omega_n)\cdot\boldsymbol{\mu}_n\\
&\qquad\qquad+i\sum_{n\neq m}\hat{b}_n^\dagger(t)\hat{b}_m(t)\left[\frac{\mu_0\omega_n^2}{\hbar}\boldsymbol{\mu}_m^*\cdot\mathbf{K}(\mathbf{R}_m,\mathbf{R}_n,\omega_n)\cdot\boldsymbol{\mu}_n\right]^*. \qquad \text{(B.2.10)}
\end{aligned}$$

We identify the decay rate as

$$\beta=\frac{\mu_0\omega_n^2}{\hbar}\mathrm{Im}\left\{\boldsymbol{\mu}_m^*\cdot\mathbf{K}(\mathbf{R}_m,\mathbf{R}_m,\omega_m)\cdot\boldsymbol{\mu}_m\right\} \qquad \text{(B.2.11)}$$

and furthermore we see that

$$\boldsymbol{\mu}_m^*\cdot\left[\mathbf{U}_{mm}^{(+)}(t)-\mathbf{U}_{mm}^{(-)}(t)\right]\cdot\boldsymbol{\mu}_m=i\beta+\gamma \qquad \text{(B.2.12)}$$

where $\gamma_m$ is the Lamb shift given by

$$\gamma = \frac{1}{\hbar}\mathrm{Re}\left\{\boldsymbol{\mu}_m^* \cdot \left[\mathbf{U}_{mm}^{(+)}(t) - \mathbf{U}_{mm}^{(-)}(t)\right] \cdot \boldsymbol{\mu}_m\right\}. \tag{B.2.13}$$

# C

# Details for Chapter 6

## C.1 Relation between the Green function and the coupling coefficient

The coupling amongst the atoms occurs through the electric field by the coefficients $G_{mn}$ which are related to the classical Green function through

$$G_{mn} = -\frac{\mu_0 \omega_a^2}{\hbar \beta} \boldsymbol{\mu}_m^* \cdot \mathbf{K}(\mathbf{R}_{mn}, \omega_a) \cdot \boldsymbol{\mu}_n e^{-i\mathbf{k}_0 \cdot \mathbf{R}_{mn}}, \tag{C.1.1}$$

where $\mu_0$ is the vacuum permeability, $\omega_a$ is the atomic transition frequency, $\hbar$ is the Planck constant, and $\beta$ is the atomic decay rate or half the Einstein $A$-coefficient. Finally, $\boldsymbol{\mu}_m$ is the dipole vector which for $\Delta m = 0$ transitions is real and in the same direction as the incident field having wave vector $\mathbf{k}_0$ while for $\Delta m = \pm 1$ transitions $\boldsymbol{\mu}_m$ is complex and transverse to the incident light [12], $\mathbf{R}_{mn} = \mathbf{R}_m - \mathbf{R}_n$, and the kernel is

$$\begin{aligned} \mathbf{K}(\mathbf{r}, \omega) &= c_0^2 \sum_{\mathbf{k}} \left( \frac{\omega_k}{\omega} \right)^2 \frac{e^{i\mathbf{k}\cdot\mathbf{r}}}{\omega^2 - \omega_k^2} (\mathbf{I} - \hat{\mathbf{k}} \otimes \hat{\mathbf{k}}) \\ &= \mathbf{G}^+(\mathbf{r}, \omega) - \frac{c_0^2}{\omega} \delta(\mathbf{r}) \mathbf{I}. \end{aligned} \tag{C.1.2}$$

Here, the dyadic $\mathbf{G}^+(\mathbf{r}, \omega)$ being the retarded Green function governing the classical propagation of the field, $\mathbf{I}$ is the identity matrix, and $\hat{\mathbf{k}}$ is the unit vector in the direction of $\mathbf{k}$. The retarded Green function is in vacuum given by [51]

$$\mathbf{G}^+(\mathbf{r}, \omega) = -\frac{e^{ik^+ r}}{4\pi r} \left[ P(ikr)\mathbf{I} + Q(ikr)\hat{\mathbf{r}} \otimes \hat{\mathbf{r}} \right] + \frac{c_0^2}{\omega^2} \delta(\mathbf{r}) \mathbf{I}, \tag{C.1.3}$$

where $r = |\mathbf{r}|$, $k = |\mathbf{k}| = \omega / c_0$, and $k^+$ contain an infinitesimal imaginary part. The functions $P(z)$ and $Q(z)$ are defined as

$$P(z) = 1 - \frac{1}{z} + \frac{1}{z^2}, \qquad Q(z) = -1 + \frac{3}{z} - \frac{3}{z^2}. \tag{C.1.4}$$

In our case $n \neq m$ and we get

$$\begin{aligned} G_{mn} =& \frac{3}{2}\frac{e^{ik_a^+ R_{mn}}}{k_a R_{mn}}\left[P(ik_a R_{mn}) + Q(ik_a R_{mn})\cos^2\theta_{mn}\right] e^{-i\mathbf{k}_0\cdot\mathbf{R}_{mn}} \\ =& \frac{3}{2}\frac{e^{ik_a^+ R_{mn}}}{k_a R_{mn}}\left[1-\cos^2\theta_{mn}\right] e^{-i\mathbf{k}_0\cdot\mathbf{R}_{mn}} \\ &+ \frac{3i}{2}\frac{e^{ik_a^+ R_{mn}}}{(k_a R_{mn})^2}\left[1-3\cos^2\theta_{mn}\right] e^{-i\mathbf{k}_0\cdot\mathbf{R}_{mn}} \\ &- \frac{3}{2}\frac{e^{ik_a^+ R_{mn}}}{(k_a R_{mn})^3}\left[1-3\cos^2\theta_{mn}\right] e^{-i\mathbf{k}_0\cdot\mathbf{R}_{mn}}, \end{aligned} \tag{C.1.5}$$

where $\theta_{mn}$ is the angle between $\boldsymbol{\mu}$ and $\mathbf{R}_{mn}$.

### C.1.1 Scalar approximation

If the dipoles are randomly oriented then one often integrates over the angle $\theta_{mn}$ in Eq. (C.1.5) such that

$$\begin{aligned} \langle G_{mn}\rangle_{\theta_{mn}} =& \frac{3}{2}\frac{e^{ik_a R_{mn}}}{k_a R_{mn}}\left[P(ik_a R_{mn}) + \frac{Q(ik_a R_{mn})}{3}\right] e^{-i\mathbf{k}_0\cdot\mathbf{R}_{mn}} \\ =& \frac{e^{ik_a R_{mn}}}{k_a R_{mn}} e^{-i\mathbf{k}_0\cdot\mathbf{R}_{mn}}. \end{aligned} \tag{C.1.6}$$

We will omit the angle averaging brackets.

### C.1.2 The ensemble averaged coupling coefficient

We now perform an ensemble average over the position of the atoms, i.e.

$$\overline{G_{mn}} = \int \mathrm{d}\mathbf{r} n(\mathbf{r}) \int \mathrm{d}\mathbf{r}' n(\mathbf{r}') \frac{e^{i[k_a|\mathbf{r}-\mathbf{r}'|-\mathbf{k}_0\cdot(\mathbf{r}-\mathbf{r}')]}}{k_a|\mathbf{r}-\mathbf{r}'|}. \tag{C.1.7}$$

Assuming a Gaussian cloud such that

$$n(\mathbf{r}) = \frac{1}{\sqrt{(2\pi\tilde{\rho}^2)^3}} \exp\left(-\frac{r^2}{2\tilde{\rho}^2}\right), \tag{C.1.8}$$

then making the change of variables $\mathbf{x} = k_a(\mathbf{r}-\mathbf{r}')$ and $\mathbf{y} = k_a(\mathbf{r}+\mathbf{r}')$ gives

$$\begin{aligned} n(\mathbf{r})n(\mathbf{r}') &= n[(\mathbf{x}+\mathbf{y})/(2k_a)]n[(\mathbf{y}-\mathbf{x})/(2k_a)] \\ &= \frac{k_a^6}{(2\pi\rho^2)^3} \exp\left(-\frac{x^2}{4\rho^2}\right) \exp\left(-\frac{y^2}{4\rho^2}\right), \end{aligned} \tag{C.1.9}$$

with $\rho = k_a\tilde{\rho}$ being the size of the cloud normalized with the atomic wavenumber. The integrals thus separate into two independent integrals $\overline{G_{mn}} = I_a I_b$ with

$$I_a = \frac{J(\mathbf{x},\mathbf{y})k_a^6}{(2\pi\tilde{\rho}^2)^3}\int \mathrm{d}\mathbf{y} e^{-\frac{y^2}{4\rho^2}} = \frac{1}{\pi^{3/2}(2\rho)^3} \tag{C.1.10a}$$

$$I_b = \int \mathrm{d}\mathbf{x} e^{-\frac{x^2}{4\rho^2}}\frac{e^{ix}}{x}e^{-iax\cos(\theta)} \tag{C.1.10b}$$

where $J(\mathbf{x},\mathbf{y}) = \frac{1}{8k_a^6}$ is the Jacobian determinant of the variable transformation and $a = k_0/k_a$. Notice that $a = \omega_0/\omega_a \approx 1$ even for a very large detuning and we will thus take $a = 1$ for simplicity. The integral $I_b$ is then given by

$$\begin{aligned} I_b =& \int \mathrm{d}\mathbf{x} e^{-\frac{x^2}{4\rho^2}}\frac{e^{ix}}{x}e^{-ix\cos(\theta)} \\ =& 4\pi\int_0^\infty \mathrm{d}x \exp\left[-\left(\frac{x}{2\rho}\right)^2 + ix\right]\sin(x) \\ =& 2i\pi^{3/2}\rho\left(1-e^{-4\rho^2}\right) + 2e^{-4\rho^2}\pi^{3/2}\rho\mathrm{Erfi}(2\rho) \end{aligned} \tag{C.1.11}$$

and thus

$$\begin{aligned} \overline{G_{mn}} &= \frac{1}{(2\rho)^2}\left[e^{-4\rho^2}\mathrm{Erfi}(2\rho) + i\left(1-e^{-4\rho^2}\right)\right] \\ &\overset{\rho\gg 1}{\to} \frac{1}{(2\rho)^2}\left[\frac{1}{2\sqrt{\pi}\rho} + i\right]. \end{aligned} \tag{C.1.12}$$

## C.2 Derivation details of the $N$-atom fluorescence spectrum

The definition of the fluorescence spectrum of a cloud of two-level atoms is given by

$$\frac{S(\mathbf{r},\omega')}{S_0} = \sum_{m,n} \mathrm{Re}\left\{ \lim_{t\to\infty} \int_0^\infty \mathrm{d}\tau e^{i\omega\tau} \left\langle \hat{b}_m^\dagger(t+\tau)\hat{b}_n(t) \right\rangle e^{i(\mathbf{k}_0-\mathbf{k}_d)\cdot(\mathbf{R}_m-\mathbf{R}_n)} \right\}, \tag{C.2.1}$$

where $\mathbf{k}_d$ is now in the direction from the center of the cloud to the detector. For simplicity, we have assumed that we can filter out the free field and have omitted the $r/c$ time contribution in the operator since we are taking the long time limit. We will split the spectrum up into two parts, i.e.

$$\frac{S_{\mathrm{loc}}(\mathbf{r},\omega')}{S_0} = \sum_{m} \mathrm{Re}\left\{ \lim_{t\to\infty} \int_0^\infty \mathrm{d}\tau e^{i\omega\tau} \left\langle \hat{b}_m^\dagger(t+\tau)\hat{b}_m(t) \right\rangle \right\}, \tag{C.2.2a}$$

$$\frac{S_{\mathrm{int}}(\mathbf{r},\omega')}{S_0} = \sum_{m,n\neq m} \mathrm{Re}\left\{ \lim_{t\to\infty} \int_0^\infty \mathrm{d}\tau e^{i\omega\tau} \left\langle \hat{b}_m^\dagger(t+\tau)\hat{b}_n(t) \right\rangle e^{i\delta\mathbf{k}\cdot\mathbf{R}_{mn}} \right\}, \tag{C.2.2b}$$

where $\delta\mathbf{k} = \mathbf{k}_0 - \mathbf{k}_d$ and $\mathbf{R}_{mn} = \mathbf{R}_m - \mathbf{R}_n$.

In order to calculate the spectrum we need the Laplace transform of $\left\langle \hat{b}_m^\dagger(t)\hat{b}_n(t+\tau) \right\rangle$ with respect to $\tau$. We do this in the same way as the calculation of the single atom fluorescence spectrum in Sec. 6.1 by finding the Laplace transform of $\hat{\mathbf{x}}(t+\tau)$. This give a similar expression as in the calculation of the atomic population in Sec. 6.3

$$\begin{aligned} \mathbf{0} = &-(\mathbf{M}-i\omega\mathbf{I})\,\hat{\mathbf{x}}_m(\omega) - \frac{i}{\omega}\mathbf{e}_3 + \hat{\mathbf{x}}_m(t) \\ &+ \left(i\mathbf{Q}G_m - i\tilde{\mathbf{Q}}G_m^*\right)(\mathbf{A}-i\omega\mathbf{I})^{-1}\mathbf{B}\hat{\mathbf{x}}_m(\omega) \\ &+ \sum_{n\neq m}\left(i\mathbf{Q}G_{mn} - i\tilde{\mathbf{Q}}G_{mn}^*\right)(\mathbf{A}-i\omega\mathbf{I})^{-1}\left[\mathbf{B}^i\hat{\mathbf{x}}_n(\omega) - \hat{\mathbf{y}}_{mn}(t)\right]. \end{aligned} \tag{C.2.3}$$

Consistent with the single scattering approximation we omit the terms $\hat{\mathbf{y}}_{mn}(t)$ since, in the evaluation of $\left\langle \hat{b}_m^\dagger(t)\hat{b}_n(t+\tau) \right\rangle$, this term concern three atom correlations. Now, we write Eq. (C.2.3) as a $3N \times 3N$ matrix equation. We define the frequency dependent counterparts of the matrices $\mathbf{M}^{(N)}$, $\mathbf{\Lambda}$ and $\mathbf{\Pi}$

as

$$\{\mathbf{M}^{(N)}(\omega)\}_{mn} = (\mathbf{M} - i\omega\mathbf{I})\delta_{mn}, \tag{C.2.4a}$$

$$\{\mathbf{\Lambda}(\omega)\}_{mn} = \left(i\mathbf{Q}G_m - i\tilde{\mathbf{Q}}G_m^*\right)(\mathbf{A} - i\omega\mathbf{I})^{-1}\mathbf{B}\delta_{mn}, \tag{C.2.4b}$$

$$\{\mathbf{\Pi}(\omega)\}_{mn} = \left(i\mathbf{Q}G_{mn} - i\tilde{\mathbf{Q}}G_{mn}^*\right)(\mathbf{A} - i\omega\mathbf{I})^{-1}\tilde{\mathbf{B}}(1-\delta_{mn}). \tag{C.2.4c}$$

With these and to first order in the interaction we obtain

$$\begin{aligned}\hat{\mathbf{X}}(\omega) \approx &-[\mathbf{M}^{(N)}(\omega)]^{-1}\left[\frac{i}{\omega}\mathbf{C} - \hat{\mathbf{X}}(t)\right] \\ &- [\mathbf{M}^{(N)}(\omega)]^{-1}(\mathbf{\Lambda}(\omega) + \mathbf{\Pi}(\omega))[\mathbf{M}^{(N)}(\omega)]^{-1}\left[\frac{i}{\omega}\mathbf{C} - \hat{\mathbf{X}}(t)\right].\end{aligned}$$

The validity of these first order solutions are given by

$$||\mathbf{\Lambda}(\omega) + \mathbf{\Pi}(\omega)|| \ll ||\mathbf{M}^{(N)}(\omega)||, \tag{C.2.5}$$

which is further investigated in App. C.4. In order to calculate the spectrum we need to know

$$\begin{aligned}\left\langle \hat{b}_m^\dagger \hat{\mathbf{X}}(\omega)\right\rangle_{ss} = &-[\mathbf{M}^{(N)}(\omega)]^{-1}\left[\frac{i}{\omega}\left\langle \hat{b}_m^\dagger \mathbf{C}\right\rangle_{ss} - \left\langle \hat{b}_m^\dagger \hat{\mathbf{X}}\right\rangle_{ss}\right] \\ &- [\mathbf{M}^{(N)}(\omega)]^{-1}\left[\mathbf{\Lambda}(\omega) + \mathbf{\Pi}(\omega)\right][\mathbf{M}^{(N)}(\omega)]^{-1}\left[\frac{i}{\omega}\left\langle \hat{b}_m^\dagger \mathbf{C}\right\rangle_{ss} - \left\langle \hat{b}_m^\dagger \hat{\mathbf{X}}\right\rangle_{ss}\right].\end{aligned}$$

The steady-state expectation values of $\left\langle \hat{b}_m^\dagger(t)\mathbf{C}\right\rangle$ and $\left\langle \hat{b}_m^\dagger(t)\hat{\mathbf{X}}(t)\right\rangle$ are related to the steady-state expectation values $\mathbf{x}_m(\infty)$ and $\mathbf{y}_{mn}(\infty)$ through

$$\left\{\left\langle \hat{b}_m^\dagger(t)\mathbf{C}\right\rangle_{ss}\right\}_n = \mathbf{V}\mathbf{x}_m(\infty), \tag{C.2.6a}$$

$$\left\{\left\langle \hat{b}_m^\dagger(t)\hat{\mathbf{X}}(t)\right\rangle_{ss}\right\}_n = \mathbf{P}\mathbf{y}_{mn}(\infty)(1-\delta_{mn}) + \left[\mathbf{U}\mathbf{x}_m(\infty) + \frac{\mathbf{e}_2}{2}\right]\delta_{mn}, \tag{C.2.6b}$$

where $\mathbf{P}$ is a sparse $9\times 3$ matrix, written out in App. C.5, that single out elements in $\mathbf{y}_{mn}$ while the $\mathbf{e}_1 = [1,0,0]^T$ term arrive due to a contraction of for products of two operators of the same atom similar to the single atom calculations, see Eq. (6.1.13). Using the above notation the fluorescence spectra can be written as

$$\frac{S_{\rm loc}(\mathbf{r},\omega')}{S_0} = \sum_m \mathrm{Re}\left\{\mathbf{e}_2 \cdot \left\{\left\langle \hat{b}_m^\dagger(t)\hat{\mathbf{X}}(\omega)\right\rangle_{ss}\right\}_m\right\}, \tag{C.2.7a}$$

$$\frac{S_{\rm int}(\mathbf{r},\omega')}{S_0} = \sum_{m,n\neq m} \mathrm{Re}\left\{\mathbf{e}_2 \cdot \left\{\left\langle \hat{b}_m^\dagger(t)\hat{\mathbf{X}}(\omega)\right\rangle_{ss}\right\}_n e^{i\delta\mathbf{k}\cdot\mathbf{R}_{mn}}\right\}. \tag{C.2.7b}$$

We can write $\left\langle \hat{b}_m^\dagger(t)\hat{\mathbf{X}}(\omega)\right\rangle_{ss}$ as a zeroth and a first order term

$$\left\langle \hat{b}_m^\dagger(t)\hat{\mathbf{X}}(\omega)\right\rangle_{ss} \approx \left\langle \hat{b}_m^\dagger(t)\hat{\mathbf{X}}(\omega)\right\rangle_{ss}^{(0)} + \left\langle \hat{b}_m^\dagger(t)\hat{\mathbf{X}}(\omega)\right\rangle_{ss}^{(1)}. \tag{C.2.8a}$$

The elements of the zeroth order term

$$\left\{\left\langle \hat{b}_m^\dagger(t)\hat{\mathbf{X}}(\omega)\right\rangle_{ss}^{(0)}\right\}_m = -(\mathbf{M}-i\omega\mathbf{I})^{-1}\left[\left(\frac{i}{\omega}\mathbf{V}-\mathbf{U}\right)\mathbf{x}_m^{(0)}(\infty)+\frac{\mathbf{e}_2}{2}\right], \tag{C.2.9a}$$

$$\left\{\left\langle \hat{b}_m^\dagger(t)\hat{\mathbf{X}}(\omega)\right\rangle_{ss}^{(0)}\right\}_n = -(\mathbf{M}-i\omega\mathbf{I})^{-1}\left[\frac{i}{\omega}\mathbf{V}\mathbf{x}_m^{(0)}(\infty)+\mathbf{P}\mathbf{y}_{mn}^{(0)}(\infty)\right] \tag{C.2.9b}$$

and for the first order term

$$\begin{aligned}\left\{\left\langle \hat{b}_m^\dagger(t)\hat{\mathbf{X}}(\omega)\right\rangle_{ss}^{(1)}\right\}_m =& -(\mathbf{M}-i\omega\mathbf{I})^{-1}\left(\frac{i}{\omega}\mathbf{V}-\mathbf{U}\right)\mathbf{x}_m^{(1)}(\infty)\\ &-\boldsymbol{\epsilon}_m(\omega)\left[\left(\frac{i}{\omega}\mathbf{V}-\mathbf{U}\right)\mathbf{x}_m^{(0)}(\infty)+\frac{\mathbf{e}_2}{2}\right] \qquad \text{(C.2.10a)}\\ \left\{\left\langle \hat{b}_m^\dagger(t)\hat{\mathbf{X}}(\omega)\right\rangle_{ss}^{(1)}\right\}_n =& -(\mathbf{M}-i\omega\mathbf{I})^{-1}\left[\frac{i}{\omega}\mathbf{V}\mathbf{x}_m^{(1)}(\infty)+\mathbf{P}\mathbf{y}_{mn}^{(1)}(\infty)\right]\\ &-\boldsymbol{\epsilon}_n(\omega)\left[\frac{i}{\omega}\mathbf{V}\mathbf{x}_m^{(0)}(\infty)+\mathbf{P}\mathbf{y}_{mn}^{(0)}(\infty)\right]. \qquad \text{(C.2.10b)}\end{aligned}$$

For brevity we have defined the matrix

$$\boldsymbol{\epsilon}_m(\omega) = (\mathbf{M}-i\omega\mathbf{I})^{-1}\left(i\mathbf{Q}G_m - i\tilde{\mathbf{Q}}G_m^*\right)(\mathbf{A}-i\omega\mathbf{I})^{-1}(\mathbf{B}+\tilde{\mathbf{B}})(\mathbf{M}-i\omega\mathbf{I})^{-1}. \tag{C.2.11}$$

The steady-state operators of the $m$'th atom can be written as $\mathbf{x}_m(\infty) \approx \mathbf{x}_m^{(0)}(\infty)+\mathbf{x}_m^{(1)}(\infty)$ with

$$\mathbf{x}_m^{(0)}(\infty) = -\mathbf{M}^{-1}\mathbf{e}_3, \tag{C.2.12a}$$

$$\mathbf{x}_m^{(1)}(\infty) = -\boldsymbol{\epsilon}_m(0)\mathbf{e}_3, \tag{C.2.12b}$$

and similar we can write $\mathbf{y}_{mn}(\infty) \approx \mathbf{y}_{mn}^{(0)}(\infty)+\mathbf{y}_{mn}^{(1)}(\infty)$ with

$$\mathbf{y}_{mn}^{(0)}(\infty) = \mathbf{A}^{-1}(\mathbf{B}+\tilde{\mathbf{B}})\mathbf{M}^{-1}\mathbf{e}_3, \tag{C.2.13a}$$

$$\mathbf{y}_{mn}^{(1)}(\infty) = \mathbf{A}^{-1}\mathbf{B}\boldsymbol{\epsilon}_m(0)\mathbf{e}_3 + \mathbf{A}^{-1}\tilde{\mathbf{B}}\boldsymbol{\epsilon}_n(0)\mathbf{e}_3. \tag{C.2.13b}$$

For consistency we write the elements of $\left\langle \hat{b}_m^\dagger(t)\hat{\mathbf{X}}(\omega)\right\rangle_{ss}$ using only the matrices defined for the equations of motion. The elements of the zeroth order term are thus

$$\left\{\left\langle \hat{b}_m^\dagger(t)\hat{\mathbf{X}}(\omega)\right\rangle_{ss}^{(0)}\right\}_m = (\mathbf{M}-i\omega\mathbf{I})^{-1}\left[\left(\frac{i}{\omega}\mathbf{V}-\mathbf{U}\right)\mathbf{M}^{-1}\mathbf{e}_3+\frac{\mathbf{e}_2}{2}\right], \tag{C.2.14a}$$

$$\left\{\left\langle \hat{b}_m^\dagger(t)\hat{\mathbf{X}}(\omega)\right\rangle_{ss}^{(0)}\right\}_n = (\mathbf{M}-i\omega\mathbf{I})^{-1}\left[\frac{i}{\omega}\mathbf{V}+\mathbf{P}\mathbf{A}^{-1}(\mathbf{B}+\tilde{\mathbf{B}})\right]\mathbf{M}^{-1}\mathbf{e}_3 \tag{C.2.14b}$$

and for the first order term

$$\begin{aligned}\left\{\left\langle \hat{b}_m^\dagger(t)\hat{\mathbf{X}}(\omega)\right\rangle_{ss}^{(1)}\right\}_m =&(\mathbf{M}-i\omega\mathbf{I})^{-1}\left(\frac{i}{\omega}\mathbf{V}-\mathbf{U}\right)\boldsymbol{\epsilon}_m(0)\mathbf{e}_3\\ &+\boldsymbol{\epsilon}_m(\omega)\left[\left(\frac{i}{\omega}\mathbf{V}-\mathbf{U}\right)\mathbf{M}^{-1}\mathbf{e}_3+\frac{\mathbf{e}_2}{2}\right]\end{aligned} \tag{C.2.15a}$$

$$\begin{aligned}\left\{\left\langle \hat{b}_m^\dagger(t)\hat{\mathbf{X}}(\omega)\right\rangle_{ss}^{(1)}\right\}_n =&(\mathbf{M}-i\omega\mathbf{I})^{-1}\left[\frac{i}{\omega}\mathbf{V}+\mathbf{P}\mathbf{A}^{-1}\mathbf{B}\right]\boldsymbol{\epsilon}_m(0)\mathbf{e}_3\\ &-(\mathbf{M}+i\omega\mathbf{I})^{-1}\mathbf{P}\mathbf{A}^{-1}\tilde{\mathbf{B}}\boldsymbol{\epsilon}_n(0)\mathbf{e}_3\\ &+\boldsymbol{\epsilon}_n(\omega)\left[\frac{i}{\omega}\mathbf{V}+\mathbf{P}\mathbf{A}^{-1}(\mathbf{B}+\tilde{\mathbf{B}})\right]\mathbf{M}^{-1}\mathbf{e}_3.\end{aligned} \tag{C.2.15b}$$

### C.2.1 Local spectrum

We now write the local spectrum as a zeroth order contribution and a first order correction, i.e. $S_{\mathrm{loc}}(\mathbf{r},\omega')\approx S_{\mathrm{loc}}^{(0)}(\mathbf{r},\omega')+S_{\mathrm{loc}}^{(1)}(\mathbf{r},\omega')$, with

$$\begin{aligned}\frac{S_{\mathrm{loc}}^{(0)}(\mathbf{r},\omega')}{S_0} &= \sum_m \mathrm{Re}\left\{\mathbf{e}_2\cdot\left\{\left\langle \hat{b}_m^\dagger(t)\hat{\mathbf{X}}^{(0)}(\omega)\right\rangle_{ss}\right\}_m\right\}\\ &= N\mathrm{Re}\left\{\mathbf{e}_2\cdot(\mathbf{M}-i\omega\mathbf{I})^{-1}\left[\left(\frac{i}{\omega}\mathbf{V}-\mathbf{U}\right)\mathbf{M}^{-1}\mathbf{e}_3+\frac{\mathbf{e}_2}{2}\right]\right\},\end{aligned} \tag{C.2.16a}$$

$$\begin{aligned}\frac{S_{\mathrm{loc}}^{(1)}(\mathbf{r},\omega')}{S_0} &= \sum_m \mathrm{Re}\left\{\mathbf{e}_2\cdot\left\{\left\langle \hat{b}_m^\dagger(t)\hat{\mathbf{X}}^{(1)}(\omega)\right\rangle_{ss}\right\}_m\right\}\\ &= \mathrm{Re}\left\{\mathbf{e}_2\cdot(\mathbf{M}-i\omega\mathbf{I})^{-1}\left(\frac{i}{\omega}\mathbf{V}-\mathbf{U}\right)\sum_m\boldsymbol{\epsilon}_m(0)\mathbf{e}_3\right\}\\ &\quad+\mathrm{Re}\left\{\mathbf{e}_2\cdot\sum_m\boldsymbol{\epsilon}_m(\omega)\left[\left(\frac{i}{\omega}\mathbf{V}-\mathbf{U}\right)\mathbf{M}^{-1}\mathbf{e}_3+\frac{\mathbf{e}_2}{2}\right]\right\}.\end{aligned} \tag{C.2.16b}$$

### Elastic local spectrum

The elastic part of the local spectrum is given by the delta function from the $\frac{1}{\omega}$ term, i.e.

$$\frac{S^{(0)}_{\mathrm{loc},el}(\mathbf{r},\omega')}{S_0} = \pi N \mathrm{Re}\left\{\mathbf{e}_2 \cdot \mathbf{M}^{-1}\mathbf{V}\mathbf{M}^{-1}\mathbf{e}_3\right\}\delta(\omega) = \frac{\pi N \tilde{\Omega}_R^2}{2\left(1+\tilde{\Omega}_R^2\right)^2}\delta(\omega), \tag{C.2.17a}$$

$$\begin{aligned}\frac{S^{(1)}_{\mathrm{loc},el}(\mathbf{r},\omega')}{S_0} &= \pi \mathrm{Re}\left\{\mathbf{e}_2 \cdot \left[\mathbf{M}^{-1}\mathbf{V}\sum_m \boldsymbol{\epsilon}_m(0) + \sum_m \boldsymbol{\epsilon}_m(0)\mathbf{V}\mathbf{M}^{-1}\right]\mathbf{e}_3\right\}\delta(\omega) \\ &= -\frac{\pi\left(\mathrm{Im}\left\{\sum_m G_m\right\} + \mathrm{Re}\left\{\sum_m G_m\right\}\Delta\right)\tilde{\Omega}_R^2\left(1-\tilde{\Omega}_R^2\right)}{(1+\Delta)\left(1+\tilde{\Omega}_R^2\right)^4}. \end{aligned} \tag{C.2.17b}$$

### C.2.2 Interference spectrum

Likewise, the interference spectrum is written as a zeroth order contribution and a first order correction, i.e. $S_{\mathrm{int}}(\mathbf{r},\omega') \approx S^{(0)}_{\mathrm{int}}(\mathbf{r},\omega') + S^{(1)}_{\mathrm{int}}(\mathbf{r},\omega')$, with

$$\begin{aligned}\frac{S^{(0)}_{\mathrm{int}}(\mathbf{r},\omega')}{S_0} &= \sum_{m,n\neq m}\mathrm{Re}\left\{\mathbf{e}_2 \cdot \left\{\left\langle \hat{b}^\dagger_m(t)\hat{\mathbf{X}}^{(0)}(\omega)\right\rangle_{ss}\right\}_n e^{i\delta\mathbf{k}\cdot\mathbf{R}_{mn}}\right\} \\ &= \mathrm{Re}\left\{\sum_{m,n\neq m} e^{i\delta\mathbf{k}\cdot\mathbf{R}_{mn}}\mathbf{e}_2\cdot(\mathbf{M}-i\omega\mathbf{I})^{-1}\left[\frac{i}{\omega}\mathbf{V}+\mathbf{P}\mathbf{A}^{-1}(\mathbf{B}+\tilde{\mathbf{B}})\right]\mathbf{M}^{-1}\mathbf{e}_3\right\}\end{aligned} \tag{C.2.18a}$$

$$\begin{aligned}\frac{S^{(1)}_{\mathrm{int}}(\mathbf{r},\omega')}{S_0} &= \sum_{m,n\neq m}\mathrm{Re}\left\{\mathbf{e}_2 \cdot \left\{\left\langle \hat{b}^\dagger_m(t)\hat{\mathbf{X}}^{(1)}(\omega)\right\rangle_{ss}\right\}_n e^{i\delta\mathbf{k}\cdot\mathbf{R}_{mn}}\right\} \\ &= \mathrm{Re}\left\{\mathbf{e}_2\cdot(\mathbf{M}-i\omega\mathbf{I})^{-1}\left[\frac{i}{\omega}\mathbf{V}+\mathbf{P}\mathbf{A}^{-1}\mathbf{B}\right]\sum_{m,n\neq m} e^{i\delta\mathbf{k}\cdot\mathbf{R}_{mn}}\boldsymbol{\epsilon}_m(0)\mathbf{e}_3\right\} \\ &\quad + \mathrm{Re}\left\{\mathbf{e}_2\cdot(\mathbf{M}-i\omega\mathbf{I})^{-1}\mathbf{P}\mathbf{A}^{-1}\tilde{\mathbf{B}}\sum_{m,n\neq m} e^{i\delta\mathbf{k}\cdot\mathbf{R}_{mn}}\boldsymbol{\epsilon}_n(0)\mathbf{e}_3\right\} \\ &\quad + \mathrm{Re}\left\{\mathbf{e}_2\cdot\sum_{m,n\neq m} e^{i\delta\mathbf{k}\cdot\mathbf{R}_{mn}}\boldsymbol{\epsilon}_n(\omega)\left[\frac{i}{\omega}\mathbf{V}+\mathbf{P}\mathbf{A}^{-1}(\mathbf{B}+\tilde{\mathbf{B}})\right]\mathbf{M}^{-1}\mathbf{e}_3\right\}.\end{aligned} \tag{C.2.18b}$$

### Elastic interference spectrum

The elastic part of the interference spectrum is again given by the delta function from the $\frac{1}{\omega}$ term, i.e.

$$\begin{aligned}\frac{S^{(0)}_{\mathrm{int},el}(\mathbf{r},\omega')}{S_0} =&\pi\mathrm{Re}\left\{\sum_{m,n\neq m} e^{i\delta\mathbf{k}\cdot\mathbf{R}_{mn}}\mathbf{e}_2\cdot\mathbf{M}^{-1}\mathbf{V}\mathbf{M}^{-1}\mathbf{e}_3\right\}\delta(\omega)\\ =&\sum_{m,n\neq m} e^{i\delta\mathbf{k}\cdot\mathbf{R}_{mn}}\frac{\pi\tilde{\Omega}_R^2}{2\left(1+\tilde{\Omega}_R^2\right)^2}\delta(\omega), \qquad \text{(C.2.19a)}\\ \frac{S^{(1)}_{\mathrm{int},el}(\mathbf{r},\omega')}{S_0} =&\pi\mathrm{Re}\left\{\mathbf{e}_2\cdot\mathbf{M}^{-1}\mathbf{V}\sum_{m,n\neq m} e^{i\delta\mathbf{k}\cdot\mathbf{R}_{mn}}\boldsymbol{\epsilon}_m(0)\mathbf{e}_3\right\}\delta(\omega)\\ &+\pi\mathrm{Re}\left\{\mathbf{e}_2\cdot\sum_{m,n\neq m} e^{i\delta\mathbf{k}\cdot\mathbf{R}_{mn}}\boldsymbol{\epsilon}_n(0)\mathbf{V}\mathbf{M}^{-1}\mathbf{e}_3\right\}\delta(\omega)\\ =&-\frac{\pi\mathrm{Im}\left\{\sum_{m,n\neq m} e^{i\delta\mathbf{k}\cdot\mathbf{R}_{mn}}G_m\right\}\tilde{\Omega}_R^2\left(1-\tilde{\Omega}_R^2\right)}{2\left(1+\Delta^2\right)\left(1+\tilde{\Omega}_R^2\right)^4}\delta(\omega)\\ &-\frac{\pi\mathrm{Re}\left\{\sum_{m,n\neq m} e^{i\delta\mathbf{k}\cdot\mathbf{R}_{mn}}G_m\right\}\Delta\tilde{\Omega}_R^2\left(1-\tilde{\Omega}_R^2\right)}{2\left(1+\Delta^2\right)\left(1+\tilde{\Omega}_R^2\right)^4}\delta(\omega)\\ &-\frac{\pi\mathrm{Im}\left\{\sum_{m,n\neq m} e^{i\delta\mathbf{k}\cdot\mathbf{R}_{mn}}G_n\right\}\tilde{\Omega}_R^2\left(1-\tilde{\Omega}_R^2\right)}{2\left(1+\Delta^2\right)\left(1+\tilde{\Omega}_R^2\right)^4}\delta(\omega)\\ &-\frac{\pi\mathrm{Re}\left\{\sum_{m,n\neq m} e^{i\delta\mathbf{k}\cdot\mathbf{R}_{mn}}G_n\right\}\Delta\tilde{\Omega}_R^2\left(1-\tilde{\Omega}_R^2\right)}{2\left(1+\Delta^2\right)\left(1+\tilde{\Omega}_R^2\right)^4}\delta(\omega). \qquad \text{(C.2.19b)}\end{aligned}$$

## C.3 Ensemble averages for the spectrum

In order to calculate the first order correction to the "local" part of the fluorescence spectrum we need to average the following sums

$$\sum_{m}^{N}\sum_{n\neq m}^{N} G_{mn}, \qquad \sum_{m}^{N}\sum_{n\neq m}^{N} G^{*}_{mn} \tag{C.3.1}$$

and for the "interference" part we need

$$\sum_{m}^{N}\sum_{n\neq m}^{N}\sum_{n'\neq m}^{N} e^{i\delta\mathbf{k}\cdot\mathbf{R}_{mn}} G_{mn'}, \qquad \sum_{m}^{N}\sum_{n\neq m}^{N}\sum_{n'\neq m}^{N} e^{i\delta\mathbf{k}\cdot\mathbf{R}_{mn}} G^{*}_{mn'}, \tag{C.3.2a}$$

$$\sum_{m}^{N}\sum_{n\neq m}^{N}\sum_{n'\neq n}^{N} e^{i\delta\mathbf{k}\cdot\mathbf{R}_{mn}} G_{nn'}, \qquad \sum_{m}^{N}\sum_{n\neq m}^{N}\sum_{n'\neq n}^{N} e^{i\delta\mathbf{k}\cdot\mathbf{R}_{mn}} G^{*}_{nn'}. \tag{C.3.2b}$$

Here $\mathbf{R}_{mn} = \mathbf{R}_m - \mathbf{R}_n$, with the $\mathbf{R}_m$ being the position of the $m$'th atom, and $\delta\mathbf{k} = \mathbf{k} - \mathbf{k}_0$, where $\mathbf{k}_0$ is the wave vector of the incident light and $\mathbf{k} = k_0\hat{\mathbf{r}}_d$ is the wave vector of the detected light in the far field with magnitude $k_0 = |\mathbf{k}_0|$ and $\hat{\mathbf{r}}_d$ is the normalized direction from the center of the cloud to the detector. By noticing that

$$\begin{aligned}
&\sum_{m}^{N}\sum_{n\neq m}^{N}\sum_{n'\neq m}^{N} e^{i\delta\mathbf{k}\cdot\mathbf{R}_{mn}} G_{mn'} \\
&= \sum_{m}^{N}\sum_{\substack{n'\neq m\\ n'\neq n}}^{N} e^{i\delta\mathbf{k}\cdot\mathbf{R}_{m}} G_{mn'} \sum_{n\neq m}^{N} e^{-i\delta\mathbf{k}\cdot\mathbf{R}_{n}} + \sum_{m}^{N}\sum_{n\neq m}^{N} e^{i\delta\mathbf{k}\cdot\mathbf{R}_{mn}} G_{mn},
\end{aligned} \tag{C.3.3}$$

then by defining the averaged functions

$$f(\mathbf{k}) = \int \mathrm{d}\mathbf{r} n(\mathbf{r}) e^{-i\mathbf{k}\cdot\mathbf{r}} \tag{C.3.4}$$

and

$$G(\mathbf{k},\mathbf{k}') = \int \mathrm{d}\mathbf{r} \int \mathrm{d}\mathbf{r}' n(\mathbf{r}) n(\mathbf{r}') e^{i\mathbf{k}\cdot\mathbf{r}} e^{-i\mathbf{k}'\cdot\mathbf{r}'} \frac{e^{ik_a|\mathbf{r}-\mathbf{r}'|}}{k_a|\mathbf{r}-\mathbf{r}'|} e^{-i\mathbf{k}_0\cdot(\mathbf{r}-\mathbf{r}')} e^{i\mathbf{k}\cdot\mathbf{r}} e^{-i\mathbf{k}'\cdot\mathbf{r}'} \tag{C.3.5}$$

we can write the ensemble averages of the sums Eq. (C.3.1) as

$$\overline{\sum_{m}^{N}\sum_{n\neq m}^{N} G_{mn}} = N(N-1)G(\mathbf{0},\mathbf{0}), \tag{C.3.6a}$$

$$\overline{\sum_{m}^{N}\sum_{n\neq m}^{N} G^{*}_{mn}} = N(N-1)G^{*}(\mathbf{0},\mathbf{0}), \tag{C.3.6b}$$

while the averages of the sums in Eqs. (C.3.2) can be written as

$$\overline{\sum_{m}^{N}\sum_{n\neq m}^{N}\sum_{n'\neq m}^{N} e^{i\delta\mathbf{k}\cdot\mathbf{R}_{mn}} G_{mn'}} = N(N-1)(N-2)f(\delta\mathbf{k})G(\delta\mathbf{k},\mathbf{0}) + N(N-1)G(\delta\mathbf{k},\delta\mathbf{k}), \tag{C.3.7a}$$

$$\overline{\sum_{m}^{N}\sum_{n\neq m}^{N}\sum_{n'\neq m}^{N} e^{i\delta\mathbf{k}\cdot\mathbf{R}_{mn}} G^{*}_{mn'}} = N(N-1)(N-2)f(\delta\mathbf{k})G^{*}(-\delta\mathbf{k},\mathbf{0}) + N(N-1)G^{*}(-\delta\mathbf{k},-\delta\mathbf{k}), \tag{C.3.7b}$$

$$\overline{\sum_{m}^{N}\sum_{n\neq m}^{N}\sum_{n'\neq n}^{N} e^{i\delta\mathbf{k}\cdot\mathbf{R}_{mn}} G_{nn'}} = N(N-1)(N-2)f(-\delta\mathbf{k})G(-\delta\mathbf{k},\mathbf{0}) + N(N-1)G(-\delta\mathbf{k},-\delta\mathbf{k}), \tag{C.3.7c}$$

$$\overline{\sum_{m}^{N}\sum_{n\neq m}^{N}\sum_{n'\neq n}^{N} e^{i\delta\mathbf{k}\cdot\mathbf{R}_{mn}} G^{*}_{nn'}} = N(N-1)(N-2)f(-\delta\mathbf{k})G^{*}(\delta\mathbf{k},\mathbf{0}) + N(N-1)G^{*}(\delta\mathbf{k},\delta\mathbf{k}). \tag{C.3.7d}$$

We thus need to calculate $f(\delta\mathbf{k})$, $G(\mathbf{0},\mathbf{0})$, $G(\delta\mathbf{k},\mathbf{0})$, $G(-\delta\mathbf{k},\mathbf{0})$, $G(\delta\mathbf{k},\delta\mathbf{k})$, $G(-\delta\mathbf{k},-\delta\mathbf{k})$, and their complex conjugates.

### C.3.1 The ensemble average

Let us evaluate the function

$$G(\mathbf{k},\mathbf{k}') = \int \mathrm{d}\mathbf{r} \int \mathrm{d}\mathbf{r}' n(\mathbf{r}) n(\mathbf{r}') e^{i\mathbf{k}\cdot\mathbf{r}} e^{-i\mathbf{k}'\cdot\mathbf{r}'} \frac{e^{ik_a|\mathbf{r}-\mathbf{r}'|}}{k_a|\mathbf{r}-\mathbf{r}'|} e^{-i\mathbf{k}_0\cdot(\mathbf{r}-\mathbf{r}')} e^{i\mathbf{k}\cdot\mathbf{r}} e^{-i\mathbf{k}'\cdot\mathbf{r}'}. \tag{C.3.8}$$

With a Gaussian cloud and the integrand transformation $\mathbf{x} = k_a(\mathbf{r}-\mathbf{r}')$ and $\mathbf{y} = k_a(\mathbf{r}+\mathbf{r}')$ such that $\mathbf{r} = (\mathbf{y}-\mathbf{x})/2k_a$ and $\mathbf{r}' = (\mathbf{y}+\mathbf{x})/2k_a$ we get

$G_N(\mathbf{k},\mathbf{k}') = I_a(\mathbf{k}-\mathbf{k}')I_b(\mathbf{k}+\mathbf{k}')$ where

$$\begin{aligned} I_a(\mathbf{k}-\mathbf{k}') =& \frac{J(\mathbf{x},\mathbf{y})k_a^6}{(2\pi\tilde{\rho}^2)^3}\int \mathrm{d}\mathbf{y} e^{-\frac{y^2}{4\rho^2}+i\frac{(\mathbf{k}-\mathbf{k}')}{2k_a}\cdot\mathbf{y}} \\ =& \frac{1}{\pi^{3/2}(2\rho)^3}\exp[-(\rho b)^2] \end{aligned} \tag{C.3.9a}$$

$$I_b(\mathbf{k}) = \int \mathrm{d}\mathbf{x} e^{-\frac{x^2}{4\rho^2}}\frac{e^{ix}}{x}e^{-idx\cos(\theta)}. \tag{C.3.9b}$$

Here $b = |\mathbf{k}-\mathbf{k}'|/2k_a$, $d = |2\mathbf{k}_0 - \mathbf{k} - \mathbf{k}'|/2k_a$, and here we use $\theta$ as the angle between $2\mathbf{k}_0 - \mathbf{k} - \mathbf{k}'$ and $\mathbf{x}$.

The integral $I_b$ is given by

$$\begin{aligned} I_b(\mathbf{k}) =& \int \mathrm{d}\mathbf{x} e^{-\frac{x^2}{4\rho^2}}\frac{e^{ix}}{x}e^{-idx\cos(\theta)} \\ =& \frac{4\pi}{d}\int_0^\infty \mathrm{d}x \exp\left[-\left(\frac{x}{2\rho}\right)^2 + ix\right]\sin(dx) \\ =& -\frac{2\pi^{3/2}\rho}{d}e^{-(1-d)^2\rho^2}\mathrm{Erfi}[(1-d)\rho] \\ &+ \frac{2\pi^{3/2}\rho}{d}e^{-(1+d)^2\rho^2}\mathrm{Erfi}[(1+d)\rho] \\ &+ \frac{2i\pi^{3/2}\rho}{d}e^{-(1-d)^2\rho^2}\left(1-e^{-4d\rho^2}\right) \end{aligned} \tag{C.3.10}$$

such that

$$\begin{aligned} G(\mathbf{k},\mathbf{k}') =& -\frac{1}{d(2\rho)^2}e^{-[b^2+(1-d)^2]\rho^2}\mathrm{Erfi}[(1-d)\rho] \\ &+ \frac{1}{d(2\rho)^2}e^{-[b^2+(1+d)^2]\rho^2}\mathrm{Erfi}[(1+d)\rho] \\ &+ i\frac{1}{d(2\rho)^2}e^{-[b^2+(1-d)^2]\rho^2}\left(1-e^{-4d\rho^2}\right), \end{aligned} \tag{C.3.11}$$

which for $b = 0$ and $d = 1$ reduce to the previous found expression for $G_N(\mathbf{0},\mathbf{0})$.

In a similar way we get that

$$f(\mathbf{k}) = \int \mathrm{d}\mathbf{r} n(\mathbf{r}) e^{-i\mathbf{k}\cdot\mathbf{r}} = \exp\left[-\left(\frac{\rho|\mathbf{k}|}{2k_a}\right)^2\right]. \tag{C.3.12}$$

We thus have

$$f(\delta\mathbf{k}) = \exp\left[-\rho^2\left|\sin\left(\frac{\theta_d}{2}\right)\right|^2\right], \tag{C.3.13}$$

where we have used that $|\delta\mathbf{k}|^2 = 2k_0^2(1-\cos\theta_d) = 4k_0^2\sin^2(\theta_d/2)$ and $k_0/k_a \approx 1$.

For $G(\mathbf{k},\mathbf{k}')$ and $\delta\mathbf{k} = \mathbf{k}_0 - \mathbf{k}_d$ we have that the coefficients $b$ and $d$ of Eq. (C.3.11) are given by

| $G(\mathbf{k},\mathbf{k}')$, | $b = \lvert\mathbf{k}-\mathbf{k}'\rvert/2k_a$, | $d = \lvert 2\mathbf{k}_0 - \mathbf{k} - \mathbf{k}'\rvert/2k_a$ | |
|---|---|---|---|
| $G(\mathbf{0},\mathbf{0})$, | $b = 0$, | $d = 1$ | (C.3.14a) |
| $G(\delta\mathbf{k},\mathbf{0})$, | $b = \left\lvert\sin\left(\frac{\theta_d}{2}\right)\right\rvert$, | $d = \lvert\cos(\theta_d/2)\rvert$ | (C.3.14b) |
| $G(-\delta\mathbf{k},\mathbf{0})$, | $b = \left\lvert\sin\left(\frac{\theta_d}{2}\right)\right\rvert$, | $d = \sqrt{1+3\sin^2\left(\frac{\theta_d}{2}\right)}$ | (C.3.14c) |
| $G(\delta\mathbf{k},\delta\mathbf{k})$, | $b = 0$, | $d = 1$ | (C.3.14d) |
| $G(-\delta\mathbf{k},-\delta\mathbf{k})$, | $b = 0$, | $d = \sqrt{1+8\sin^2\left(\frac{\theta_d}{2}\right)}$ | (C.3.14e) |

where $\theta_d$ is the detection angle between the propagation direction of the incoming driving field and the detection direction.

## C.4 Validity of the single-scattering approximation

The validity of the single-scattering approximation will now be investigated. It occurs in two different forms in the calculation of the atomic population and the fluorescence spectrum. We shortly find that if the criterion for the population calculations are obeyed then the criterion for the spectrum is as well. The singlesscattering approximation validity for the calculation of the spectrum is given by

$$||\mathbf{\Lambda}(\omega) + \mathbf{\Pi}(\omega)|| \ll ||\mathbf{M}^{(N)}(\omega)||, \tag{C.4.1}$$

with the $N$ by $N$ block diagonal matrices

$$\{\mathbf{M}^{(N)}(\omega)\}_{mn} = (\mathbf{M} - i\omega\mathbf{I})\delta_{mn}, \tag{C.4.2a}$$

$$\{\mathbf{\Lambda}(\omega)\}_{mn} = \left(i\mathbf{Q}G_m - i\tilde{\mathbf{Q}}G_m^*\right)(\mathbf{A} - i\omega\mathbf{I})^{-1}\mathbf{B}\delta_{mn}, \tag{C.4.2b}$$

$$\{\mathbf{\Pi}(\omega)\}_{mn} = \left(i\mathbf{Q}G_{mn} - i\tilde{\mathbf{Q}}G_{mn}^*\right)(\mathbf{A} - i\omega\mathbf{I})^{-1}\tilde{\mathbf{B}}(1 - \delta_{mn}). \tag{C.4.2c}$$

The criterion for the population calculations is given by $\omega = 0$. The norm $||\cdots||$ denotes the infinity norm and thus $||\mathbf{\Lambda}(\omega) + \mathbf{\Pi}(\omega)|| = ||\mathbf{\Lambda}(\omega)||$ and since $\mathbf{M}^{(N)}$ is block diagonal with identical elements in the different blocks we also have $||\mathbf{M}^{(N)}(\omega)|| = N||\mathbf{M} - i\omega\mathbf{I}||$. Thus, the validity criterion becomes

$$\sum_m || \left(i\mathbf{Q}G_m - i\tilde{\mathbf{Q}}G_m^*\right)(\mathbf{A} - i\omega\mathbf{I})^{-1}\mathbf{B}|| \ll N||\mathbf{M} - i\omega\mathbf{I}||. \tag{C.4.3}$$

At this point both sides of the inequality depend on both cloud type (size and number of atoms) and driving field (detuning and Rabi frequency). Let us make a new estimate that separates the cloud and the field parameters. We have that

$$\begin{aligned} &|| \left(i\mathbf{Q}G_m - i\tilde{\mathbf{Q}}G_m^*\right)(\mathbf{A} - i\omega\mathbf{I})^{-1}\mathbf{B}|| \\ &\qquad \leq |G_m|||\mathbf{Q}(\mathbf{A} - i\omega\mathbf{I})^{-1}\mathbf{B}|| + |G_m^*|||\tilde{\mathbf{Q}}(\mathbf{A} - i\omega\mathbf{I})^{-1}\mathbf{B}|| \\ &\qquad\qquad = 4|G_m|||(\mathbf{A} - i\omega\mathbf{I})^{-1}||, \end{aligned} \tag{C.4.4}$$

since $|G_m| = |G_m^*|$, $||\mathbf{B}|| = ||\tilde{\mathbf{B}}|| = 1$, and $||\mathbf{Q}|| = ||\tilde{\mathbf{Q}}|| = 2$. In order to get further physical intuition on the range of validity we note that from numerical investigations $4||(\mathbf{A} - i\omega\mathbf{I})^{-1}|| < 1$ and furthermore $||\mathbf{M} - i\omega\mathbf{I}||$ is minimal for $\omega = 0$. This signifies that if the validity criterion for $\omega = 0$ is obeyed, i.e. the criterion used in calculating the population, then the criterion for

the spectrum is also obeyed. At last, $\sum_m |G_m| < \sum_m \sum_{n\neq m} |G_{mn}|$ and thus we get the inequality

$$\frac{\sum_m \sum_{n\neq m} |G_{mn}|}{N} \ll ||\mathbf{M}|| \tag{C.4.5}$$

and this also respects Eq. (C.4.3). Here, the left hand side only depends on cloud properties such as size and number of atoms while the right hand side only depends on the driving properties Rabi frequency and detuning. The matrix norm is

$$||\mathbf{M}|| = \begin{cases} 2\Omega_\mathrm{R}, & 2\sqrt{1+\Delta^2} < \Omega_\mathrm{R} \\ 2\sqrt{1+\Delta^2} + \Omega_\mathrm{R}, & 2 < \Omega_\mathrm{R} < 2\sqrt{1+\Delta^2} \\ 2(1+\sqrt{1+\Delta^2}), & \Omega_\mathrm{R} < 2 \end{cases} . \tag{C.4.6}$$

The significance of this is that the perturbative treatment is only valid if the dipole-dipole interaction is much smaller than the interaction with the driving field. That is, the analysis is valid when we pump it hard or if we are far detuned. For large intensity we thus have the condition

$$\frac{\sum_m \sum_{n\neq m} |G_{mn}|}{N} \ll 2\Omega_\mathrm{R} \tag{C.4.7}$$

while for large detuning and intensity below $\Omega_\mathrm{R} < 2$ the condition is

$$\frac{\sum_m \sum_{n\neq m} |G_{mn}|}{N} \ll 2(1+\sqrt{1+\Delta^2}) \tag{C.4.8}$$

and at last for the intermediate region we have

$$\frac{\sum_m \sum_{n\neq m} |G_{mn}|}{N} \ll 2\sqrt{1+\Delta^2} + \Omega_\mathrm{R}. \tag{C.4.9}$$

The ensemble average of $|G_{mn}|$ assuming a Gaussian cloud with normalized thickness $\rho$, like in App. C.1, is

$$\overline{|G_{mn}|} = \frac{1}{\sqrt{\pi}\rho}. \tag{C.4.10}$$

## C.5 The $N$-atom matrices

Here we state the matrices used for calculating the steady-state population and fluorescence spectra of a cloud of $N$ atoms.

### C.5.1 Single-atom matrices

The vectors and matrices connected to the single-atom evolution, $\hat{\mathbf{x}}_m(t)$, $\mathbf{M}$, $\mathbf{U}$, and $\mathbf{V}$, are

$$\hat{\mathbf{x}}_m(t) = \begin{bmatrix} \hat{b}_m^\dagger(t) \\ \hat{b}_m(t) \\ \hat{\sigma}_m(t) \end{bmatrix}, \qquad \mathbf{M} = \begin{bmatrix} 1+i\Delta & 0 & -i\Omega_{\mathrm{R}} \\ 0 & 1-i\Delta & i\Omega_{\mathrm{R}} \\ -\frac{i\Omega_{\mathrm{R}}}{2} & \frac{i\Omega_{\mathrm{R}}}{2} & 2 \end{bmatrix}, \tag{C.5.1}$$

$$\mathbf{V} = \begin{bmatrix} 0 & 0 & 0 \\ 0 & 0 & 0 \\ 1 & 0 & 0 \end{bmatrix}, \qquad \mathbf{U} = \begin{bmatrix} 0 & 0 & 0 \\ 0 & 0 & 1 \\ -\frac{1}{2} & 0 & 0 \end{bmatrix}. \tag{C.5.2}$$

### C.5.2 Two-atom coupling matrices

The vectors and matrices connected to the coupling amongst atoms, $\hat{\mathbf{y}}_{mn}(t)$, $\mathbf{A} = \mathbf{A}_{\mathrm{diag}} + \mathbf{A}_{\Omega_{\mathrm{R}}}$, $\mathbf{B}$, $\tilde{\mathbf{B}}$, $\mathbf{Q}$, $\tilde{\mathbf{Q}}$, and $\mathbf{P}$, are given by

$$\hat{\mathbf{y}}_{mn}(t) = \begin{bmatrix} \hat{b}_m^\dagger(t)\hat{b}_n(t) \\ \hat{b}_n^\dagger(t)\hat{b}_m(t) \\ \hat{b}_m^\dagger(t)\hat{b}_n^\dagger(t) \\ \hat{b}_m(t)\hat{b}_n(t) \\ \hat{b}_m^\dagger(t)\hat{\sigma}_n(t) \\ \hat{b}_n^\dagger(t)\hat{\sigma}_m(t) \\ \hat{\sigma}_n(t)\hat{b}_m(t) \\ \hat{\sigma}_m(t)\hat{b}_n(t) \\ \hat{\sigma}_m(t)\hat{\sigma}_n(t) \end{bmatrix}, \qquad \mathbf{A}_{\mathrm{diag}} = \mathrm{diag}\begin{bmatrix} 2 \\ 2 \\ 2(1+i\Delta) \\ 2(1-i\Delta) \\ 3+i\Delta \\ 3+i\Delta \\ 3-i\Delta \\ 3-i\Delta \\ 4 \end{bmatrix}, \tag{C.5.3}$$

$$\mathbf{A}_{\Omega_{\mathrm{R}}} = i\Omega_{\mathrm{R}} \begin{bmatrix} 0 & 0 & 0 & 0 & 1 & 0 & 0 & -1 & 0 \\ 0 & 0 & 0 & 0 & 0 & 1 & -1 & 0 & 0 \\ 0 & 0 & 0 & 0 & -1 & -1 & 0 & 0 & 0 \\ 0 & 0 & 0 & 0 & 0 & 0 & 1 & 1 & 0 \\ \frac{1}{2} & 0 & -\frac{1}{2} & 0 & 0 & 0 & 0 & 0 & -1 \\ 0 & \frac{1}{2} & -\frac{1}{2} & 0 & 0 & 0 & 0 & 0 & -1 \\ 0 & -\frac{1}{2} & 0 & \frac{1}{2} & 0 & 0 & 0 & 0 & 1 \\ -\frac{1}{2} & 0 & 0 & \frac{1}{2} & 0 & 0 & 0 & 0 & 1 \\ 0 & 0 & 0 & 0 & -\frac{1}{2} & -\frac{1}{2} & \frac{1}{2} & \frac{1}{2} & 0 \end{bmatrix}, \tag{C.5.4}$$

$$\mathbf{B} = \begin{bmatrix} 0 & 0 & 0 \\ 0 & 0 & 0 \\ 0 & 0 & 0 \\ 0 & 0 & 0 \\ 1 & 0 & 0 \\ 0 & 0 & 0 \\ 0 & 1 & 0 \\ 0 & 0 & 0 \\ 0 & 0 & 1 \end{bmatrix}, \quad \tilde{\mathbf{B}} = \begin{bmatrix} 0 & 0 & 0 \\ 0 & 0 & 0 \\ 0 & 0 & 0 \\ 0 & 0 & 0 \\ 0 & 0 & 0 \\ 1 & 0 & 0 \\ 0 & 0 & 0 \\ 0 & 1 & 0 \\ 0 & 0 & 1 \end{bmatrix}, \tag{C.5.5}$$

$$\mathbf{Q} = \begin{bmatrix} 0 & 0 & 0 & 0 & 0 & 0 & 0 & 0 & 0 \\ 0 & 0 & 0 & 0 & 0 & 0 & 0 & 2 & 0 \\ -1 & 0 & 0 & 0 & 0 & 0 & 0 & 0 & 0 \end{bmatrix}, \tag{C.5.6}$$

$$\tilde{\mathbf{Q}} = \begin{bmatrix} 0 & 0 & 0 & 0 & 0 & 2 & 0 & 0 & 0 \\ 0 & 0 & 0 & 0 & 0 & 0 & 0 & 0 & 0 \\ 0 & -1 & 0 & 0 & 0 & 0 & 0 & 0 & 0 \end{bmatrix}, \tag{C.5.7}$$

$$\mathbf{P} = \begin{bmatrix} 0 & 0 & 1 & 0 & 0 & 0 & 0 & 0 & 0 \\ 1 & 0 & 0 & 0 & 0 & 0 & 0 & 0 & 0 \\ 0 & 0 & 0 & 0 & 1 & 0 & 0 & 0 & 0 \end{bmatrix}. \tag{C.5.8}$$

# Bibliography


[1] G. I. Taylor, "Interference fringes with feeble light," *Proc. Cam. phil. Soc.*, vol. **15**, p. 114, (1909).

[2] P. W. Anderson, "Absence of diffusion in certain random lattices," *Phys. Rev.*, vol. **109**, p. 1492, (1958).

[3] M. P. V. Albada and A. Lagendijk, "Observation of weak localization of light in random medium," *Phys. Rev. Lett.*, vol. **55**, p. 2692, (1985).

[4] P. E. Wolf and G. Maret, "Weak localization and coherent backscattering," *Phys. Rev. Lett.*, vol. **55**, p. 2696, (1985).

[5] P. A. Lee and A. D. Stone, "Universal conductance fluctuations in metals," *Phys. Rev. Lett.*, vol. **55**, p. 1622, (1985).

[6] M. C. W. van Rossum and Th. M. Nieuwenhuizen, "Multiple scattering of classical waves: microscopy, mesoscopy, and diffusion," *Rev. Mod. Phys.*, vol. **71**, p. 313, (1999).

[7] C. W. J. Beenakker, "Random-matrix theory of quantum transport," *Rev. Mod. Phys.*, vol. **69**, p. 731, (1997).

[8] L. Sapienza, H. Thyrrestrup, S. Stobbe, P. D. Garcia, S. Smolka, and P. Lodahl, "Cavity quantum electrodynamics with Anderson-localized modes," *Science*, vol. **327**, p. 1352, (2010).

[9] J. C. Maxwell, "On physical lines of forces, parts I-IV: The theory of molecular vortices applied to magnetic phenomena," *Phil. Mag. J. Sci.*, vol. **21** & **23**, (1861).

[10] J. C. Maxwell, "A dynamical theory of the electromagnetic field," *Phil. Trans. of the Royal Soc. of London*, vol. **155**, p. 459, (1865).

[11] R. Loudon, *The Quantum Theory of Light*. New York: Oxford University Press, 3rd ed., 2007.

[12] L. Mandel and E. Wolf, *Optical Coherence and Quantum Optics*. Cambridge: Cambridge University Press, 1995.

[13] R. J. Glauber and M. Lewenstein, "Quantum optics of dielectric media," *Phys. Rev. A*, vol. **43**, p. 467, (1991).

[14] D. S. Fisher and P. A. Lee, "Relation between conductivity and transmission matrix," *Phys. Rev. A*, vol. **23**, p. 6851, (1981).

[15] S. Datta, *Electronic Transport in Mesoscopic Systems*. Cambridge: Cambridge University Press, 1st ed., 1995.

[16] G. Cwilich, L. S. Froufe-Pérez, and J. J. Sáenz, "Spatial wave intensity correlations in quasi-one-dimensional wires," *Phys. Rev. E*, vol. **74**, p. 045603(R), (2006).

[17] O. N. Dorokhov, "On the coexistence of localized and extended electronic states in the metallic phase," *Solid State Commun.*, vol. **51**, p. 381, (1984).

[18] P. A. Mello, P. Pereyra, and N. Kumar, "Macroscopic approach to multichannel disordered conductors," *Ann. of Phys.*, vol. **181**, p. 290, (1988).

[19] J. J. Sáenz, L. S. Froufe-Pérez, and A. García-Martín, *Wave Scattering in Complex Media*, Chap. 5. Dordrecht: Kluwer, 2003.

[20] S. Feng, C. Kane, P. A. Lee, and A. D. Stone, "Correlations and fluctuations of coherent wave transmission through disordered media," *Phys. Rev. Lett.*, vol. **61**, p. 834, (1988).

[21] P. A. Mello, E. Akkermans, and B. Shapiro, "Macroscopic approach to correlations in the electronic transmission and reflection from disordered conductors," *Phys. Rev. Lett.*, vol. **61**, p. 459, (1988).

[22] P. A. Mello, "Averages on the unitary group and applications to the problem of disordered conductors," *J. Phys. A*, vol. **23**, p. 4061, (1990).

[23] A. García-Martín, F. Scheffold, M. Nieto-Vesperinas, and J. J. Sáenz, "Finite-size effects on intensity correlations in random media," *Phys. Rev. Lett.*, vol. **88**, 143901, (2002).

[24] P. A. M. Dirac, *The Principles of Quantum Mechanics*. New York: Oxford University Press, 4th ed., 1958.

[25] H. Goldstein, *Classical Mechanics*. Singapore: Addison-Wesley, 2nd ed., 1980.

[26] R. J. Glauber, "The quantum theory of optical coherence," *Phys. Rev.*, vol. **130**, p. 2529, (1963).

[27] C. W. J. Beenakker, "Thermal radiation and amplified spontaneous emission from a random medium," *Phys. Rev. Lett.*, vol. **81**, p. 1829, (1998).

[28] M. Patra and C. W. J. Beenakker, "Propagation of squeezed radiation through amplifying or absorbing random media," *Phys. Rev. A*, vol. **61**, 063805, (2000).

[29] P. Kok, W. J. Munro, K. Nemoto, T. C. Ralph, J. P. Dowling, and G. J. Milburn, "Linear optical quantum computing with photonic qubits," *Rev. Mod. Phys*, vol. **79**, p. 135, (2007).

[30] R. A. Campos, B. E. A. Saleh, and M. C. Teich, "Quantum-mechanical lossless beam splitter: SU(2) symmetry and photon statistics," *Phys. Rev. A*, vol. **40**, p. 1371, (1989).

[31] R. Hanbury Brown and R. Q. Twiss, "Corrrelation between photons in two coherent beams of light," *Nature*, vol. **177**, p. 27, (1956).

[32] L.-M. Duan, G. Giedke, J. I. Cirac, and P. Zoller, "Inseparability criterion for continuous variable systems," *Phys. Rev. Lett.*, vol. **84**, p. 2722, (2000).

[33] R. Simon, "Peres-Horodecki separability criterion for continuous variable systems," *Phys. Rev. Lett.*, vol. **84**, p. 2726, (2000).

[34] S. Mancini, V. Giovannetti, D. Vitali, and P. Tombesi, "Entangling macroscopic oscillators exploiting radiation pressure," *Phys. Rev. Lett.*, vol. **88**, 120401, (2002).

[35] M. D. Reid, P. D. Drummond, W. P. Bowen, P. K. Lam, H. A. Bacher, U. L. Andersen, and G. Leuchs, "The Einstein-Podolsky-Rosen paradox: From concepts to applications," *Rev. Mod. Phys.*, vol. **81**, p. 1727, (2009).

[36] J. S. Bell, "On the Einstein-Podolsky-Rosen paradox," *Physics*, vol. **1**, p. 195, (1964).

[37] J. R. Ott, N. A. Mortensen, and P. Lodahl, "Quantum interference and entanglement induced by multiple scattering of light," *Phys. Rev. Lett.*, vol. **105**, 090501, (2010).

[38] P. Lodahl, A. P. Mosk, and A. Lagendijk, "Spatial quantum correlations in multiple scattered light," *Phys. Rev. Lett.*, vol. **95**, 173901, (2005).

[39] S. Smolka, H. Thyrrestrup, L. Sapienza, T. B. Lehmann, K. R. Rix, L. S. Froufe-Pérez, P. D. García, and P. Lodahl, "Probing the statistical properties of Anderson localization with quantum emitters," *New J. Phys.*, vol. **13**, 063044, (2011).

[40] Th. M. Nieuwenhuizen and M. C. W. van Rossum, "Intensity distribution of transmitted waves through multiple scattering medium," *Phys. Rev. Lett.*, vol. **74**, p. 2674, (1995).

[41] W. H. Peeters, J. J. D. Moerman, and M. P. van Exter, "Observation of two-photon speckle patterns," *Phys. Rev. Lett.*, vol. **104**, 173601, (2010).

[42] S. Smolka, A. Huck, U. L. Andersen, A. Lagendijk, and P. Lodahl, "Observation of spatial quantum correlations induced by multiple scattering of nonclassical light," *Phys. Rev. Lett.*, vol. **102**, 193901, (2009).

[43] S. M. Popoff, G. Lerosey, R. Carminati, M. Fink, A. C. Boccara, and S. Gigan, "Measuring the transmission matrix in optics: An approach to the study and control of light propagation in disordered media," *Phys. Rev. Lett.*, vol. **104**, 100601, (2010).

[44] S. Smolka, A. Huck, U. L. Andersen, A. Lagendijk, and P. Lodahl, "Observation of spatial quantum correlations induced by multiple scattering of nonclassical light - erratum," *Phys. Rev. Lett.*, In Prep.

[45] P. Lodahl, "Quantum correlations induced by multiple scattering of quadrature squeezed light," *Opt. Express*, vol. **14**, p. 6919, (2006).

[46] J. D. Jackson, *Classical Electrodynamics*. New York: John Wiley & Sons, Inc., 3rd ed., 1999.

[47] M. L. Andersen, S. Stobbe, A. S. Sørensen, and P. Lodahl, "Strongly modified plasmon–matter interaction with mesoscopic quantum emitters," *Nature Physics*, vol. **7**, p. 215, (2011).

[48] E. A. Power and S. Zienau, "Coulomb gauge in non-relativistic quantum electrodynamics and the shape of spectral lines," *Phil. Trans. R. Soc. Lond. A*, vol. **251**, p. 427, (1959).

[49] P. G. Woolley, "Molecular quantum electrodynamics," *Proc. R. Soc. Lond. A*, vol. **321**, p. 557, (1971).

[50] M. Wubs, L. G. Suttorp, and A. Lagendijk, "Multiple-scattering approach to interatomic interactions and superradiance in inhomogeneous dielectrics," *Phys. Rev. A*, vol. **70**, 053823, (2004).

[51] P. D. Vries, D. V. van Coevorden, and A. Lagendijk, "Point scatterers for classical waves," *Rev. Mod. Phys.*, vol. **70**, p. 447, (1998).

[52] C. Cohen-Tannoudji, J. Dupont-Roc, and G. Grynberg, *Photons and Atoms. Introduction to Quantum Electrodynamics*. New York: Wiley, 1st ed., 1989.

[53] B. R. Mollow, "Power spectrum of light scattered by two-level systems," *Phys. Rev.*, vol. **188**, p. 1969, (1969).

[54] F. Schuda, C. R. Stroud Jr., and M. Hercher, "Observation of resonant Stark effect at optical frequencies," *J. Phys. B*, vol. **7**, p. L198, (1974).

[55] S. Ates, S. M. Ulrich, S. Reitzenstein, A. Löffler, A. Forchel, and P. Michler, "Post-selected indistinguishable photons from the resonance fluorescence of a single quantum dot in a microcavity," *Phys. Rev. Lett.*, vol. **103**, 167402, (2009).

[56] M. Dagenais and L. Mandel, "Investigation of two-time correlations in photon emissions from a single atom," *Phys. Rev. A*, vol. **18**, p. 2217, (1978).

[57] P. Lodahl, A. F. van Driel, I. S. Nikolaev, A. Irman, K. Overgaag, D. Vanmaekelbergh, and W. L. Vos, "Controlling the dynamics of spontaneous emission from quantum dots by photonic crystals," *Nature*, vol. **430**, p. 654, (2004).

[58] M. D. Leistikow, A. P. Mosk, E. Yeganegi, S. R. Huisman, A. Lagendijk, and W. L. Vos, "Inhibited spontaneous emission of quantum dots observed in a 3d photonic band gap," *Phys. Rev. Lett.*, vol. **107**, 193903, (2011).

[59] H. J. Kimble and L. Mandel, "Theory of resonance flourescence," *Phys. Rev. A*, vol. **13**, p. 2123, (1976).

[60] T. Bienaimé, S. Bux, E. Lucioni, P. W. Courteille, N. Piovella, and R. Kaiser, "Observation of a cooperative radiation force in the presence of disorder," *Phys. Rev. Lett.*, vol. **104**, 183602, (2010).

[61] L. Jin, J. Evers, and M. Macovei, "Photon scattering from strongly driven atomic ensembles," *Phys. Rev. A*, vol. **84**, 043812, (2011).

[62] S. Bux, E. Lucioni, H. Bender, T. Bienaimé, K. Lauber, C. Stehle, C. Zimmermann, S. Slama, P. W. Courteille, N. Piovella, and R. Kaiser,

"Cooperative scattering by cold atoms," *J. of Mod. Phys.*, vol. **57**, p. 1841, (2010).

[63] T. Bienaimé, M. Petruzzo, D. Bigerni, N. Piovella, and R. Kaiser, "Atom and photon measurement in cooperative scattering by cold atoms," *J. of Mod. Phys.*, vol. **58**, p. 1, (2011).

[64] T. G. Rudolph, Z. Ficek, and B. J. Dalton, "Two-atom resonance fluorescence in running- and standing-laserwave fields," *Phys. Rev. A*, vol. **52**, p. 636, (1995).

[65] T. Savels, A. P. Mosk, and A. Lagendijk, "Gain narrowing in few-atom systems," *Phys. Rev. Lett.*, vol. **98**, 103601, (2007).

[66] S. Das, G. S. Agarwal, and M. O. Scully, "Quantum interference in cooperative Dicke emission from spatial variation of the laser phase," *Phys. Rev. Lett.*, vol. **101**, 153601, (2008).

[67] J. D. Pritchard, C. S. Adams, and K. Mølmer, "Correlated photon emission from multiatom Rydberg dark states," *Phys. Rev. Lett.*, vol. **108**, 043601, (2012).

[68] M. D. Birowosuto, S. E. Skipetrov, W. L. Vos, and A. P. Mosk, "Observation of spatial fluctuations of the local density of states in random photonic media," *Phys. Rev. Lett.*, vol. **105**, 013904, (2010).

[69] E. Akkermans and G. Montambaux, *Mesoscopic Physics of Electrons and Photons*. Cambridge: Cambridge, 1st ed., 2007.

[70] N. Cherroret and A. Buchleitner, "Entanglement and Thouless times from coincidence measurements across disordered media," *Phys. Rev. A*, vol. **83**, 033827, (2011).